TECHNICAL REPORT STANDARD TITLE PAGE

1. REPORT NO.	2. GOVERNMENT ACCESSION NO.	3. RECIPIENT'S CATALOG NO.
NASA CR-150162		

4. TITLE AND SUBTITLE	5. REPORT DATE
Ignition Transients of Large Segmented Solid Rocket Boosters	April 1976
	6. PERFORMING ORGANIZATION CODE
7. AUTHOR(S)	8. PERFORMING ORGANIZATION REPORT #
Leonard H. Caveny and Kenneth K. Kuo	
9. PERFORMING ORGANIZATION NAME AND ADDRESS	10. WORK UNIT NO.
Princeton Resources, Inc. P. O. Box 211 Princeton, New Jersey, 08540	11. CONTRACT OR GRANT NO. NAS8-31666
	13. TYPE OF REPORT & PERIOD COVERED
12. SPONSORING AGENCY NAME AND ADDRESS	Contractor Report Final
National Aeronautics and Space Administration Washington, D. C. 20546	14. SPONSORING AGENCY CODE

15. SUPPLEMENTARY NOTES

16. ABSTRACT

Analytical procedures were developed and computerized to predict and analyze the ignition transients of high performance, segmented solid rocket boosters, of the type being developed by NASA for the Space Shuttle. The analysis accounts for the following: (1) temporal and spatial development of the flow field set up by the head-end igniter discharge, (2) ignition and flame spreading coupled to chamber flow, (3) the steep velocity, pressure, and temperature gradients that occur during the early phases of ignition, and (4) the interactions that produce "ignition spikes" (i.e., compression of chamber gases during pressurization, erosive burning, and mass-added effect of igniter discharge). The point of departure of this analysis is the 1973 model of Peretz, Caveny, Kuo and Summerfield; in this study, the flow interactions between the slots and main chamber are accounted for and the original computer program for monolithic motors was improved. The procedures were used to predict the ignition transients of the current design for the Space Shuttle booster.

17. KEY WORDS	18. DISTRIBUTION STATEMENT
	Unclassified-Unlimited A. A. McCool Director, Structures & Propulsion Lab.

19. SECURITY CLASSIF. (of this report)	20. SECURITY CLASSIF. (of this page)	21. NO. OF PAGES	22. PRICE
Unclassified	Unclassified	109	NTIS

ACKNOWLEDGEMENT

The authors express appreciation to personnel at the George C. Marshall Space Flight Center and the Wasatch Division of the Thiokol Corporation whose input materially aided this project and, in particular, to B. W. Shackelford, Jr. (NASA Project Coordinator) who provided overall technical guidance.

This project applied and extended analytical techniques developed at the Guggenheim Laboratories of Princeton University under a series of NASA Grants. Accordingly, it incorporates some of the results the authors obtained in a previous collaboration with A. Peretz and M. Summerfield.

This project was carried under NASA Contract NAS8-31666 by the authors working as consultants to Princeton Resources, Inc., P.O. Box 211, Princeton, NJ 08540.

TABLE OF CONTENTS

Table of Contents - Continued

LIST OF FIGURES

List of Figures - Continued

LIST OF TABLES

NOMENCLATURE*

A_b = burning surface of propellant, cm^2

A_p = cross-sectional area of the port, cm^2

A_t = motor nozzle throat area, cm^2

a = pre-exponential factor in burning rate law, ap^n

B_ℓ, B_r = points at left boundary and right boundary, see Figs. 3-3 and 3-4.

b = burning perimeter, cm

C_D = discharge coefficient

$C_{F\lambda m}$ = thrust coefficient accounting for losses

C_{FV} = thrust coefficient

C_m = nozzle coefficient for thrust loss

c = sonic velocity, cm/sec

c^* = characteristic velocity in nozzle discharge relationship, cm/sec

c_p = specific heat at constant pressure, cal/g-K

d_h = hydraulic diameter of the port, $4A_p/b$, cm

E = total stored energy, cal/g

F = thrust, newtons

f = friction coefficient, $2g\tau_w/\rho u^2$

G = mass flow rate, ρu, g/cm^2-sec

g = conversion factor

h = enthalpy of gases, cal/g

h_c = local convective heat-transfer coefficient, cal/cm^2-sec-K

I = inhomogeneous terms in the governing equations

J_c, J = mechanical equivalent of heat

k_e = erosive burning constant in Eq. (2-20), cm^3-K/cal

M = Mach number

m = mass flow rate, g/sec

N = number of spacewise mesh points

n = pressure exponent in the non-erosive burning rate law

Pr = Prandtl number

p = static pressure, atm

p_w = wetted perimeter (after ignition, only the inert perimeter), cm

*Appendices A and B provide further definitions of the symbols and units.

q_ℓ = rate of heat transfer, cal/cm^2-sec

R = gas constant for the combustion gases

R_u, R_g = universal gas constant

r, r_b = burning rate of the solid propellant, including the erosive burning contribution, cm/sec

r_0 = burning rate under nonerosive conditions, cm/sec

T = temperature (without subscript, static gas temperature), K

T_{af} = average film gas temperature, $(T + T_{ps})/2$, K

T_f = adiabatic flame temperature of the solid propellant, K

T_{ig} = effective mean temperature of the igniter gas, K

T_{pi}, T_0 = initial propellant temperature, K

T_{ps} = propellant surface temperature, K

$T_{ps,ig}$ = propellant surface temperature, at which propellant ignition occurs, K

t = time, sec

u = gas velocity, cm/sec

V = volume, cm^3

W = molecular weight of the combustion gases, g/g-mole

w = width of opening to slot, cm

x = axial distance from head end, cm

x_{seg} = effective distance from the leading edge of the corresponding segment, cm

x_{slot} = distance from head end of motor to the upstream edge of the segment, cm

y = perpendicular distance from the propellant surface into the solid, cm

α = thermal diffusivity, cm^2/sec

α_e = pre-exponential factor in erosive burning relationship

α_N = nozzle half-angle at exit plane, deg

β_e = erosive burning exponential factor

γ = ratio of specific heats

ε_{ex} = nozzle exit expansion ratio

ε_s = equivalent sand roughness, cm

θ = weighting parameter for implicit numerical scheme

λ = thermal conductivity, cal/cm-sec-K

λ_N = nozzle divergence loss

μ = viscosity of the combustion gases, g/cm-sec (poise)

ρ = density (without subscript, gas density), g/cm^3

σ_p = temperature sensitivity of burning rate, K^{-1}

τ_w = shear stress on the port wall

ϕ = temperature gradient at propellant surface, K/cm

Subscripts

A2,$\bar{A}$2 = values at points A_2 and $\bar{A}_2$, see Figs. 3-3 and 3-4.

act = actual

am = ambient

ch = chamber

E = entrance to motor nozzle (motor chamber aft-end)

es = entrance section at head-end of motor

ex = exit of nozzle

gen = generated in slot

h = head-end

i = initial value

ig = igniter

in = into slot

int = initial

meas = measured

mtr = motor

n = index for mesh points in the axial direction

n = nozzle end

out = out of slot

p = pressure

pd = latest predictor calculation

pr,c = solid propellant (condensed phase)

ref = reference conditions, T_0 = 298K and p = 68.08 atm

sldv = per unit volume containing slot

slot = slot

stag = stagnation

T = temperature

u = velocity

I = along right-running characteristic

II = along left-running characteristic

III = along particle-path line

1,2,3,4= station numbers

Superscripts

j = index for mesh time increments

$\bar{}$ = mean value

1.0 INTRODUCTION

This report describes the application of analytical techniques which are being developed to predict the ignition transients of segmented, solid propellant rocket boosters. Particular attention is given to the large, solid-rocket booster (SRB) which is being developed for the Space Shuttle (e.g., thrust > 10^6 lb and length > 100 ft). The booster is referred to as a segmented motor (as opposed to a monolithic motor) since it consists of several large motor segments which are joined together. The development of large SRB's is accompanied by a number of questions pertaining to optimizing performance, improving reliability, and reducing the costs of qualification tests. During the formative phases of development, it is natural to employ analytical techniques that yield a more comprehensive understanding of complex interactions between the igniter gas flow, heat transfer to the propellant, flame spreading, developing flow field, and erosive burning. Indeed, because of the costs of manufacturing and testing each solid rocket booster, predictions and design recommendations based on comprehensive analytical models can play an important role in defining the SRB configurations.

The essential elements that are incorporated into the analysis are: (a) techniques to account for the strong contribution of erosive burning, coupled to the chamber gas dynamics; (b) ability to consider significant pressure, temperature, and velocity spatial gradients, encountered in high loading density motors, and their variation with time during the starting transient, and (c) calculation of propellant surface heat-up to ignition and flame spreading, coupled to both temporal and spatial changes of flow parameters in the chamber. Indeed, to account for the experimentally observed steep pressure rise and pressure overshoots, the dominant influences of erosive burning and the spatial gradients of pressure, temperature, and velocity

must be accurately taken into account. Thus, using the techniques described in this report, analysts will be able to prescribe with greater confidence the upper limits of volumetric loading density and predict more accurately the pressure-thrust-time motor performance during the starting transient.

While the emphasis of this report is on large SRB's, the methodology is not dependent on motor diameter and thus can be applied to a wide variety of high length-to-diameter ratio motors.

The point of departure for this study was the analytical solution and computer program described in Ref. 1. The analytical development in Ref. 1 is for monolithic motor configurations and is sufficiently complete to treat most high performance motors; however, the computer program described in Ref. 1 dealt with a rather narrow subset of the overall analytical formulation. Thus, the computer program described in Ref. 1 (while well suited for the special geometry, igniter, and burning conditions of the laboratory slab motor) is not suitable for analyzing high-performance, operational motors. Also, the Ref. 1 computer program was not prepared in modular form and, as a consequence, changes in geometry, burning rate laws, friction factor equations, convective heating equations, etc., are extremely difficult to perform. During this study these limitations were overcome by redoing the computer program and emphasizing the requirements that occur during the design of high performance motors.

2.0 DESCRIPTION OF MODEL

2.1 Physical Situation Considered

The emphasis of this study was on the type of segmented motor configuration and ignition events illustrated in Fig. 2-1. At the onset of igniter discharge, a flow pattern with pressure, temperature, and velocity distributions develops in the motor port. Subsonic flow with friction and heat transfer to the propellant at low pressure (usually between 1 and 3 atm for the low port-to-throat area ratios under investigation) is established in the chamber. During the early part of the transient, the motor nozzle flow is unchoked. The first phase of the starting transient is the induction interval (ignition lag), which ends with the appearance of the first flame on the propellant surface (see Fig. 2-1b). The ignition criterion (used in this study) is that a point on the propellant surface ignites when it attains some critical ignition temperature, typically between 800 and 900 K. Thus, the process of flame spreading along the propellant surface, which starts at first ignition and ends when the entire surface is ignited, is described by the model of successive ignitions. Once started, the flame spreading is accelerated by the increased heat flux due to the rapidly increasing mass flow originating from the already ignited propellant surface. As the flow encounters the separations between the segments, the boundary layer is disturbed producing local increases in the convective heating rates. Rapid chamber pressurization usually begins with the onset of fast flame spreading. The last phase of the starting transient is the chamber filling period, which follows the completion of flame spreading. Prior to this time, the nozzle flow usually becomes choked. Erosive burning may take place during this period and thereafter, due to high gas velocities in the chamber. Also, the compression effects during the rapid pressurization will significantly increase the temperature of the chamber gases. Thus, the maximum

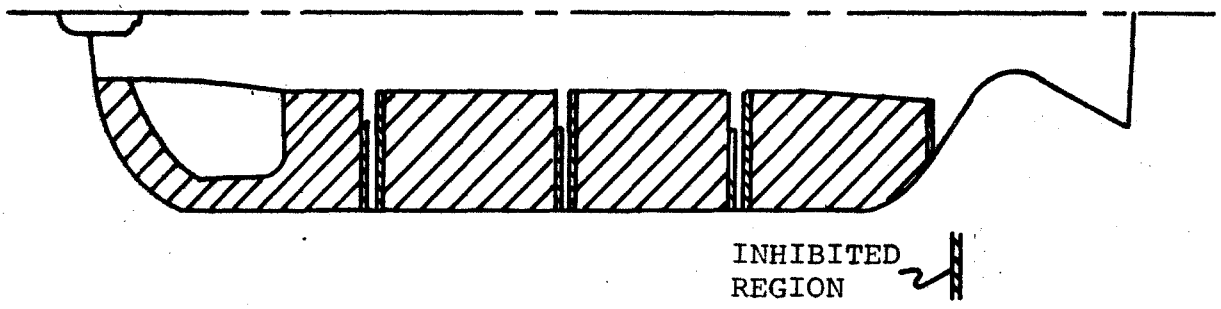

(a) Segmented rocket motor configuration

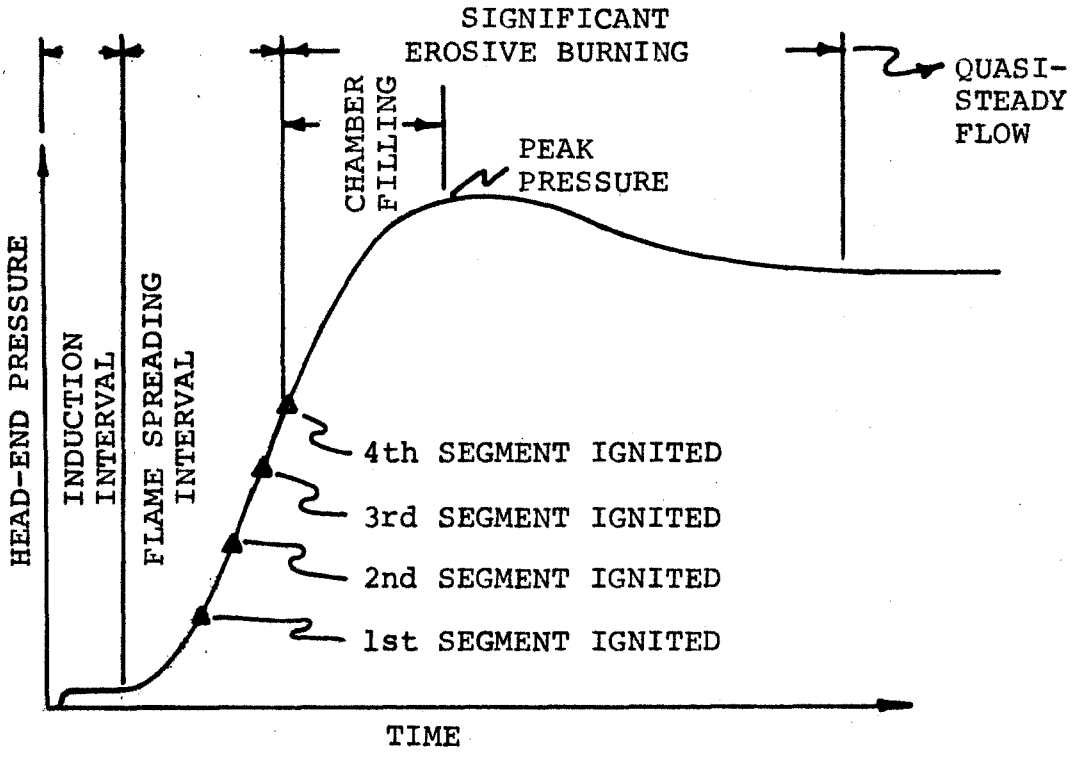

(b) Significant ignition intervals.

Fig. 2-1 Type of rocket motor and time intervals considered during study.

pressure may be much higher than the eventual equilibrium pressure. Significant pressure and temperature drops as well as velocity increases are established along the port. Following the pressure peak, a quasi-steady situation develops and pressure decreases toward an equilibrium value due to diminishing erosive burning, as the port area increases.

2.2 Types of Ignition Transient Models

Numerous studies have dealt with a particular fundamental process taking place during the start of solid propellant motors or have focused on practical correlations to facilitate igniter design. A detailed review of previous studies is given in Ref. 1. The analytical models directed at the analysis of the overall starting transient, can be categorized into three major groups: (a) lumped chamber-parameter, or p(t) models (e.g., Refs. 2-6), (b) quasi-steady one-dimensional flow, or p(x) models (e.g., Refs. 7 & 8), and (c) temporal and spatial development of flow field (Ref. 1.).

As shown on Fig. 2-2a, the models of the first group assume uniform pressure and temperature distributions in the combustion chamber port. Accordingly, such models are incapable of considering those driving forces which control ignition and flame spreading rates.

In the models of the second type (see Fig. 2-2b), quasi-steady pressure, temperature, and velocity distributions along the port are considered at each instant of time during the transient. Flame spreading is often treated in ways unsuitable for predictive use, e.g., an experimentally determined function of time; partially or fully instantaneous; linear function of the burning rate; proceeding in a constant average rate; or calculated from an experimental pressure-time plot.

Many high-performance solid propellant rocket motors have high volumetric loading densities, small port-to-throat area ratios, and, frequently, large length-to-diameter ratios. Such motors, referred to as HVT (High Velocity Transient)

ENERGY EQN. NOT USED
$T_{ch} = T_f \neq f[p(t)]$
ENERGY EQN. USED
$T_{ch} = f(p(t), V...)$
$T_f = f(\phi, r, ...)$

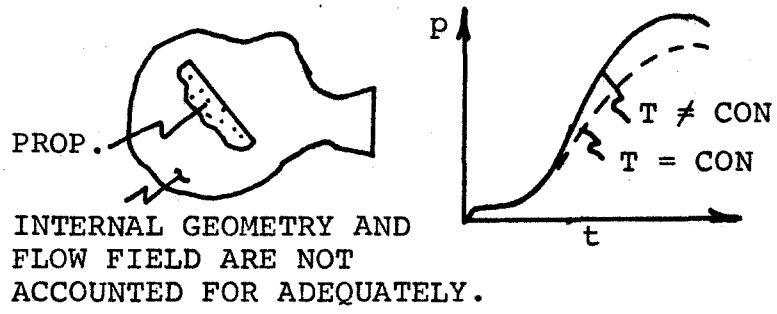

INTERNAL GEOMETRY AND FLOW FIELD ARE NOT ACCOUNTED FOR ADEQUATELY.

(a) p(t) model, chamber parameters are lumped.

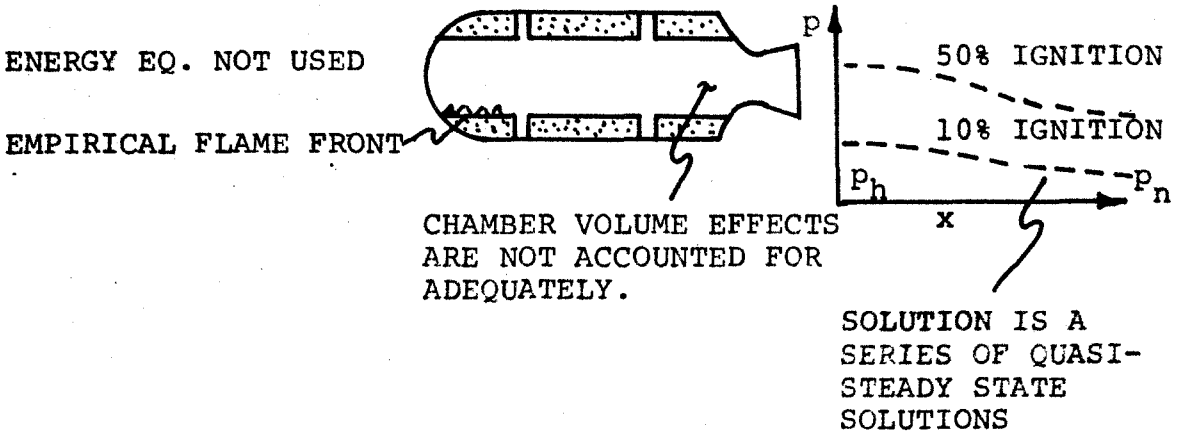

(b) p(x) model, quasi-steady 1-D flow.

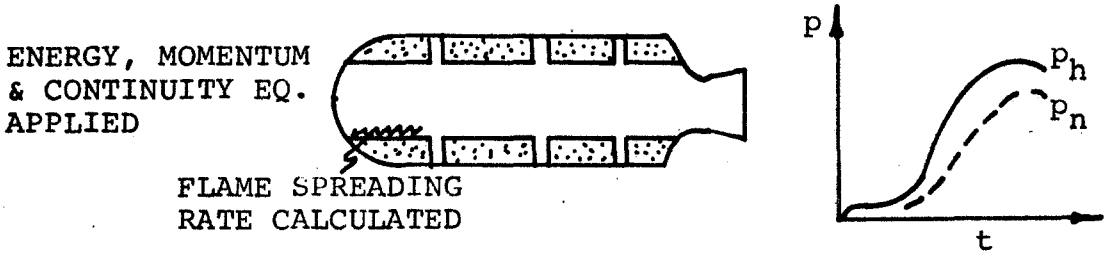

(c) p(x,t) model, transient flow field.

Fig. 2-2 Several types of ignition models.

motors, are characterized by high internal gas velocities (Mach numbers > 0.3), significant axial pressure and temperature gradients, pressure over-shoots, and relatively short ignition transient times. The large solid boosters are properly classified as HVT motors. The starting transients of the HVT motors (and SRB's) are inadequately predicted and incompletely analyzed by either one of the above-mentioned classes of approaches. In particular, pressure, temperature, and velocity variations with time and axial position in the motor [p(t,x) model] must be considered (see Fig. 2-2c). Interactions between processes, such as the developing flow field, igniter gas flow, convective heat transfer to the solid propellant, flame spreading, and erosive burning must be taken into account.

2.3 Description of Model Used in This Study

The analytical model [referred to as the p(x,t) model] is capable of treating the following:

General -

- Goes from onset of igniter flow through the ignition transient to steady state operation.

Igniter -

- Igniter discharge is an arbitrary function of time.
- Pyrogen igniter located at head-end.

Main Chamber - either monolithic or segmented configurations:

- Axial gradients of pressure, temperature, and velocity.
- Nozzle flow either choked or unchoked.
- Axial variation of port area.
- Wall friction and heating losses.
- Propellant surface temperature and gradient varies in axial direction.
- Flame spreading is governed by coupling between main chamber flow field, convective heating rates, and propellant temperature profile.
- Erosive burning is accounted for.

The key to quantitative p_{max} predictions for SRB designs is expected to be an accurate determination of the erosive burning during chamber pressurization.

Even though the physical model and mathematical formulation given in Ref. 1 were rather comprehensive with respect to high performance rocket motors of monolithic configuration, the Ref. 1 computer program was very specialized and suitable only for analyzing the laboratory slab motor. Thus, the program was not sufficiently general to handle conventional rocket motor designs. Accordingly, during this study the computer program was reorganized, improved greatly, and expanded to give it the capability to analyze high performance rocket motors. Thus, the reader may refer to Ref. 1 for the details of the equation development for monolithic motors. Of course, the extensions required to consider the slots between the segments are documented in this report. The duplication between Ref. 1 and this report has been kept to a minimum. Furthermore, the Ref. 1 nomenclature has been retained.

2.4 Basic Assumptions

The following basic assumptions are used in the p(x,t) model:

(a) All chemical reactions occur on the propellant surface in a combustion zone which is so thin that it can be considered as a plane. The combustion products enter the main stream in the port with zero axial momentum.

(b) The flow in the main chamber port is one-dimensional. This assumption is a good approximation to the real situation in view of the highly turbulent flows encountered in HVT motors. Changes of flow properties across the boundary layer are considered in the expressions for heat transfer and friction coefficients used in the analysis. It is further assumed that the slots are designed so that their interactions do not affect the one-dimensionality of the flow.

(c) Rate processes at the propellant surface are quasi-steady in the sense that their characteristic times are short compared to that of the pressure transient.

(d) The propellant combustion products and the pyrogen igniter gas have the same values of c_p, W, and γ.

(e) The gases flowing in the port obey the perfect gas law.

2.5 Governing Equations

The mathematical formulations of the approach to the above described problem consist of the following:

(a) Mass, momentum, and energy conservation equations in unsteady, quasi-one-dimensional form for the gas phase;

(b) Equation of state for the gas flowing in the motor;

(c) Proper initial conditions at the start of the transient (onset of igniter flow);

(d) Two boundary conditions at the fore-end of the propellant section, obtained from a pair of ordinary differential equations, which describe the rate of change of pressure and temperature in the entrance section;

(e) A third boundary condition, which describes the gas velocity at the entrance to the motor nozzle, for either choked or unchoked flow;

(f) Semi-empirical correlations for the convective heat-transfer and friction coefficients for the highly-turbulent flow in the port;

(g) Burning rate law for the solid propellant, including the effects of initial temperature, pressure, and velocity over the surface (erosive burning). (The burning rate equations are in subroutine form so that they can be easily modified.)

(h) A solid phase heat-up equation for determination of the propellant surface temperature during the induction interval coupled to an ignition criterion for the propellant; and

(i) Thrust calculations based on nozzle-end stagnation pressure.

First, the conservation equations along a section of the port that does not contain slots will be summarized. For a more detailed development, the reader is referred to Ref. 1. The mass conservation equation for the control volume in Fig. 2-3, written for a unit volume, is

$$\frac{\partial \rho}{\partial t} + \frac{\partial (\rho u)}{\partial x} + \frac{\rho u}{A_p}\frac{\partial A_p}{\partial x} = \frac{rb}{A_p}(\rho_{pr} - \rho) \quad (2\text{-}1)$$

RATE OF INCREASE OF MASS	SPATIAL INCREASE OF MASS FLOW RATE	INCREASE OF MASS FLOW RATE DUE TO INCREASE OF PORT AREA	RATE OF MASS ADDITION DUE TO BURNING

The momentum conservation equation is

$$\frac{\partial (\rho u)}{\partial t} + \frac{\partial (\rho u^2)}{\partial x} + \frac{\rho u^2}{A_p}\frac{\partial A_p}{\partial x} =$$

RATE OF INCREASE OF MOMENTUM	SPATIAL INCREASE OF MOMENTUM FLUX	CHANGE OF MOMENTUM FLUX DUE TO INCREASE OF PORT AREA

$$-\frac{\partial p}{\partial x} + \frac{4}{3}\mu\left[\frac{\partial^2 u}{\partial x^2} + \frac{1}{A_p}\frac{\partial A_p}{\partial x}\frac{\partial u}{\partial x}\right] - \frac{f\rho u^2 p_w}{2A_p} \quad (2\text{-}2)$$

PRESSURE GRADIENT FORCE	VISCOUS FORCE DUE TO NORMAL STRESS	FRICTION FORCE ACTING ON FLUID BY THE DUCT

The energy conservation equation, written in terms of the total stored (internal and kinetic) energy per unit mass, E, is

$$\frac{\partial}{\partial t}\left(\rho A_p E\right) + \frac{\partial}{\partial x}\left(\rho A_p u E\right) =$$

RATE OF ACCUMULATION OF STORED TOTAL ENERGY	RATE OF SPATIAL INCREASE OF STORED TOTAL ENERGY

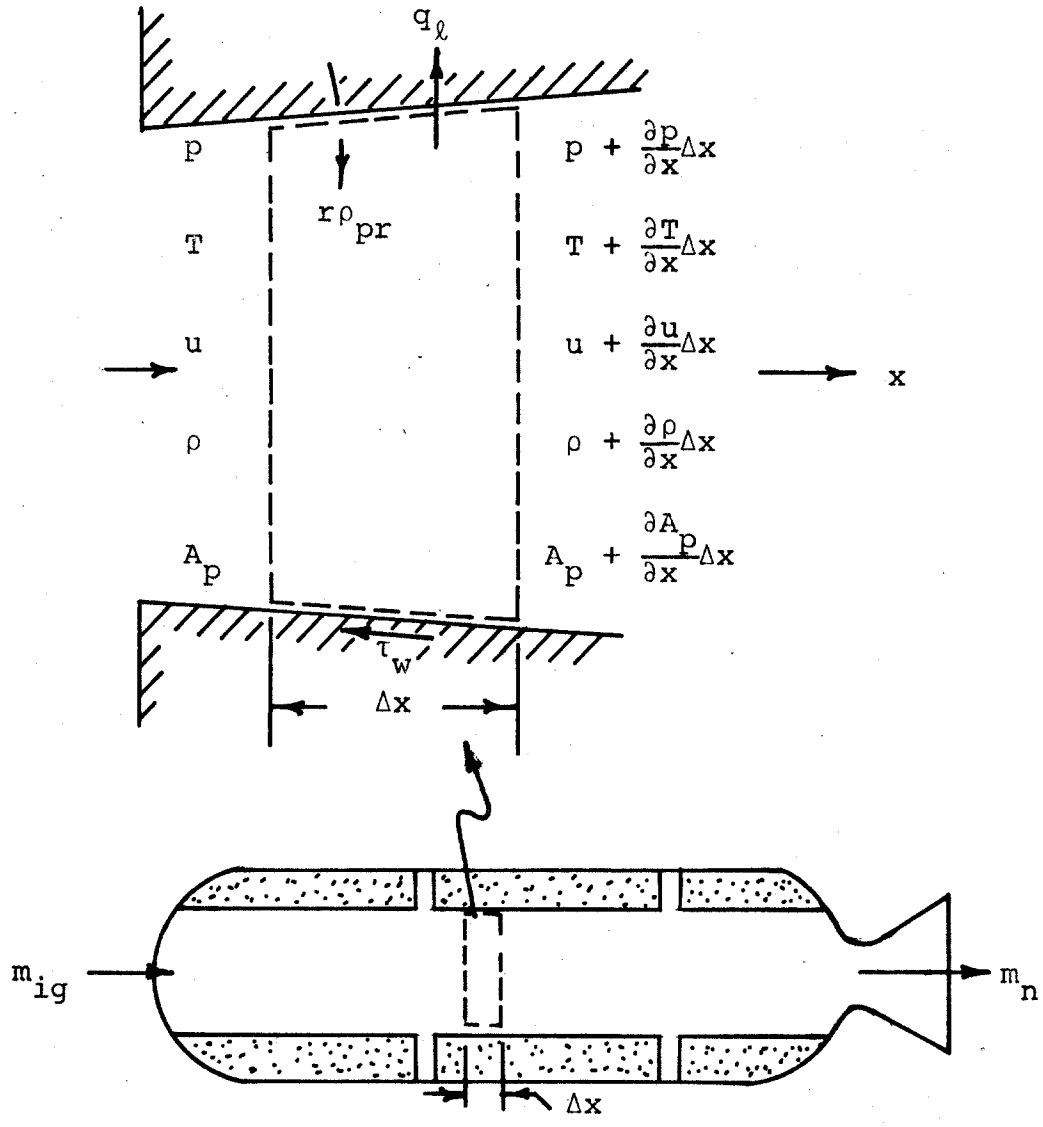

Fig. 2-3 Control volume used to consider transient flow field in chamber region of motor that does not contain a slot.

$$\frac{\partial}{\partial x}\left[A_p \lambda_g \frac{\partial T}{\partial x}\right] - \frac{\partial}{\partial x}\left(puA_p\right)\frac{1}{J_c} + \frac{\partial}{\partial x}\left[\frac{4}{3}\mu A_p \frac{\partial u}{\partial x}\right]\frac{1}{J_c} +$$

NET RATE OF ENERGY INPUT BY HEAT CONDUCTION

RATE OF WORK DONE ON THE FLUID BY PRESSURE FORCES

RATE OF WORK DONE ON THE FLUID BY VISCOUS FORCES

$$\rho_{pr} r h_f p_w - q_\ell p_w \qquad (2\text{-}3)$$

RATE OF ENTHALPY ADDED BY BURNING OF SOLID PROPELLANT

RATE OF HEAT LOST TO THE SURROUNDINGS

The above conservation equations constitute a set of inhomogeneous, nonlinear, partial differential equations (PDE). After nondimensionalization and an order of magnitude analysis, the effects of the following terms were neglected (indicated in Eqs. 2-2 and 2-3): (a) forces between gas molecules due to the viscous stress in the axial direction, created by the axial velocity gradient; (b) viscous dissipation and rate of work done by the internal viscous forces, and (c) axial heat conduction between gas molecules. The wall friction at a station in the propellant section is neglected after ignition occurs and appreciable blowing starts.

The present formulation is more general than the Ref. 1 formulation since it accounts for the rate of mass accumulation in the free volume created by the propellant surface regression.

2.6 Provisions for Circumferential Slots in Segmented Motors

As shown in Fig. 2-1, segmented motors consist of a series of sections which when joined together form circumferential slots which contain an appreciable volume and burning surface area. The interactions produced by the slots are accounted for by solving a set of ordinary differential equations for each slot and using those solutions as boundary conditions for the main stream flow equations.

Two flow interaction conditions between the main chamber and the slots are considered: (1) when the pressure gradient between the main chamber and slot is significant (such as during the passage of the first strong pressure wave), and (2) when the pressures in chamber and slot are nearly equal. In principle, the first condition could be used throughout the ignition transient but to do so greatly increases the computer time without increasing the accuracy of the solution.

2.6.1 Pressure Differential Between Main Chamber and Slot is Significant

Whenever the pressure differential between the main chamber and the slots is significant, the coupling of the fluid flow processes between the several circumferential slots and the main chamber is accounted for by simultaneously solving the continuity, energy and momentum equations for flow into (or out of) each slot and coupling the result with the complete PDE solution for the main chamber flow.

In Fig. 2-4, the control volume of the slot is shown interacting with the main stream flow. The flow in (or out of) the slot is described by the following equations.

When the main chamber pressure is greater than the slot pressure, the flow into the slot is

$$m_{in} = C_D b w_{slot} \rho_{ch} \left\{ 2 g J c_p T_{ch} \left[\left(p_{slot}/p_{ch} \right)^{2/\gamma} - \left(p_{slot}/p_{ch} \right)^{(\gamma+1)/\gamma} \right] \right\}^{1/2} \qquad (2\text{-}4)$$

and $m_{out} = 0$

Conversely, as the slot begins to generate mass and the pressure in the slot exceeds the pressure in the main chamber, flow is out of the slot,

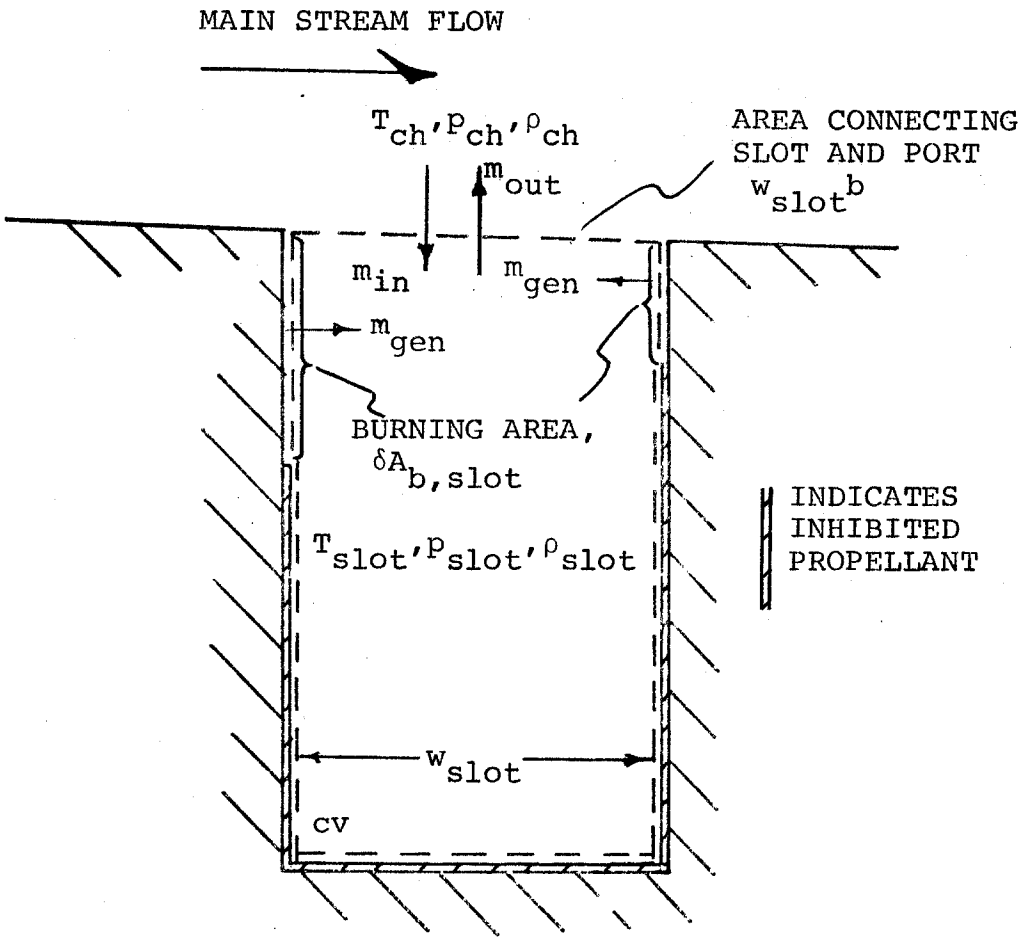

Fig. 2-4 Longitudinal section through slot showing nomenclature used in analysis of slot.

$$m_{out} = C_D b w_{slot} \rho_{slot} \left\{ 2gJc_p T_{slot} \left[\left(p_{ch}/p_{slot} \right)^{2/\gamma} - \left(p_{ch}/p_{slot} \right)^{(\gamma+1)/\gamma} \right] \right\}^{1/2} \quad (2\text{-}5)$$

and $m_{in} = 0$

After ignition, the mass generated in the slot is

$$m_{gen} = r_b \rho_{pr} A_{b,slot} \quad (2\text{-}6)$$

The rate of increase of slot volume is

$$dV_{slot}/dt = r(A_{b,slot} - w_{slot} b) \quad (2\text{-}7)$$

The rate of mass increase in the slot is

$$d(V_{slot}\rho_{slot})/dt = -m_{out} + m_{in} + m_{gen} \quad (2\text{-}8)$$

where either m_{in} or m_{out} is zero.

In terms of the sign convention for the main chamber equation

$$m_{slot} = m_{out} - m_{in} \quad (2\text{-}9)$$

The pressurization rate of the gases in the slot is

$$dp_{slot}/dt = - \frac{Jc_p [m_{out} T_{slot} - m_{in} T_{ch} - m_{gen} T_f + p_{slot} (d(V)_{slot}/dt)/R]}{V_{slot}(1 - c_p J/R)} \quad (2\text{-}10)$$

Gas temperature in the slot is calculated from the perfect gas law.

2.6.2 Pressures in Slot and Chamber Nearly Equal

After the pressures in the main chamber and slot become nearly equal, the coupling of the fluid flow processes between the slot and main chamber is accounted for by simultaneously solving the energy and continuity equations for the flow into or out of each slot.

Combining the energy and continuity equations yields an expression for the rate of temperature change of the slot,

$$\frac{dT_{slot}}{dt} = \left(\frac{RT}{Vp}\right)_{slot}\left[m_{gen}\left(\gamma T_f - T_{slot}\right) + m_{in}\left(\gamma T_{ch} - T_{slot}\right) - m_{out}(\gamma-1)T_{slot} - (\gamma-1)\rho_{slot}T_{slot}\frac{dV_{slot}}{dt}\right] \tag{2-11}$$

Differentiating the equation of state produces an expression for rate of mass increase in the slot

$$\frac{d(\rho V)_{slot}}{dt} = -\left(\frac{pV}{RT^2}\right)_{slot}\frac{dT_{slot}}{dt} + \left(\frac{V}{RT}\right)_{slot}\frac{dp}{dt} + \left(\frac{p}{RT}\right)_{slot}\frac{dV}{dt} \tag{2-12}$$

In terms of the sign convention for the main chamber equations

$$m_{slot} = -\frac{d(\rho V)_{slot}}{dt} + m_{gen} \tag{2-13}$$

When $m_{slot} > 0$, net flow into main stream.

When $m_{slot} \leq 0$, net flow out of main stream.

The above set of equations which specify p, ρV, V, and T for a slot were solved using a fourth order Runge-Kutta Method at each Δt.

2.7 Coupling Slot Flow to Main Chamber Flow

The elements considered in the main chamber continuity, momentum, and energy equations are illustrated in Figs. 2-5a, 2-5b, and 2-5c respectively. An order of magnitude analysis revealed that for pressures and accelerations being considered, viscous normal stresses and axial heat conduction in the gas produced relatively small effects and could be neglected with no loss in accuracy. The derivation of the

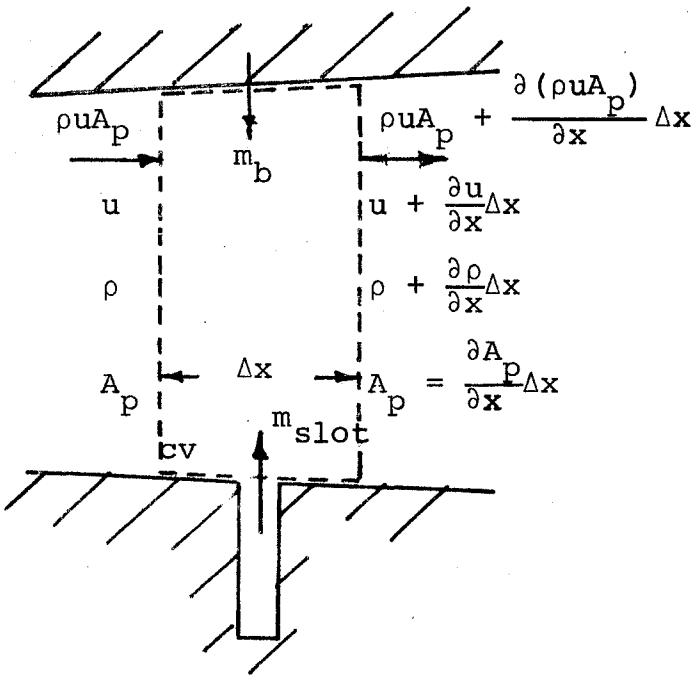

Fig. 2-5a Elements considered by continuity equation.

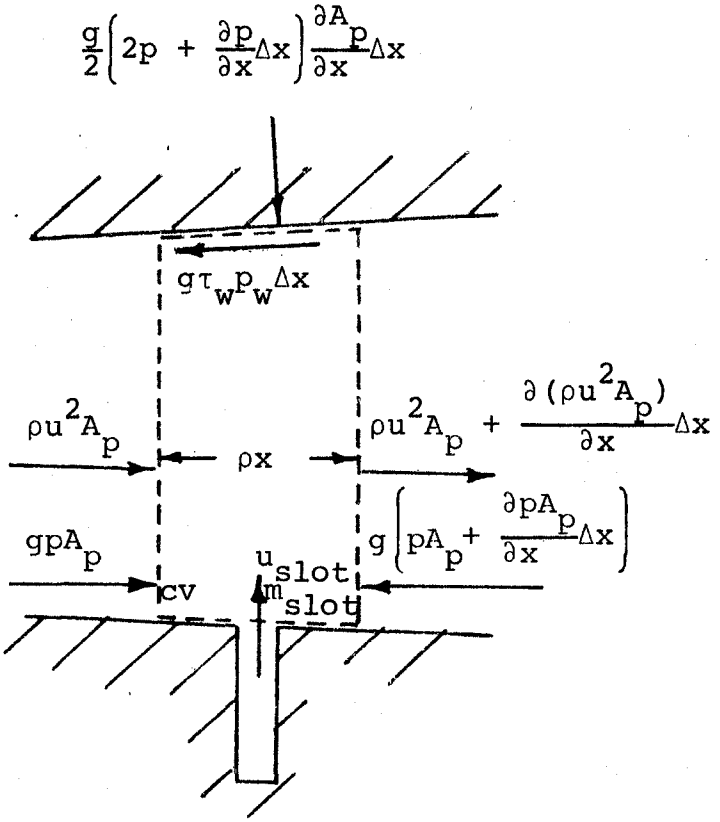

Fig. 2-5b Elements considered in momentum equation.

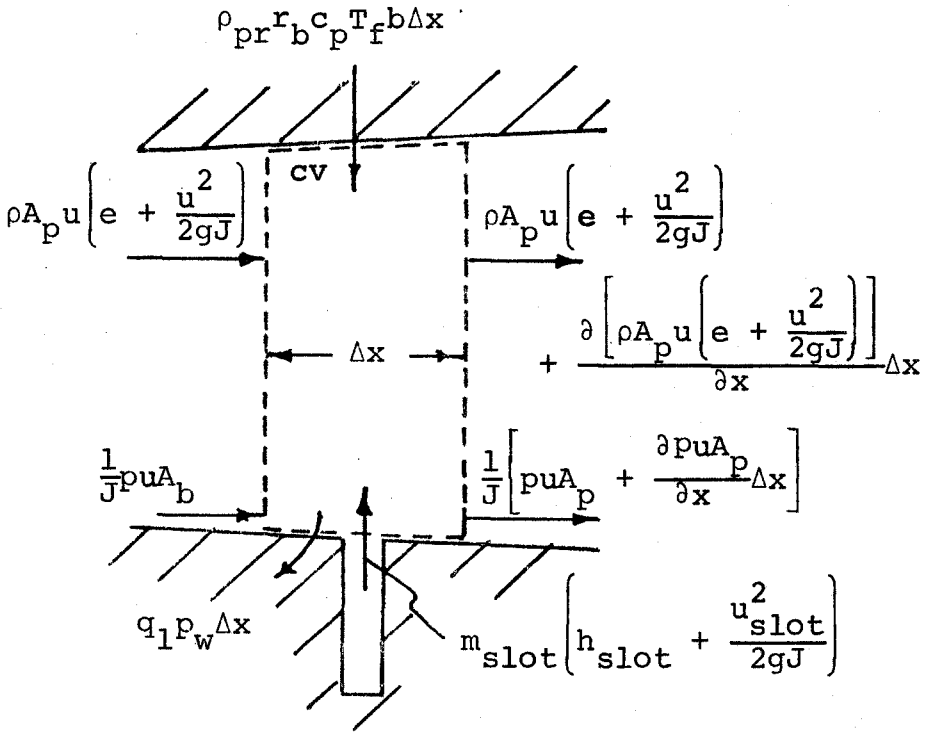

Fig. 2-5c Elements considered in energy equation.

interaction of the slot flow with the main chamber flow yields the following governing equations for those increments which contain slots.

$$\frac{\partial u}{\partial t} + u\frac{\partial u}{\partial x} + g\frac{RT}{p}\frac{\partial p}{\partial x} = \frac{-\rho_{pr} r_b b}{A_p}\frac{RTu}{p} - \frac{m_{sldv} RTu}{p} - \frac{f p_w u^2}{2A_p} \quad (2\text{-}14)$$

$$\frac{\partial T}{\partial t} + u\frac{\partial T}{\partial x} + (\gamma-1)T\frac{\partial u}{\partial x} = -\frac{(\gamma-1)uT}{A_p}\frac{\partial A_p}{\partial x} + \gamma\rho_{pr}R\frac{r_b b}{A_p}\frac{T}{p}\left[T_f - \frac{T}{\gamma} + \frac{u^2}{2gJc_p}\right]$$

$$+ (\gamma - 1)\frac{JTm_{sldv}}{p}\left[h_{slot} + \frac{u_{slot}^2}{2gJ} - \frac{RT}{(\gamma-1)J}\right]$$

$$- (\gamma - 1)\frac{p_w T}{A_p p}\left[Jq_\ell - \frac{f\rho u^3}{2gRT}\right] \quad (2\text{-}15)$$

$$\frac{\partial p}{\partial t} + u\frac{\partial p}{\partial x} + \gamma p\frac{\partial u}{\partial x} = -\frac{\gamma p u}{A_p}\frac{\partial A_p}{\partial x} + (\gamma - 1)\frac{\rho_{pr} r_b b}{A_p}\left[c_p J\left(T_f - \frac{T\rho}{\gamma\rho_{pr}}\right) + \frac{u^2}{2g}\right]$$

$$+ (\gamma - 1)J\, m_{sldv}\left[h_{slot} + \frac{u_{slot}^2}{2gJ}\right] - (\gamma-1)\frac{p_w}{A_p}\left[Jq_\ell - \frac{f\rho u^3}{2gRT}\right] \quad (2\text{-}16)$$

where m_{sldv} is mass flux from slot per unit volume of increment containing slot, e.g., $m_{slot}/\bar{A}_p\Delta x$.

Equations (2-14), (2-15), and (2-16) for the segmented configuration are the counterparts of Eqs. (4), (5), and (6) respectively in Ref. 1 for monolithic configurations. The primary difference in the two sets of equations is the addition of inhomogeneous terms to each equation when slots are considered.

2.8 Empirical Correlations for the Heat-Transfer and Friction Coefficients

The expression for the local convective heat-transfer coefficient h_c is deduced from the conventional Dittus-Boelter correlation for turbulent flow in pipes. Entrance effects, observed by many investigators (e.g., Refs. 9-13) are accounted for by including a power function of the length and diameter.[1,12] Variation of the gas physical properties across the boundary layer is considered by evaluating the properties at an average film temperature T_{af}. The expression for h_c used in this study, is

$$h_c = 1.56 \times 10^{-3} Pr^{-0.6} c_p \left(\frac{pu}{R}\right)^{0.8} W^{0.1} T_{af}^{-0.67} \left(x_{seg} d_h\right)^{-0.1} \tag{2-17}$$

where x_{seg} is the effective distance from the leading edge of the segment being considered. To avoid complications that arise when unrealistically small values of characteristic length are used in convective heating relationships, the minimum value of x_{seg} is considered to be one-half of a distance increment, Δx, as used in the numerical solution. After ignition, convective heating to the propellant surface is terminated. However, the calculation of h_c is continued for use in the erosive burning calculations.

The friction coefficient, f, is deduced from Colebrook's expression for turbulent flow in pipes with roughness. Observed[14] entrance effects and variation of fluid properties across the boundary layer are taken into account. The friction factor is expressed in the following form:

$$f = \frac{0.449 \left(d_h / x_{seg}\right)^{0.1}}{\left\{ \ln \left[\frac{\varepsilon_s / d_h}{3.7} + \frac{1.27 RW^{0.5} T_{af}^{1.65} \left(d_h / x_{seg}\right)^{0.05}}{10^6 p u d_h f^{0.5}} \right] \right\}^2} \tag{2-18}$$

2.9 Burning Rate Law

Two versions of the Lenoir-Robillard burning rate law[15,16] can be used to account for erosive burning. The first is the conventional form

$$r = r_0 + \alpha_e G^{0.8} d_h^{-0.2} \exp\left(- |\beta_e r \rho_{pr}/G| \right) \qquad (2\text{-}19)$$

where d_h is the hydraulic diameter, $4A_p/b$, at the point being considered. Equation (2-19) accounts for the convective effects by incorporating the important functional dependencies on free stream flow and geometry, i.e., $G^{0.8}/d_h^{0.2}$.

The second is a form which is particularly well suited for analyzing segmented motors.

$$r = r_0 + k_e h_c(d_H, x, L_{slot}, u, \ldots) \exp\left(- |\beta_e r \rho_{pr}/G| \right) \qquad (2\text{-}20)$$

where h_c is any convective heat transfer coefficient which accounts for the intricacies of the solid rocket geometry and flow field, in particular, those produced by the segments.

In principle, k_e and α_e can be estimated from theoretical considerations,[15] but in practice they are usually deduced from experimental data. Values of β_e are always determined from experimental correlations and generally are in the range between 75 and 200. In all cases, it is necessary that the k_e and β_e pairs and the α_e and β_e pairs be consistent.

2.10 Determination of the Propellant Surface Temperature

The heat equation for an unignited propellant grain at each of the series of axial locations (e.g., 20 to 29) is

$$\frac{\partial T_{pr}(t,y)}{\partial t} = \alpha_{pr} \frac{\partial^2 T_{pr}(t,y)}{\partial y^2} \qquad (2\text{-}21)$$

with the initial condition

$$T_{pr}(0,y) = T_{pi} \qquad (2\text{-}22)$$

and with the following boundary conditions:

$$T_{pr}(t,\infty) = T_{pi} \tag{2-23a}$$

$$\partial T_{pr}(t,0)/\partial y = -(h_c/\lambda_{pr})(T - T_{pr}) \tag{2-23b}$$

Equation (2-21) along with its boundary conditions is solved using Goodman's integral method.[17]

For purposes of this study, ignition of a particular section of the propellant surface is accomplished when a prescribed critical ignition temperature is attained. This simple ignition criterion is satisfactory whenever high convective heating rates assure rapid ignition. However, if ignition failures (i.e., hang fires and misfires) are to be studied, a more comprehensive ignition model may be required.

2.11 Head-end and Nozzle-end Boundary Conditions

The three physical boundary conditions are as follows: two boundary conditions at the entrance to the propellant section (denoted by x_p), and one boundary condition at the entrance to the motor nozzle (denoted by x_E).

The gas properties in the entrance section are assumed to be uniform. Heat-transfer and shock-pattern losses taking place at the exit of the igniter may lower the effective mean temperature of the igniter gas, T_{ig}. From the continuity and energy conservation equations for the entrance section, the rate of change of pressure and temperature at the entrance to the propellant section are derived:

$$\frac{dp_{es}}{dt} = \frac{1}{V_{es}}\left[\gamma R T_{ig} m_{ig}(t) - \gamma A_{p,es} p_{es}(t) u_{es}(t) - \frac{(\gamma - 1) A_{p,es} p_{es}(t) u_{es}(t)^3}{2gRT_{es}(t)}\right] \tag{2-24}$$

$$\frac{dT_{es}}{dt} = \frac{1}{V_{es}}\left\{\frac{RT_{es}(t)m_{ig}(t)}{p_{es}(t)}\left[\gamma T_{ig} - T_{es}(t)\right] - (\gamma - 1)A_{p,es}u_{es}(t)\left[T_{es}(t) + \frac{u_{es}(t)^2}{2gR}\right]\right\} \qquad (2\text{-}25)$$

The igniter mass flow rate m_{ig} is a prescribed function of time.

Equations (2-24) and (2-25) form a pair of coupled ordinary differential equations for the unknowns p_{es} and T_{es}. Their solution provides two boundary conditions for the governing Eqs. (2-14 to 2-16). The two initial conditions for this pair of equations are

$$p_{es}(0) = p_{es,i} \quad \text{and} \quad T_{es}(0) = T_{es,i} \qquad (2\text{-}26)$$

The boundary condition at the aft end of the motor chamber is derived assuming isentropic flow between the entrance to the motor nozzle and the nozzle exit. Using continuity and energy conservation relations between these two sections, the following equation applies:

$$u_E(t)^2 = \frac{2g\gamma}{\gamma-1}RT_E(t)\frac{1 - [p_{ex}(t)/p_E(t)]^{(\gamma-1)/\gamma}}{(A_p/A_{ex})^2[p_{ex}(t)/p_E(t)]^{-2/\gamma} - 1} \qquad (2\text{-}27)$$

When the motor nozzle is unchoked (the usual case during the induction intervals, when very low port-to-throat area ratios are used) the pressure at the nozzle exit, p_{ex} in Eq. (2-27), equals the ambient pressure. For the case of a choked motor nozzle Eq. (2-27) becomes the following implicit relation:

$$u_E(t)^2 = \frac{\gamma g R T_E(t)}{[A_p/A_t]^2}\left[\left(\frac{2}{\gamma+1}\right)\left(1 + \frac{\gamma-1}{2}\frac{u_E(t)^2}{\gamma g R T_E(t)}\right)\right]^{(\gamma+1)/(\gamma-1)}$$

3.0 NUMERICAL SOLUTION

This section extends the discussion of the numerical solution in Ref. 1 by describing the organization of the revised computer program and by describing the methods used to account for the slots. The overall numerical solution is summarized in this section. However, the reader is referred to Ref. 1 for a more general discussion of the specific numerical techniques which are used.

3.1 Provisions for Circumferential Slots in Segmented Motors

As shown in Fig. 3-1, segmented motors consist of a series of sections which when joined together form circumferential slots which contain an appreciable volume and burning surface area. The interactions between the main chamber flow and the slots are accounted for by coupling the equations for the main chamber with the ordinary differential equations for each slot. During the development of the numerical solution, certain conventions regarding geometry were adopted:

(1) Segmented motors are divided into equal axial distance increments (Δx) regardless of whether an individual increment includes a circumferential slot. Circumferential slots provide an additive volume (δV_{slot}) and an additive burning surface area ($\delta A_{b,slot}$) but do not alter the port area, i.e., the mainstream flow does not pass through the slot.

(2) Port area A_p is the part of the flow passage above the slot and $A_{p,t+\Delta t} = A_{p,t} + br\Delta t$ where b is the burning perimeter along the port.

(3) Burning surface area of an increment which includes a slot is $\Delta A_{b,slot} = b\Delta x + \delta A_{b,slot}$. Note that the value $\delta A_{b,slot}$ must be input as the burning area in the slot less bw_{slot}. The burning surface

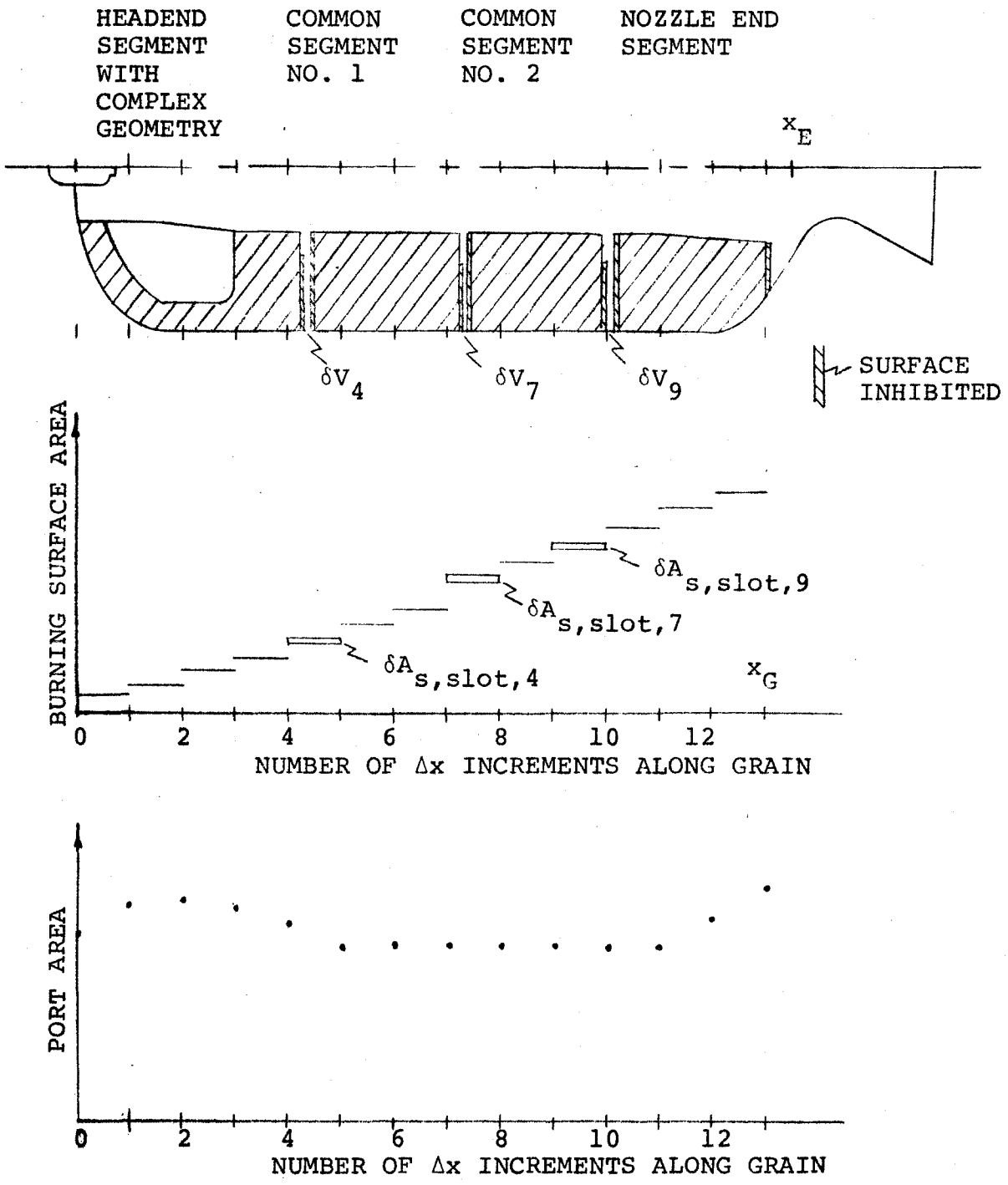

Fig. 3-1 Geometrical description of segmented rocket motor showing lumped parameter method of treating volumes and surface areas associated with slots.

in the slot may be quite small since the circumferential area in the slot may be partially inhibited to prevent burning. $\delta A_{b,slot}$ is considered to be constant during the ignition interval.

(4) The total volume of an increment which includes a slot is $\Delta V = A_p \Delta x + \delta V_{slot}$. However, only $A_p \Delta x$ is associated with the main stream. During each Δt, the volume of the slot increases by $r\Delta t(\delta A_{b,slot} - bw_{slot})$.

(5) The pre-ignition heat loss and friction are affected by the slots since the slots disturb the boundary layer and accumulate gases during pressurization.

(6) Ignition of the exposed propellant in the slots is controlled by the flame spreading along the main port. Since in the present SRB design the burning surface area in the slots is a small fraction of the total burning surface area, the burning surface area in a slot is assumed to ignite at the same time as the axial increment that contains it.

(7) The passage area into a slot is bw_{slot} and increases by $2r\Delta t$ during each time interval. The mass from the slots is injected normal-to-the-centerline.

The tabular inputs required to describe segmented rocket motor geometry are:

For both monolithic and segmented motors:

x	Distance from head end of motor, i.e., $x = 0$ at head end of motor.
A_p	Port area of main channel.
b	Perimeter of propellant surface in main channel.
p_w	Total perimeter of propellant and inert surface (i.e., wetted perimeter before ignition).

For segmented motors, when slot begins in interval from x to $x + \Delta x$:

x_{slot} Distance to the upstream edge of the slot from the head end of the motor, i.e., $x = 0$.

$A_{b,slot}$ Burning surface area in slot. (The lack of surface area along the main port because the slot width is accounted for in this input value, i.e., subtract bw_{slot} from the actual burning surface area in the slot.)

V_{slot} Volume (region of gas not in the flow field) of slot.

w_{slot} Width of slot

The geometry inputs x_p, x_E and x_G are the same for both monolithic and segmented motors. Figure 3-2 illustrates the conventions used in defining the geometry. Note that the head-end region between $x = 0$ and $x = x_p$ is a flow passage that does not contain propellant and that the last $\Delta x/2$ is a flow passage that does not contain propellant.

3.2 Implementation Scheme

Numerical mathematical techniques were implemented for the simultaneous integration of the three governing equations, [Eqs. (2-14), (2-15), and (2-16)], the equations for the entrance section [Eqs. (2-24) and (2-25)] and exit section [Eqs. (2-27) or (2-28)], and the equation describing rate of change of the propellant surface temperature, [Eq. (III-50) in Ref. 1]. The numerical steps were organized in modular form into a program for a large capacity digital computer.

The set of governing equations is totally hyperbolic in nature.[18,19] All three eigenvalues of its characteristic equation are distinct and real. A generalized implicit scheme based on central differences in spacewise derivatives[20,21] was chosen to solve numerically the governing equations. Let the net of points in the t-x plane be given by $t = j\Delta t$ and $x = n\Delta x$, where $j = 0,1,2...$, and $n = 0,1,2...$. The mesh size of the net is determined by Δt and Δx. Then the derivatives of pressure, for instance, are expressed in the following difference form:

FOR MONOLITHIC MOTORS -
FROM INPUT TABLES OF PORT AREA AND PROPELLANT PERIMETER VS DISTANCE PROGRAM INTERPOLATES FOR b AND A_p AT EACH STATION 1 THROUGH NDELX.

FOR SEGMENTED MOTORS -
PORT AREA, PERIMETERS ARE INPUT FOR EACH Δx.

$$x_E - x_G = \Delta x/2$$

$$\Delta x = \frac{x_E - x_p}{NDELX}$$

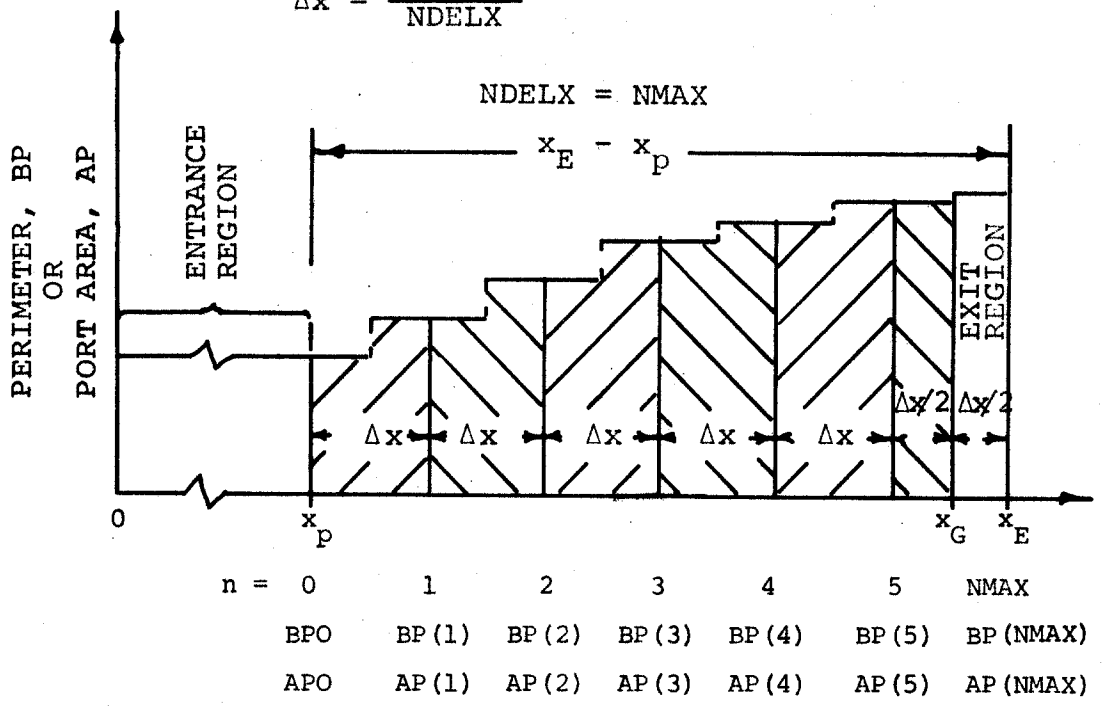

n =	0	1	2	3	4	5	NMAX
	BPO	BP(1)	BP(2)	BP(3)	BP(4)	BP(5)	BP(NMAX)
	APO	AP(1)	AP(2)	AP(3)	AP(4)	AP(5)	AP(NMAX)

PROPELLANT AREA:

$$A_b = \frac{\Delta x}{2}BPO + \sum_{1}^{NDELX-1} \Delta x BP(I) \approx \int_{x_p}^{x_G} b\,dx$$

CHAMBER VOLUME:

$$V = x_p APO + \frac{\Delta x}{2}APO + \sum_{1}^{NDELX-1} \Delta x AP(I) + \frac{\Delta x}{2}AP(NDELX) \approx \int_{0}^{x_E} A_p\,dx$$

Fig. 3-2 Accounting for surface area and volume.

$$\left.\begin{aligned} \left.\frac{\partial p}{\partial t}\right|_n &= \frac{p_n^{j+1} - p_n^j}{\Delta t} \\ \left.\frac{\partial p}{\partial x}\right|_n &= \frac{\theta\left(p_{n+1}^{j+1} - p_{n-1}^{j+1}\right) + (1-\theta)\left(p_{n+1}^{j} - p_{n-1}^{j}\right)}{2\Delta x} \end{aligned}\right\} \quad (3\text{-}1)$$

where $p_n^j = p(j\Delta t, n\Delta x)$.

The weighting parameter θ is a real constant, lying in the interval $0 \leqq \theta \leqq 1$. For the implicit formulation no stability restriction exists if $0.5 \leqq \theta \leqq 1$.[20] Usually a value of $\theta = 0.6$ was used in the calculations.

3.3 Quasi-linearization and Predictor-Corrector Calculations of the Non-linear Terms in the Governing Equations

The governing equations may be written in the following matrix form

$$\frac{\partial}{\partial t}\begin{pmatrix} u \\ T \\ p \end{pmatrix} + \begin{pmatrix} F_{u,u} & F_{u,T} & F_{u,p} \\ F_{T,u} & F_{T,T} & F_{T,p} \\ F_{p,u} & F_{p,T} & F_{p,p} \end{pmatrix} \frac{\partial}{\partial x}\begin{pmatrix} u \\ T \\ p \end{pmatrix} = \begin{pmatrix} I_u \\ I_T \\ I_p \end{pmatrix} \quad (3\text{-}2)$$

where $F[u(t,x),T(t,x),p(t,x)]$ are the functional coefficients of the partial spacewise derivatives, and $I[u(t,x),T(t,x),p(t,x)]$ are the corresponding inhomogeneous terms in Eqs. (2-14), (2-15), and (2-16). These latter terms account for the interactions with the slots.

To obtain a system of linear algebraic difference equations which can be solved simultaneously by matrix methods, the nonlinear coefficients $F(u,T,p)$ and inhomogeneous terms $I(u,T,p)$ are linearized in a way described in the following paragraphs.

The inhomogeneous terms were quasi-linearized as follows:[22]

$$I_n^{j+\theta} \approx I\left(u_n^j, T_n^j, u_n^j\right) + \theta\left(u_n^{j+1} - u_n^j\right)\frac{\partial I}{\partial u}\bigg|_n^{j+\frac{\theta}{2}}$$

$$+ \theta\left(T_n^{j+1} - T_n^j\right)\frac{\partial I}{\partial T}\bigg|_n^{j+\frac{\theta}{2}} + \theta\left(p_n^{j+1} - p_n^j\right)\frac{\partial I}{\partial p}\bigg|_n^{j+\frac{\theta}{2}} \quad (3\text{-}3)$$

where the partial derivatives, which are actually algebraic terms, are evaluated with the flow properties at $(j + \theta/2, n)$, such as, for instance, $p_n^{j+\theta/2} = p_n^j + \theta\left(p_n^{j+1} - p_n^j\right)/2$.

A predictor-corrector technique was applied to the non-linear coefficients $F(u,T,p)$ and the partial derivatives in Eq. (3-3). According to this method, a predictor calculation is first made, in which previous-time flow properties are used to evaluate all the coefficients F and partial derivatives in the quasi-linearized inhomogeneous terms. Then, a corrector calculation is made in which the coefficients F and the partial derivatives are evaluated with weight-averaged flow properties. The iterations may continue until sufficient covergence is achieved.

After substitution of the aforementioned finite-difference representations into the governing equations, the velocity variation equation, Eq. (2-14), becomes

$$\frac{u_n^{j+1} - u_n^j}{\Delta t} + \bar{u}_n^j\left[\frac{\theta\left(u_{n+1}^{j+1} - u_{n-1}^{j+1}\right) + (1-\theta)\left(u_{n+1}^j - u_{n-1}^j\right)}{2\Delta x}\right]$$

$$+ gR\frac{\bar{T}_n^j}{\bar{p}_n^j}\left[\frac{\theta\left(p_{n+1}^{j+1} - p_{n-1}^{j+1}\right) + (1-\theta)\left(p_{n+1}^j - p_{n-1}^j\right)}{2\Delta x}\right] =$$

$$I_u\left(u_n^j, T_n^j, p_n^j\right) + \theta\left(u_n^{j+1} - u_n^j\right)\frac{\partial I_u}{\partial u}\bigg|_n^{j+\frac{\theta}{2}}$$

$$+ \theta\left(T_n^{j+1} - T_n^j\right)\frac{\partial I_u}{\partial T}\bigg|_n^{j+\frac{\theta}{2}} + \theta\left(p_n^{j+1} - p_n^j\right)\frac{\partial I_u}{\partial p}\bigg|_n^{j+\frac{\theta}{2}} \quad (3\text{-}4)$$

The temperature and pressure variation equations, Eqs. (2-15) and (2-16) are treated in an analogous manner.

The barred parameters are weight-averaged quantities as follows, e.g.,

$$\bar{u}_n^j = \theta\left(u_n^{j+1}\right)_{pd} + (1 - \theta)u_n^j \tag{3-5}$$

whereas the flow parameters in the partial derivative form in Eq. (3-4) are

$$u_n^{j+\frac{\theta}{2}} = \frac{\theta}{2}\left(u_n^{j+1}\right)_{pd} + \left(1 - \frac{\theta}{2}\right)u_n^j \tag{3-6}$$

The parameters $\left(u_n^{j+1}\right)_{pd}$ are the quantities calculated from the latest predictor iteration. In the first step predictor calculation they have the values of the previous time step.

Negligibly small differences were found between final solutions obtained by single-step and multi-step predictor calculations. Therefore, to reduce computing time, single-step predictor-corrector calculations are used in the actual computations. The final solution at every time step is obtained implicitly by a matrix method discussed in Section 3.6.

3.4 Extraneous Boundary Conditions

The use of central-difference formulation, as described in Eq. (3-1), for all spacewise derivatives in the governing equations, requires six boundary conditions for the solution. In other words, the set of finite-difference equations corresponds to a hyperbolic system of 6th order.[19] Therefore, three boundary conditions, in addition to the physical ones [defined by Eqs. (2-24), (2-25), and (2-27) or (2-28)] are needed. These so-called extraneous boundary conditions for the hyperbolic system of governing equations studied are derived from the compatibility relations at the boundaries. The latter are obtained by solving the governing equations by the method of characteristics.[23]

The compatibility relations along the right-running and left-running Mach lines (defined by $dx/dt = u \pm c$, respectively), in terms of p-u characteristics, are

$$\left(\frac{dp}{dt}\right)_{I,II} = \mp \frac{\gamma p}{c}\left(\frac{du}{dt}\right)_{I,II} \pm \left(I_p + \frac{\gamma p}{c} I_u\right) \qquad (3\text{-}7)$$

The relation along the particle-path line (defined by $dx/dt = u$), in terms of T-p characteristics, is

$$\left(\frac{dT}{dt}\right)_{III} = \frac{\gamma-1}{\gamma}\frac{T}{p}\left(\frac{dp}{dt}\right)_{III} + \left(I_T - \frac{\gamma-1}{\gamma}\frac{T}{p} I_p\right) \qquad (3\text{-}8)$$

In relations (3-7) and (3-8), I_u, I_T, and I_p are the inhomogeneous terms in the governing equations [see Eq. (3-2)].

For a subsonic flow toward the nozzle in the motor which is the case during most of the transient in the physical model, described in Section 2, the left-running characteristic line is considered at the left boundary, whereas the right-running characteristic line together with the particle-path line are considered at the right boundary of the region of numerical computation. Taking into account the conditions at the right boundary, which is the aft-end of the motor (uniform perimeter, no area change, and no mass addition), the compatibility relation along the right-running characteristic is the same as given in Ref. 1 as Eq.(IV-12). The compatibility relation along the left-running characteristic is the same as Eq. (IV-13) in Ref. 1. The compatibility relation along the particle-path line, at the right boundary, is the same as Eq. (IV-14) in Ref. 1.

3.5 Treatment of the boundary Conditions

The compatibility relation along the left-running characteristic line, Eqs. (2-24) and (2-25), form a closed system of ordinary differential equations to determine the gas velocity, temperature, and pressure at the entrance to the propellant section. The system, formed by

the other two compatibility relations, Eqs. (2-27) or (2-28), (unchoked or choked flow, respectively) determines the flow parameters at the chamber aft-end. The equations in each system are expressed in a finite-difference form and quasi-linearized in an implicit form, using a predictor-corrector iteration calculation in the same manner which is utilized for the governing equations. As a result, a set of three linear inhomogeneous algebraic equations is obtained for every boundary. Each set of equations is solved by 3 × 3 matrix, using Kramer's rule, to yield the gas velocity, temperature, and pressure at the boundary for the next time step calculations. The characteristic line segments near the left and right boundary of the calculated domain are shown in Figs. 3-3 and 3-4, respectively. These figures also show the numerical calculation grid in an x,t-diagram.

In Fig. 3-3, the line sent out from A_2^j to the left-boundary point $B_\ell(x_0,t^{j+1})$ with a slope $(dx/dt)_{II} = u - c$ is the left-running characteristic. The process of determination of the boundary values is carried out in the following steps:

(1) With the calculation completed for the time step $j\Delta t$, all properties are determined at the point $\bar{A}_2^j$ by linear interpolation between the boundary (x_1,t^j). The position of $\bar{A}_2^j$ is taken from the previous-time-step calculations, as described below.

(2) The left-boundary system of equations [Eqs. (2-24), (2-25), and (IV-13) in Ref. 1] is solved for u, T, and p at $B_\ell(x_0,t^{j+1})$. The flow parameters, present in the coefficients and inhomogeneous terms of these equations, are iterated with the solutions until sufficient convergence is reached.

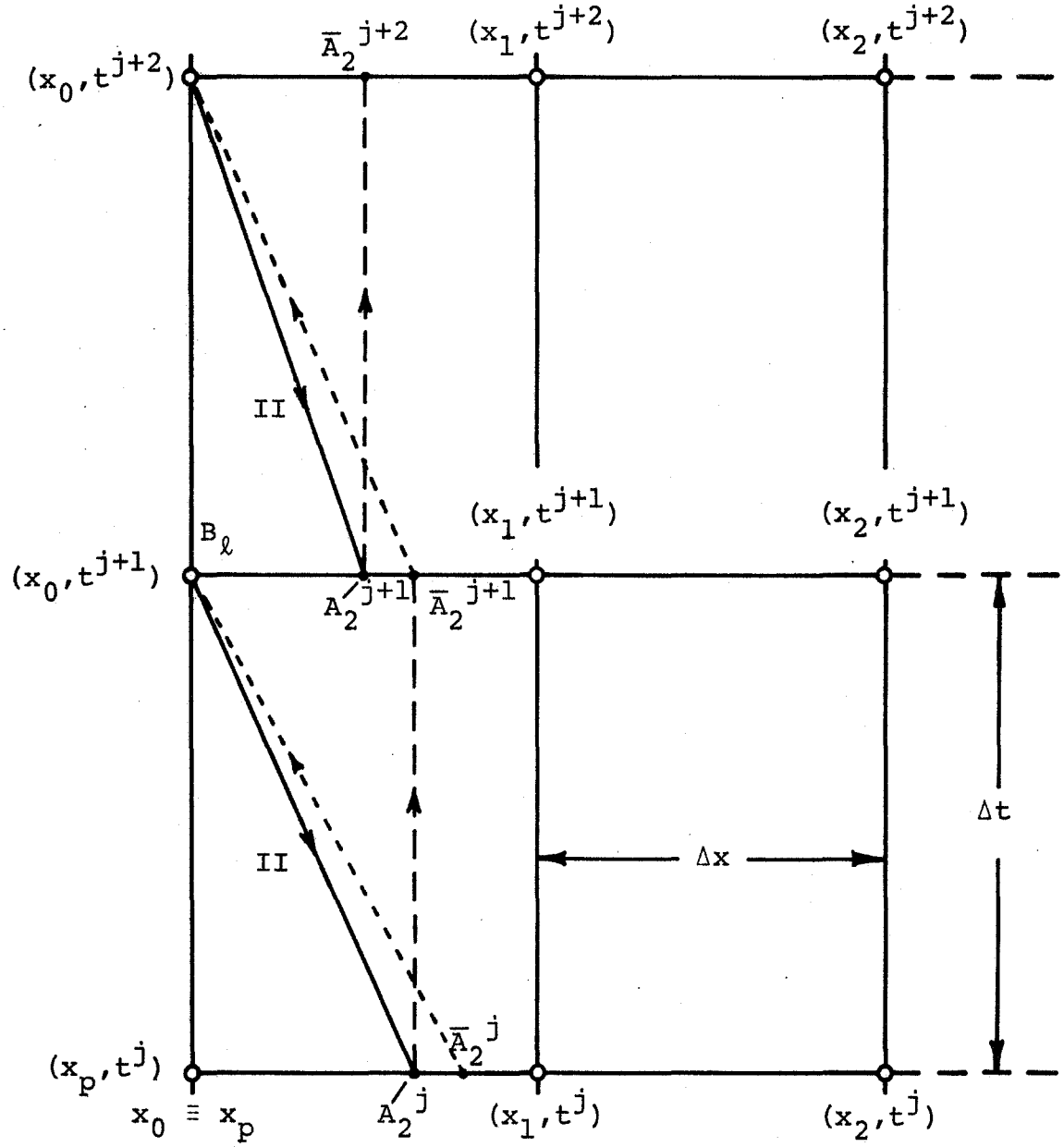

Fig. 3-3 Numerical calculation grid and characteristic directions at the left boundary of the calculated domain.

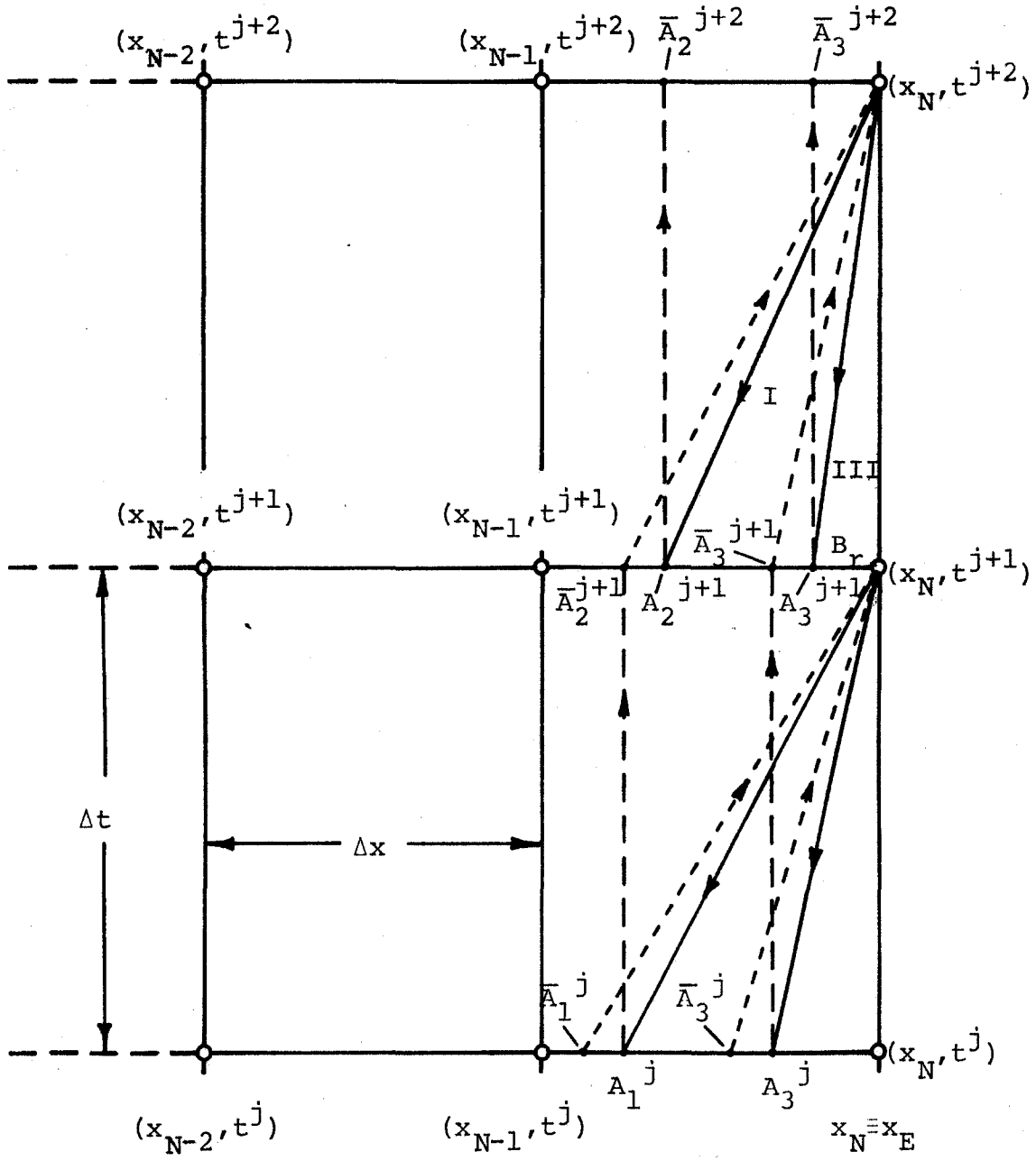

Fig. 3-4 Numerical calculation grid and characteristic directions at the right boundary of the calculated domain.

(3) The corrected location of A_2^j at the current time is found from the slope of the left-running characteristic (solid line $A_2^j - B_\ell$ in Fig. 3-3), i.e.,

$$x_{A_2}^j = x_0 - \frac{\Delta t}{2}\left[\left(u_{x_0}^{j+1} + u_{\bar{A}_2}^j\right) - \left(c_{x_0}^{j+1} + c_{\bar{A}_2}^j\right)\right] \quad (3\text{-}9)$$

If $|x_{A_2} - x_{\bar{A}_2}|/x_{\bar{A}_2} > 0.002$, steps (1), (2), and (3) are repeated with $(x_{\bar{A}_2})_{i+1} = 0.8\, x_{A_2} + 0.2(x_{\bar{A}_2})_i$, where the subscript "i" denotes the number of the iteration step.

When the convergence condition for the point A_2^j is met (usually in two iterations), the distance x of this point becomes the distance for the first iteration in the next time step, i.e., $x_{\bar{A}_2}^{j+1} = x_{A_2}^j$ (dotted vertical line in Fig. 3-3).

In Fig. 3-4, the lines sent out from A_1^j and A_3^j to the right-boundary point $B_r(x_N, t^{j+1})$ are the right-running characteristic and particle path, respectively. The calculation of the right-boundary values by the simultaneous solution of the above-mentioned pertinent system of equations is similar to that of the left-boundary values.

The positions of the points A_1, A_2, and A_3 change very slowly with respect to time. The directions of exaggerated shifts shown in Figs. 3-3 and 3-4 are typical for the chamber-filling interval of the transient.

It should be noted that some solutions, based on separate integrations along the characteristic lines,[19] can result in oscillations of the boundary values. The quasi-linearized simultaneous-solution method results in a smooth and stable solution. The method may be applied, however, with caution to other configurations which cause different boundary conditions, such as zero aft-end velocity during part of the transient due to use of a nozzle closure, and change of velocity direction at the fore-end due to short igniter operation.

3.6 Computation Efficiency and Convergence Tests

The numerical calculation solves Eq. (3-4) along with the analogous equations for T and p, which represent the governing equations in their implicit difference algorithm. For the N-1 spacewise interior points considered, $3(N-1)$ linear algebraic equations have to be solved simultaneously for every time step for $3(N-1)$ unknowns. The value of $N-1$ depends upon the given lengths of the propellant and aft sections, $x_E - x_p$, and the spatial mesh size, Δx, used in the calculation. The faster the pressurization process, the smaller the value of Δx that must be used, and therefore, the larger the number of interior calculation points. Also, the time step, or temporal mesh size, Δt, should be kept small enough, so that the variations in flow properties with respect to time can be studied, and the quasi-linearized nonlinear and inhomogeneous terms can be properly represented.

For efficient computation, the finite-difference equations are arranged into so-called block-tridiagonal matrix form.[24] In this particular form, the $3(N-1) \times 3(N-1)$ matrix of the coefficients of the unknowns has $(3N-5)$ 3×3 square sub-matrices as single elements. An economical solution is obtained through block-factorization into two block-bidiagonal matrices.[24] For accurate computation, the computer option of double precision is used in the matrix calculation.

Variation of the mesh sizes, Δt and Δx, was carried out to test the convergence of the solution. This variation was conducted in connection with the so-called Courant-Friedrichs-Lewy stability condition for one-step space difference equations,[20] which is

$$(|u| + c)\Delta t/\Delta x \leq 1 \qquad (3\text{-}10)$$

However, when an implicit difference scheme is used, the numerical solution should be unconditionally stable.*[20] Once a stable and uniform solution is obtained, further reduction in Δt does not significantly alter the calculated

*In practice, during the initial phases of pressurization, the stability conditions for the entrance region and the slots require a smaller Δt than that which satisfies Eq. (3-10).

results. Mesh sizes, for which the maximum value of $(|u| + c)\Delta t/\Delta x$ is slightly greater than one, can often be used. However, during the initial portion of the solution much smaller values of Δt are necessary.

Various tests were performed on the sensitivity of the solution to changes in initial conditions and small changes in important input parameters, such as the igniter mass flow rate, burning rate law, propellant ignition temperature, adiabatic flame temperature, and propellant density. In all these tests the solutions were bounded and smooth, and changed only slightly for small changes in these parameters. This demonstrates the existence of neighboring solutions and the convergence of the entire numerical solution.

3.7 Organization of Computer Program

The program, consisting of over 3000 Fortran Statements, is organized into a number of modules (i.e., subroutines) which are called from MAIN as indicated in Table 3-1. A brief description of each subroutine is given in Table 3-2. The program is written in a reasonably general form so as to reduce the need for user initiated modifications. However, those subroutines which control the input (i.e., SDATAC) and the output (i.e., ANS, SRNBUG, THRUS1, PNCH) are largely self-explanatory and can be readily interpreted by the user. Similarly, those subroutines which calculate the interface conditions (i.e., MIGDOT, HCCAL, FCCAL, TSCAL and BRCAL) correspond closely to the descriptions given in Section 2 and are relatively uncomplicated. Three of the subroutines (i.e., TRID, LAGIN and RUNGE) are standard packages for performing standard numerical operations. The heart of the numerical solution consists of subroutines (i.e., PREPP, SOLUTP, PREPC, SOLUTC, INHOMO) coupled to the left boundary (LBC) and to the right boundary (RBC). These subroutines should be of little interest to the general user and are the domains of persistent numerical analysts. The subroutines (i.e., SLOTK, FCT, and FCT2) follow the discussion in Section 2 very closely.

Table 3-1

FLOW CHART FOR COMPUTER PROGRAM*

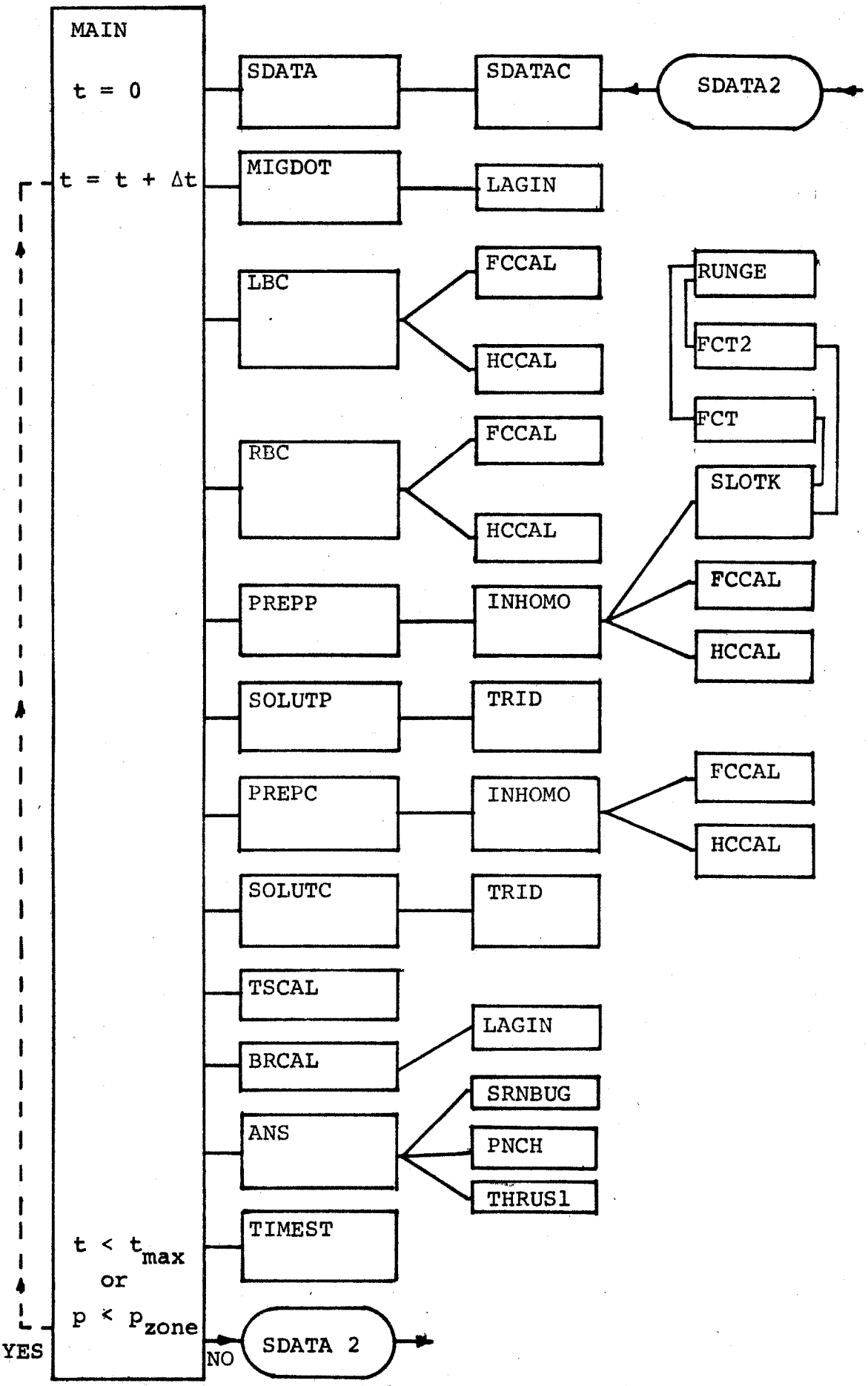

*Subroutines defined in Table 3-2.

Table 3-2

ORGANIZATION OF SUBROUTINES USED IN PROGRAM

As indicated in Table 3-1, main subroutines are called from MAIN, which is the executive portion of the program. The functions of the subroutines are indicated by their broad classification.

Initialization of variables and reading of input data:

SDATA - Initializes variables used in numerical solution.

SDATAC - Reads in data, writes out data, initializes physical constants, calculates physical properties.

Computation of parameters at the boundaries of the main stream flow:

MIGDOT - Calculates mass flow rate from igniter.

TSCAL - Calculates propellant surface temperatures.

HCCAL - Calculates convective heat transfer coefficients.

FCCAL - Calculates friction factors.

BRCAL - Calculates burning rates.

LBC - Calculates the left boundary (i.e., igniter end) flow parameters.

RBC - Calculates the right boundary (i.e., nozzle end) flow parameters.

Numerical solution for contributions from slots:

SLOTK - Solution to p, T, V, and m_{slot} for each slot.

FCT2 - Calculates derivatives to be solved by RUNGE. Used when pressures in slot and main chamber are nearly equal.

FCT - Calculates derivatives to be solved by RUNGE. Used when pressure differential between main chamber and slot is significant.

RUNGE - A fourth order Runge-Kutta solution of the set of first order ordinary differential equations which described the slot flow.

Table 3-2 (Continued)

ORGANIZATION OF SUBROUTINES USED IN PROGRAM

Numerical solution of the three PDE's:

PREPP - Prepare tables and variables for prediction step.

SOLUTP - Implicit prediction solution for T, p, and u.

PREPC - Prepares tables and variables for corrector step.

SOLUTC - Implicit corrector solution for T, p, and u.

TRID - Solves the block-tridiagonal matrix of the finite-difference equations. Called by SOLUTP and SOLUTC.

INHOMO - Prepares inhomogeneous terms used in implicit solution.

Time-dependent output:

ANS - Executive subroutine that causes the time-dependent answers to be written out.

SRNBUG - Writes tabular summary of parameters at each axial station.

THRUS1 - Calculates thrust parameters.

PNCH - Punches cards that are used as input to programs that plot graphs.

Miscellaneous subroutines:

TIMEST - Sets internal codes whenever time step is changed.

LAGIN - Interpolation used with MIGDOT to obtain $m_{ig}(t)$, with RBCAL to obtain $r(p)$, and with SDATA to obtain $A_p(x)$ and $b(x)$.

4.0 DESCRIPTION OF COMPUTER PROGRAM INPUT

The discussion in this section coupled with the samples described in Sections 5.0 and 6.0 will enable the user to prepare the input to the program.

4.1 Basis for Selection of Dimensional Units

Since this is a period of transition to the SI system of units, and since the computer program employs conventional propellant configuration dimensions (which in the U.S. are specified in inches) and combustion and thermal properties (most widely expressed in the CGS system), an effort was made to accommodate the majority of current preferences by the following:

Input:

- Propellant and motor geometry may be input either in centimeters (cm) or inches (in).
- Propellant properties are specified in the CGS system (modified so that pressure is in atmospheres)
- Igniter mass flow may be specified in either grams per second or pounds per second.

Output:

- When propellant and motor geometries are input in inches they are converted to centimeters and displayed as part of the initial output.
- In the time dependent output displays, distance along the motor is printed out in both centimeters and inches. Pressure is printed out in both atmospheres and psia, and thrust is printed out in both newtons and pounds force. All other outputs are familiar nondimensional parameters or easy to deal with parameters in the CGS system.

4.2 Definitions of Input Parameters

The initial input to the program is in four parts: a comment card identifying the run, the data by means of NAMELIST, table for m_{ig} vs t, table for geometry, and, as an option,

burning rate vs pressure. The input and output for typical runs are included in Sections 5.0 and 6.0.

Each input variable is described on the following pages. Unless indicated otherwise by the decimal or lack of decimal in the default value, the NAMELIST variables follow the usual Fortran conventions on fixed and floating point numbers. The usual caution should be used when building up a new data set, e.g.,

(1) whenever practical, pattern new data sets after sample cases,

(2) first checkout run should be for a small fraction of the ultimate time period, i.e., a short TMAX,

(3) build up the data decks for complex cases through a progression of checkout cases in which the individual features are explored separately,

(4) first few runs should explore the effects of increment size on accuracy, e.g., NDELX and DELTAT.

(5) examine output for instabilities caused by improper time and distance increments or by extrapolating beyond values in input tables, and

(6) make sure dependent variable values in input table are continuous, i.e., port area versus distance, burning perimeter versus distance, and igniter mass flux versus time.

As an option, several of the input parameters can be changed during the run by causing NAMELIST NAME to be read in at either a prescribed time or nozzle-end stagnation pressure. Indeed, causing NAMELIST NAME to be read several times during the ignition transient for the purpose of increasing Δt is a necessity if running time is to be reduced. As indicated in the sample problems, Δt can be increased as the ignition and pressurization events progress. The user should pay careful attention to learning when and how much to increase Δt.

General[@]
Limits, code words, and initial conditions

Computer Symbol	*Symbol in Text*	*Description*	*@units CGS(modified) British*
TMAX[†]	t_{max}	Maximum time. When exceeded program reads new data in NAMELIST NAME (see page 53). Should be multiple of current value of TPRINT. (0.0)	sec
LAMBDA		When time increment Δt is not input, Δt is taken as 1/20 of the hot-gas wave time for an increment, Δx. LAMBDA is a factor multiplying that Δt, for the purpose of providing a prescribed adjustment to Δt. (1.0)	
TPRINT		Time interval between print out of answers.	sec
PZONE		When stagnation pressure at end of chamber reaches PZONE, program reads new data in NAMELIST NAME. (See page 53.) (7777.0)	atm
DELTAT	Δt	Time increment, Δt. When equal to zero, program will attempt to calculate the initial time step. The initial time step should be small compared to the ratio of the distance increment, Δx, to the sonic velocity in the igniter gases. As the flow field develops, Δt should be rapidly increased using the NAMELIST NAME option described on page 53. (0.0)	

[@]In accordance with this period of transition to the SI system of units, several of the parameters may be input (as an option specified by the input UNIT) in inches and lbm/sec. Those inputs are indicated by @ in the right column. All other dimensional inputs deal with combustion and thermodynamics and are input using a modified CGS system.

[†]Numbers in parentheses are default values built into the program.

Computer Symbol	*Symbol in Text*	*Description*	*@units CGS(modified) British*
NDELX		Number of space-wise steps, Δx, along the propellant grain. (Maximum value is 29) (Fixed point number.) (20)	
TPI	T_{pi}	Initial temperature in motor chamber and propellant. Adiabatic flame temperature is adjusted by program whenever TPI $\neq$ TOREF. (298.0)	K
PAM	P_{am}	Ambient absolute pressure. (1.0)	atm
UNIT		Codeword to indicate dimensional units of selected input values. If UNIT = -1.0, calories, centimeters, grams, K, seconds and atmospheres (i.e., the modified CGS system) are used. If UNIT = -2.0, those geometry related variables indicated by @ in the right column are input in inches, the igniter mass flow is input in lbm/sec, and all other input variables are in the CGS system. (-1.0) (Not a fixed point number.)	
NINERT		When NINERT = 1, part of the wetted perimeter may be inert (i.e., not propellant). When NINERT = 0, all the perimeter is propellant. See descriptions of geometry input table. (0) (Fixed point number.)	
NPNPXT		When NPNPXT = 1, cards for plotting p, u, and T are punched every TPRINT. (0) (Fixed point number.)	

Motor Configuration Parameters

The motor geometry input parameters are illustrated in Figs. 3-1 and 3-2. The tabular inputs for port area and perimeter are described on page 51.

Computer Symbol	*Symbol in Text*	*Description*	*@units CGS(modified) British*
AT	A_t	Throat area.	cm^2 @in^2
XP	x_p	Distance downstream at which propellant begins. Flow region between $x = 0$ and x_p is considered to be inert passage with port area $A_{p,1}$. Cannot be less than XE/500. (0.1)	cm @in
XG	x_G	Position at aft end of propellant grain. Set by program as $x_G = x_E - \Delta x/2$.	cm @in
XE	x_E	Position at end of flow passage (XE > XG) and before isentropic nozzle flow begins. Distance increment is $(x_E - x_p)$/NDELX.	cm @in

Combustion Gas Properties

GAMA	γ	Effective ratio of specific heats of all combustion gases.	
W	W	Average molecular weight of all combustion gases.	g/g-mole
TIGN	T_{ig}	Effective mean temperature of the igniter gases.	K
TFREF	$T_{f,ref}$	Adiabatic flame temperature at reference conditions, i.e., $p_{ref}, T_{0,ref}$. (Actual value should be used rather than theoretical value. TFREF should be consistent with input value of W and GAMA and measured c* values. See discussion in Appendix A.)	K

Friction Factor and Heat Transfer Coefficient

Computer Symbol	Symbol in Text	Description	@units CGS(modified) British
RUFSUR	ε_s	Roughness of the port walls (used prior to ignition). When zero, friction is zero. (0.001)	cm
DDRG		A factor multiplying the friction factor, for the purpose of providing a prescribed adjustment. (1.0)	
DDHC		A factor multiplying the heat transfer coefficient, for the purpose of providing a prescribed adjustment. (1.0)	

Propellant Properties

FKPR	λ_{pr}	Thermal conductivity of solid propellant. (Btu/sec-in-°R = 178.6 cal/sec-cm-K)	cal/sec-cm-K
ROPR	ρ_{pr}	Density of solid propellant. (1 lbm/in^3 = 27.68 g/cm^3)	g/cm^3
CPR	c_{pr}	Specific heat of solid propellant.	cal/g-K
TOREF	$T_{0,ref}$	Initial propellant temperature for reference conditions. (298.0)	K
SIGP	σ_p	Temperature sensitivity of burning rate at constant pressure, $(\partial \ln r/\partial T_0)_p$. Used only with Eq. (4-1). (0.002)	K^{-1}
TPSCRI	$T_{ps,ig}$	Surface temperature at which propellant ignition occurs. (600.0)	K

*Burning Rate Relationship**

The nonerosive burning rate, r_0, can be specified either by the empirical equation

$$r_0 = r_{ref}(p/p_{ref})^n \exp[\sigma_p(T_{pi} - T_{0,ref})] \qquad (4\text{-}1)$$

*TFREF, and RREF form a consistent set of parameters evaluated at a prescribed reference condition, (e.g., TOREF = 298.0K, PREF = 68.08 atm).

or by a table (which does not include σ_p correction):

$$r_0 = f(p) \qquad (4\text{-}2)$$

The following inputs apply to the empirical equation and the erosive burning contributions. See page 52 for the inputs that prescribe the r = f(p) table.

Computer Symbol	*Symbol in Text*	*Description*	*@units CGS(modified) British*
RREF	r_{ref}	Burning rate at reference conditions. If NDATA > 0, steady state burning rates are obtained from RDATA vs PDATA table.	cm/sec
PREF	p_{ref}	Absolute pressure for reference condition propellant properties. (68.08)	atm
BREXP	n	Exponent in burning rate relationship.	

If the following modified Lenoir-Robillard erosive burning rate law is used:

$$r = r_0 + k_e h_c \exp(-\beta_e r \rho_{pr}/G) \qquad (4\text{-}3)$$

where G is $(\rho u)_{ch}$ and h_c is the convective heat transfer coefficient, then

EBC	k_e	Pre-exponential constant in Lenoir-Robillard erosive burning relationship, Eq. (4-3). (0.0)	cm^3-K/cal
EBEX	β_e	Factor in exponent of Lenoir-Robillard erosive burning relationship, Eq. (4-3). (125.0)	

If the more conventional form of the Lenoir-Robillard erosive burning rate law is used

$$r = r_0 + \alpha_e G^{0.8} d_h^{-0.2} \exp(-|\beta_e r \rho_{pr}/G|) \qquad (4\text{-}4)$$

where hydraulic diameter is $d_h = 4A_p/b$, then

EBC	α_e	Pre-exponential factor in Eq.(4-4).	
EBEX	$-\beta_e$	Code word and factor in exponent of Eq. (4-4). When < 0, signal to use Eq. (4-4).	

To convert α_e from $in^{2.8}/lbm^{0.8}\text{-}sec^{0.2}$ to CGS, multiply by 0.102.

Parameters Used in Thrust Calculation

For details of thrust calculation, see Appendix 1.

DE	D_{ex}	Exit plane diameter. If 0.0, thrust calculation is bypassed. (0.0)	cm @in
CM	c_m	Nozzle coefficient for thrust losses. (0.0)	
ALFAD	α_N	Nozzle divergence 1/2 angle. (15.0	deg
EROAT EROEXP	E_t n_t	Parameters in empirical nozzle erosion equation, dD/dt = 2*EROAT P**EROEXP. (0.0 & 0.8)	cm/sec @in/sec

Igniter Mass Discharge Versus Time Table

First table following NAMELIST NAME input.

NIGTAB*		Number of points in table. (Maximum is 30) Fixed point number; part of NAMELIST NAME.	

Use 2E10.0 Format for TIGTAB and MIGTAB.

Two point interpolation is used.

TIGTAB	t	Time after beginning of run. Second time in table should be at least 30 Δt's.	sec
MIGTAB	m_{ig}	Mass flow rate from igniter. Program will assign a small value to m_{ig} at t = 0 so as to satisfy starting conditions of solution.	g/sec @lbm/sec

*Include as part of NAMELIST NAME input.

Propellant Geometry Input Table

Second table following NAMELIST NAME input. For more details see Figs. 3-1 and 3-2.

Input which apply to both monolithic and segmented motors:

Computer Symbol	*Symbol in Text*	*Description*	*@units CGS(modified) British*
NAPDVX*		Number of points in table and stations.* (Maximum is 30) Fixed point number, part of NAMELIST NAME.	

Use 8E10.0 format for XAP, APD, BPD, WPD, XSLOT, DELABS, DELVS and WIDTH. Values in table must be consistent with XP, XG and XE.

When circumferential slots are considered, the table must include one set of entries for each x station corresponding to equally spaced stations Δx apart. The x values are to be specified so as to correspond to the leading edge of each increment.

XAP	x	Distance from head end of motor.	cm @in
APD	A_p	Port area of main channel.	cm^2 $@in^2$
BPD	b	Perimeter of propellant surface in main channel.	cm @in
WPD	p_i	Total perimeter of propellant and inert surface (i.e., wetted perimeter) before ignition.	cm @in

Inputs which apply only to segmented motors:*

XSLOT	x_{slot}	Distance to the upstream tip of the slot from the head end of the motor.	cm @in
DELABS	$\delta A_{b,slot}$	Burning surface area in slot. (Subtract bw_{slot} from actual burning surface area in the slot.)	cm^2 $@in^2$

*When segmented motors are considered, input geometry for each station, i.e., NAPDVX = NDELX + 1. When $x \leq x_{slot} < x + \Delta x$, inputs corresponding to slot at $x = x_{slot}$ are prescribed.

Computer Symbol	*Symbol in Text*	*Description*	*@units CGS(modified) British*
DELVS	δV_{slot}	Volume (region of gas not in the flow field) of slot. Program treats this as volume sink and not part of the flow passage.	cm^3 $@in^3$
WIDTH	w_{slot}	Width of axial separation between segments. (Must be sufficiently large so that flow out of slot is less than about Mach = 0.3)*	cm @in

Burning Rate Table (r vs p)

Optional third table following NAMELIST NAME. Not used when $r = r_{ref}(p/p_{ref})^n$ is desired.

Use 2E10.0 format for PDATA (in columns 1 to 10) and RDATA (in columns 11 to 20). Table is logged by the program, and interpolation is in ln r vs ln p table.

NDATA**	Length of table (i.e., the number of r,p pairs). Maximum table length is 30. If zero, table not used. (0)	
NPPR**	Number of points to be used in interpolation. Linear interpolation is prescribed by inputing 2. If three or more points are used it is important that the values in the tables be uniform and continuous. (2)	
PDATA	Values of pressure in r vs p table. (Place in columns 1 to 10)	atm
RDATA	Values of burning rate, r corresponding to pressure, PDATA. A point in the table must correspond to PREF and RREF. (Place in columns 11 to 20)	cm/sec

*Maintaining low Mach numbers out of the slot is a practical design consideration, which is discussed in Ref. 27.
**Read in as part of NAMELIST NAME.

4.3 Intermediate Insertion of New Input Parameters

There are various situations where it is either convenient or necessary to interrupt the calculations and insert new data. For example, to decrease the running time, the time step, Δt, must be increased as the flow develops. To accomplish this, the program will read in the NAMELIST NAME when nozzle-end stagnation pressure > PZONE or time > TMAX. This is illustrated in Tables 5.1 and 6.2.

The input parameters which can be read in include:

Symbol		*Units*
DELFAC	(new value of Δt = DELFAC $\times \Delta t$)	-
TMAX	(should be multiple of current value of TPRINT)	sec
DELTAT	(new time step, Δt)	sec
TPRINT		sec
AT	(throat area)	cm^2
PZONE*	NOTE ⟶	atm
TIGN		K
DDRG		-
DDHC		-

For example, if at $t = 0.01$ sec the following changes are desired:

(1) increase Δt by 40%,
(2) print out answers every 0.005 sec,
(3) next call to read NAMELIST NAME is to be at either $t = 0.04$ sec or $p_{E,stag} = 2.0$ atm,

the input should be arranged as follows:

(1) original input set should contain TMAX = 0.01.
(2) after geometry table place input array for NAMELIST NAME,&NAME DELFAC = 1.4, TPRINT = 0.005, TMAX = 0.04, PZONE = 2.0 &END

*Because of internal pressure units, this value must be input in atm and not in psi.

4.4 Punched Output for Input to Plot Programs

As specified by the codeword NPNPXT, punched cards containing many of the output variables can be obtained. Using this punched output, the user can prepare a special purpose program to plot the results.

At the beginning of each punched output deck is the title card that goes with the data set. The following values are punched in the next card using a 12A4 field:

x_p	Distance downstream at which propellant begins.	cm
x_E	Position at end of flow passage and before isentropic nozzle flow begins.	cm
A_t	Throat area.	cm^2
BLANK		
T_{int}	Initial gas temperature in chamber.	K
p_{int}	Initial chamber pressure.	atm
M_{int}	Initial Mach number	
Δx	Distance between axial stations.	cm
UNIT	Codeword to indicate units used in program.	sec
t	Time punched data begins.	sec
γ	Ratio of specific heats.	
$R_u J/W$	Gas constant divided by average molecular weight.	

The following sets of values are punched for each TPRINT interval. The first card in the set contains (in an E14.6, 2I8, 2F10.1 field):

t	Time	sec
NUT	Total Number of time steps used to this point.	-

NCARDS	Number of cards corresponding to each time interval.	-
$p_{E,stag}$	Nozzle end stagnation pressure.	atm
F	Thrust	newtons

The next NCARDS cards in the set contain NDELX+1 pressures, followed by NDELX+1 temperatures, and followed by NDELX+1 Mach numbers (using a 20A4field).

5.0 SOLID ROCKET BOOSTER CONSIDERED AS MONOLITHIC CONFIGURATION

The results presented in this section along with those of the next section serve two purposes: (1) they define and demonstrate the use of the computer program and (2) they provide information which is applicable to SRB's. The calculations presented in this section were performed during the time the procedures for analyzing the slot interactions were being developed. Accordingly, in this section the SRB is treated as a monolithic motor with a total chamber volume, length, and burning surface area similar to that of the segmented motor described in Ref. 25. Since the scope of the study did not permit all of the parametric studies to be redone using the final version of the computer program and since the results are generally applicable to the SRB described in Ref. 25, they are included in this report. In Section 6, the final version of the computer program is used to analyze the SRB as a segmented motor.

The main approximation in using a monolithic motor configuration to analyze a segmented motor is that the segmented motor geometry must be approximated in terms of port areas and perimeters. However, since the burning surface area and chamber volume in the slots of the SRB under development[25] are relatively small, the approximation is reasonable.

The input prepared to simulate the SRB design is shown in Tables 5-1 and 5-2. Table 5-1 is a listing of the input data cards and Table 5-2 is a copy of the printout prepared by the program to display the input. Note that the variables in Tables 5-1 and 5-2 are the same as described in Section 4. Preparing the input for the complex head-end geometry of the Ref. 25 SRB requires careful attention. It is important to account for all of the burning surface area, chamber volume, and port area. All of this must be done using a few distance increments and without allowing an abrupt discontinuity in the flow field. The reader should pay particular

Table 5-1

INPUT DATA FOR MONOLITHIC MOTOR (SRB1)

```
SRB1 TPSCRI850  NOERO 24
&NAME
      TMAX=.002
      TPRINT=.002
      DELTAT=.00016
      NDEIX=21
      UNIT=-2.
      NPNPXT=0
      AT=2327.
      XP=3.
      XG=1341.3
      XE=1377.
      GAMA=1.1363
      W=28.21
      TFREF=3361.
      TIGN=2650.
      RUPSUR=0.01
      FKPR=0.0011
      ROPR  = 1.758
      CPR=.3
      TPSCRI=850.
      RREF=1.0783
      BREXP = 0.35
      EBC=0.
      DE=145.64
      CM=.98
      ALFAD=12.31
      NIGTAB=6
      NAPDVX=10
&END
   0.         25.
    .020     560.
    .250     560.
    .340     300.
    .450     100.
    .50        0.
   0.         2554.     1018.92    1018.92
   3.         2554.     1018.92    1018.92
  68.4286     2554.     1018.92    1018.92
 133.8571     2554.     1018.92    1018.92
 199.2857     2870.      611.23     611.23
 264.7143     3187.      203.53     203.53
 961.6        3187.      203.53     203.53
1023.         3096.      203.53     203.53
1286.         3400.      203.53     203.53
1377.         4500.      203.53     203.53
&NAME
      TMAX=.01
      DELFAC=1.3
&END
&NAME
      TMAX=.15
      TMAX=.12
      DELFAC=2.
&END
```

Last value is retained in memory

```
&NAME
      TMAX=.2
      TPRINT=.005
&END
&NAME
      TMAX=.4
      TPRINT=.01
&END
&NAME
      TMAX=.5
      TMAX=.6
&END
```

Table 5-2 MONOLITHIC INPUT TO SIMULATE SRB DESIGN

```
HIGH PERFORMANCE ROCKET MOTOR IGNITION TRANSIENT PREDICTION PROGRAM
INCLUDES: SPATIAL & TIME DEVELOPMENT OF P,U,&T AND FLAME SPREADING

SRB1 24

GENERAL:  LIMITS, CODE WORDS, & INITIAL CONDITIONS:
TMAX      LAMBDA    TPRINT    PZONE     DELTAT     NDELX
 0.002    1.00       0.001     7777.00 0.0001600    21

TPI       PAM       UNIT      NINERT  NPNPXT
 298.0     1.00      -2.        0       0

MOTOR CONFIGURATION PARAMETERS:
AT        XP        XG        XE
 2327.00  3.00    1374.00    1374.00

COMBUSTION GAS PROPERTIES
GAMA      W         TEREF     TIGN
 1.136    28.21     3361.0    2650.0

FRICTION TRANSFER AND HEAT TRANSFER COEF.:
ROFSUR    DDRG      DDHC
0.0100     1.00      1.00

PROPELLANT PROPERTIES:
FKPR      ROPR      CPR       TOREF     SIGP      TPSCRI
0.00110  1.758       0.30      298.00    0.00200   850.00

BURNING RATE RELATIONSHIP:
RREF      PREF      BREXP     EBC       EEEX
 1.078    68.08     0.3500     0.0     125.000


PARAMETERS USED IN THRUST CALCULATIONS:
DE        CM        ALPAD     ERCAT     ERCEXP
 145.64   0.980      12.31     0.0       0.80

IGNITER MASS DISCHARGE VS. TIME TABLE:
 TIME     FLOW RATE
 0.0          25.0
 0.0200      560.0
 0.2500      560.0
 0.3400      300.0
 0.4500      100.0
 0.5000        0.0

PROPELLANT GEOMETRY TABLE:
 LENGTH   PORT AREA PROPELLANT  WETTED
                    PERIMETER   PERIMETER
    0.0    2554.00 1018.92     1018.92
    3.00   2554.00 1018.92     1018.92
   68.43   2554.00 1018.92     1018.92
  133.86   2554.00 1018.92     1018.92
  199.29   2870.00  611.23      611.23
  264.71   3187.00  203.53      203.53
  961.60   3187.00  203.53      203.53
 1023.00   3096.00  203.53      203.53
 1286.00   5595.00  203.53      203.53
 1377.00   5595.00  203.53      203.53
```

attention to entries at stations 4, 5, and 6 in Table 5-1 and note that station 5 is a transition section.

A typical time dependent output is shown on Table 5-3. The output has been annotated to define the output values. Figure 5-1 shows the calculated pressure-versus-time at four positions along the port. Also shown is an expanded portion of the curve emphasizing the reflection of the first strong wave (that arrives at the nozzle closure) and the times at which ignition occurs. Immediately apparent are the interactions produced by the nonuniform pressure at 0.08 seconds which are a result of the high velocity gases being driven ahead of the ignition front and reflecting off the nozzle converging section. (It is important to note that this nonuniform pressure is not expected to produce any structural problems since it occurs at an intermediate pressure.) The nonuniform pressure is to some degree a characteristic of this particular type of motor, i.e., a long motor with a large burning surface area in the head end and a moderately small port-to-throat area ratio. Figure 5-2 shows some of the details of the pressure wave development in the p-x plane and clearly indicates the nature of the wave reflection. When the results were tested by decreasing the time and distance steps, no important differences in the wave character or magnitude were noted.

The results of Fig. 5-1 should not be considered as detailed predictions of the SRB since much is yet to be learned from correlating previous large motor firing data. In particular, users will have to gain experience with predicting convective heat transfer rates and propellant ignition criteria.

The ripples on the p vs t curves on Fig. 5-1 are a result of longitudinal waves reflecting off the nozzle and head end closures. Note that these oscillations damp as the motor reaches its operating pressure. The oscillations are a physical characteristic of this particular SRB (as opposed to an indication of numerical difficulties) and are not observed in all calculations of large booster ignition transients.

Table 5-3 (Part 1)

OUTPUT FROM MONOLITHIC MOTOR RUN (SRB1)
- DURING FLAME SPREADING -

TIME =0.8400E-01 (196 DELTAT) DELTAT =0.5000E-03

N	DISTANCE CM	DISTANCE IN	PRESSURE ATM	PRESSURE PSIA	T DEG K	MACH NO.	RATE CM/SEC	BR/BRN	TAUB CM	FRICT. FACTOR	CONV. COEF.	M/A G/SEC CMSQ	TSURF K	PORT CMSQ
0	0.0	0.0	14.52	213.3	2654.8	0.085	0.63	1.000	0.0170	0.0	0.0313	15.09	850.	16521.4
1	173.8	68.4	13.80	202.8	2959.7	0.240	0.62	1.000	0.0123	0.0	0.0613	38.39	850.	16509.2
2	340.0	133.9	12.15	178.5	3103.3	0.425	0.59	1.000	0.0094	0.0	0.0827	58.32	850.	16501.7
3	506.2	199.3	9.46	139.0	3114.5	0.644	0.54	1.000	0.0067	0.0	0.0859	68.70	850.	18526.4
4	672.4	264.7	7.81	114.8	3096.1	0.788	0.51	1.000	0.0045	0.0	0.0750	69.64	850.	20563.5
5	838.6	330.1	7.55	110.9	3143.4	0.802	0.50	1.000	0.0036	0.0	0.0723	67.95	850.	20563.0
6	1004.8	395.6	7.30	107.2	3183.3	0.812	0.49	1.000	0.0028	0.0	0.0698	66.06	850.	20562.7
7	1170.9	461.0	7.01	103.0	3190.3	0.833	0.49	1.000	0.0021	0.0	0.0680	65.05	850.	20562.3
8	1337.1	526.4	6.73	98.9	3130.8	0.873	0.48	1.000	0.0012	0.0	0.0678	66.06	850.	20561.8
9	1503.3	591.9	6.41	94.1	2983.7	0.916	0.47	1.000	0.0005	0.0	0.0675	67.57	850.	20561.5
10	1669.5	657.3	6.18	90.7	2807.6	0.931	0.0	0.0	0.0	0.0031	0.0667	68.29	828.	20561.2
11	1835.7	722.7	6.07	89.2	2654.8	0.922	0.0	0.0	0.0	0.0031	0.0657	68.33	775.	20561.2
12	2001.9	788.1	5.97	87.7	2514.7	0.909	0.0	0.0	0.0	0.0030	0.0647	68.06	721.	20561.2
13	2168.1	853.6	5.88	86.3	2363.5	0.898	0.0	0.0	0.0	0.0030	0.0641	68.34	663.	20561.2
14	2334.3	919.0	5.77	84.8	2164.6	0.895	0.0	0.0	0.0	0.0030	0.0643	69.94	601.	20561.2
15	2500.4	984.4	5.55	81.6	1895.4	0.906	0.0	0.0	0.0	0.0030	0.0649	72.82	536.	20342.9
16	2666.6	1049.9	5.11	75.0	1569.4	0.923	0.0	0.0	0.0	0.0029	0.0640	75.01	472.	20174.4
17	2832.8	1115.3	4.54	66.6	1230.8	0.919	0.0	0.0	0.0	0.0029	0.0605	75.13	413.	20662.3
18	2999.0	1180.7	4.02	59.1	929.9	0.879	0.0	0.0	0.0	0.0029	0.0550	73.40	369.	21150.3
19	3165.2	1246.1	3.66	53.8	694.9	0.780	0.0	0.0	0.0	0.0029	0.0476	68.68	339.	21638.2
20	3331.4	1311.6	3.65	53.6	526.0	0.574	0.0	0.0	0.0	0.0029	0.0373	58.11	318.	23929.6
21	3497.6	1377.0	4.22	61.9	408.1	0.326	0.0	0.0	0.0	0.0030	0.0	42.86	306.	29032.2

PESTAG.ATM= 4.48 PESTAG.PSIA= 65.79 MASS BURNED= 0.2814E 05

THRUST NEWTONS	THRUST LBF	CFLN -	AT CM**2	EPSONG -	EPSON -	PA/PE
663280.3	149112.0	0.9738	15012.867	7.1590	2.0637	1.783

Table 5-3 (Part 2)*

OUTPUT FROM MONOLITHIC MOTOR RUN (SRB1)
- DURING RAPID PRESSURE RISE -

TIME =0.1300E 00 (278 DELTAT) DELTAT =0.1000E-02

n	x	p	T	M	r	r/r_0	$\int rdt$	f	h_c	pu	T_{ps}	A_p
N	DISTANCE CM	DISTANCE IN	PRESSURE ATM	PRESSURE PSIA	T DEG K	MACH NO.	RATE CM/SEC	BR/BRN	TAUB CM	FRICT. FACTOR	CONV. COEF.	M/A G/SEC	TSURF K	PORT CMSQ
0	0.0	0.0	23.67	347.7	2653.1	0.052	0.74	1.000	0.0488	0.0	0.0314	15.13	850.	16603.3
1	173.8	68.4	22.96	337.3	2944.1	0.176	0.74	1.000	0.0437	0.0	0.0719	46.94	850.	16590.1
2	340.0	133.9	21.47	315.4	3077.3	0.315	0.72	1.000	0.0398	0.0	0.1027	76.65	850.	16580.2
3	506.2	199.3	19.08	280.3	3105.8	0.435	0.69	1.000	0.0353	0.0	0.1099	93.61	850.	18570.7
4	672.4	264.7	18.77	275.7	3122.8	0.427	0.69	1.000	0.0322	0.0	0.0925	90.25	850.	20577.7
5	838.6	330.1	19.35	284.3	3156.0	0.400	0.69	1.000	0.0314	0.0	0.0881	86.78	850.	20577.3
6	1004.8	395.6	19.20	282.0	3176.6	0.409	0.69	1.000	0.0305	0.0	0.0875	87.59	850.	20576.8
7	1170.9	461.0	19.65	288.7	3211.3	0.388	0.70	1.000	0.0297	0.0	0.0842	84.67	850.	20576.4
8	1337.1	526.4	20.26	297.6	3249.8	0.360	0.71	1.000	0.0286	0.0	0.0801	80.53	850.	20575.9
9	1503.3	591.9	21.19	311.3	3294.4	0.320	0.72	1.000	0.0278	0.0	0.0746	74.32	850.	20575.4
10	1669.5	657.3	22.07	324.3	3338.0	0.283	0.73	1.000	0.0271	0.0	0.0691	68.10	850.	20575.1
11	1835.7	722.7	22.52	330.9	3373.3	0.267	0.73	1.000	0.0264	0.0	0.0663	65.15	850.	20574.7
12	2001.9	788.1	22.36	328.5	3396.9	0.273	0.73	1.000	0.0257	0.0	0.0665	65.98	850.	20574.4
13	2168.1	853.6	21.92	322.0	3414.2	0.295	0.73	1.000	0.0250	0.0	0.0689	69.54	850.	20574.0
14	2334.3	919.0	21.35	313.7	3428.2	0.316	0.72	1.000	0.0240	0.0	0.0708	72.47	850.	20573.5
15	2500.4	984.4	20.93	307.4	3443.5	0.343	0.71	1.000	0.0233	0.0	0.0740	77.01	850.	20354.9
16	2666.6	1049.9	20.30	298.2	3454.2	0.365	0.71	1.000	0.0226	0.0	0.0754	79.35	850.	20186.0
17	2832.8	1115.3	19.94	292.9	3469.7	0.386	0.70	1.000	0.0217	0.0	0.0770	82.14	850.	20673.4
18	2999.0	1180.7	19.38	284.8	3481.3	0.391	0.69	1.000	0.0211	0.0	0.0754	80.78	850.	21161.1
19	3165.2	1246.1	19.22	282.3	3499.3	0.411	0.69	1.000	0.0202	0.0	0.0774	84.05	850.	21648.5
20	3331.4	1311.6	18.76	275.5	3514.6	0.371	0.69	1.000	0.0154	0.0	0.0688	73.79	850.	23937.5
21	3497.6	1377.0	19.52	286.8	3524.2	0.326	0.0	0.0	0.0	0.0	0.0	67.51	860.	29040.0

PESTAG,ATM= 20.74 PESTAG,PSIA= 304.60 MASS BURNED= 0.1641E 06

F		ϵ_{flm}	A_t			P_{am}/P_{ex}
[redacted]	[redacted]	CFLM	AT	EPSONG	EPSON	PA/PE
[redacted]	LBF	-	CM**2	-	-	
				ϵ_{ex}	ϵ_{ex}	
[redacted]	945365.8	1.3335	15012.867	7.1590	7.1590	2.105

*Output symbols identified by annotations.

Table 5-3 (Part 3)

OUTPUT FROM MONOLITHIC MOTOR RUN (SRB1)
- APPROACHING FULL CHAMBER PRESSURE -

TIME =0.4200E 00 (544 DELTAT) DELTAT =0.1250E-02

N	DISTANCE CM	DISTANCE IN.	PRESSURE ATM	PRESSURE PSIA	T DEG K	MACH NO.	RATE CM/SEC	BR/BRN	TAUB CM	FRICT. FACTOR	CONV. COEF.	M/A G/SEC CMSQ	TSURF K	PORT CMSQ
0	0.0	0.0	59.43	873.0	2651.1	0.006	1.03	1.000	0.3271	0.0	0.0109	4.03	850.	17323.1
1	173.8	68.4	58.90	865.3	2924.6	0.076	1.03	1.000	0.3208	0.0	0.0780	52.33	850.	17306.8
2	340.0	133.9	58.07	853.1	3055.8	0.152	1.02	1.000	0.3149	0.0	0.1265	100.22	850.	17291.5
3	506.2	199.3	56.08	823.8	3097.3	0.207	1.01	1.000	0.3059	0.0	0.1434	131.06	850.	18990.2
4	672.4	264.7	55.76	819.4	3110.7	0.208	1.01	1.000	0.3023	0.0	0.1242	130.84	850.	20716.8
5	838.6	330.1	55.71	818.4	3123.4	0.217	1.01	1.000	0.3015	0.0	0.1256	135.84	850.	20716.4
6	1004.8	395.6	55.21	811.0	3132.5	0.232	1.00	1.000	0.2997	0.0	0.1293	143.71	850.	20715.5
7	1170.9	461.0	54.95	807.3	3142.9	0.244	1.00	1.000	0.2985	0.0	0.1324	150.39	850.	20714.9
8	1337.1	526.4	54.48	800.2	3151.2	0.258	1.00	1.000	0.2966	0.0	0.1356	157.27	850.	20713.9
9	1503.3	591.9	54.15	795.4	3159.8	0.272	1.00	1.000	0.2952	0.0	0.1392	164.63	850.	20713.1
10	1669.5	657.3	53.62	787.7	3166.5	0.285	0.99	1.000	0.2935	0.0	0.1420	170.85	850.	20712.3
11	1835.7	722.7	53.26	782.4	3173.7	0.301	0.99	1.000	0.2920	0.0	0.1461	178.80	850.	20711.5
12	2001.9	788.1	52.64	773.3	3178.6	0.314	0.99	1.000	0.2901	0.0	0.1484	184.20	850.	20710.6
13	2168.1	853.6	52.29	768.1	3184.8	0.331	0.98	1.000	0.2886	0.0	0.1529	192.96	850.	20709.8
14	2334.3	919.0	51.53	757.0	3187.8	0.343	0.98	1.000	0.2863	0.0	0.1545	197.17	850.	20708.8
15	2500.4	984.4	51.19	752.0	3193.3	0.367	0.98	1.000	0.2847	0.0	0.1612	209.23	850.	20489.5
16	2666.6	1049.9	50.10	736.0	3193.2	0.382	0.97	1.000	0.2820	0.0	0.1626	212.97	850.	20319.6
17	2832.8	1115.3	50.01	734.6	3199.8	0.398	0.97	1.000	0.2807	0.0	0.1664	221.20	850.	20806.6
18	2999.0	1180.7	49.08	721.1	3200.7	0.393	0.96	1.000	0.2785	0.0	0.1612	214.72	850.	21293.6
19	3165.2	1246.1	49.39	725.5	3209.2	0.411	0.96	1.000	0.2780	0.0	0.1665	225.59	850.	21781.5
20	3331.4	1311.6	48.58	713.7	3211.8	0.364	0.96	1.000	0.2717	0.0	0.1468	196.25	850.	24066.6
21	3497.6	1377.0	50.90	747.7	3231.4	0.325	0.0	0.0	0.0	0.0	0.0	182.88	850.	29172.8

PESTAG,ATM= 54.03 PESTAG,PSIA= 793.69 MASS BURNED= 0.1507E 07

THRUST NEWTONS	THRUST LBF	CFLM -	AT CM**2	EPSONG -	EPSON -	PA/PE
12705364.0	2856292.0	1.5463	15012.867	7.1590	7.1590	0.808

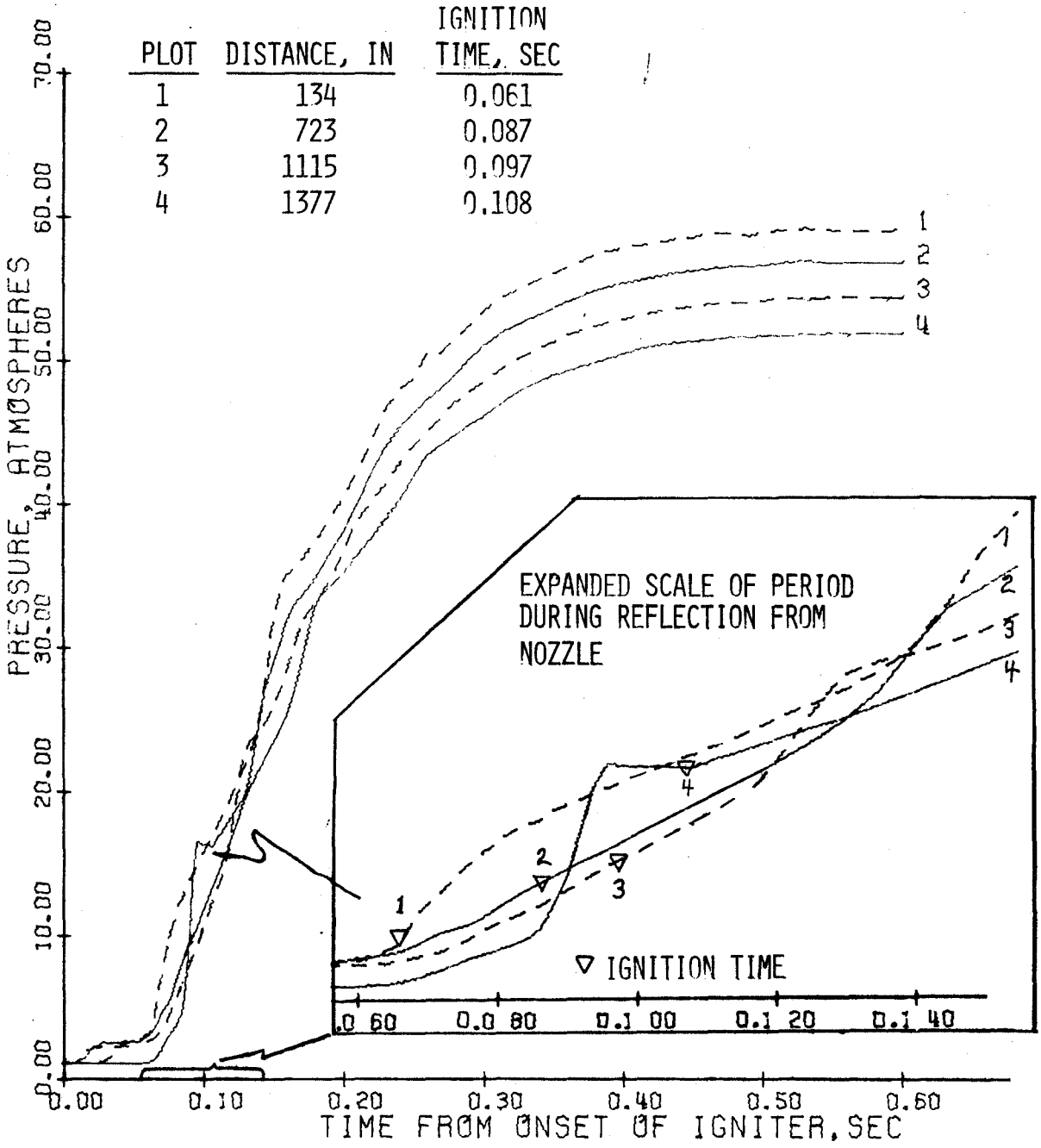

FIG. 5-1 PRESSURE DEVELOPMENT AT FOUR STATIONS ALONG THE PORT SHOWING THE REFLECTION OF THE GASES DRIVEN AHEAD OF THE IGNITION FRONT. (SRB1)

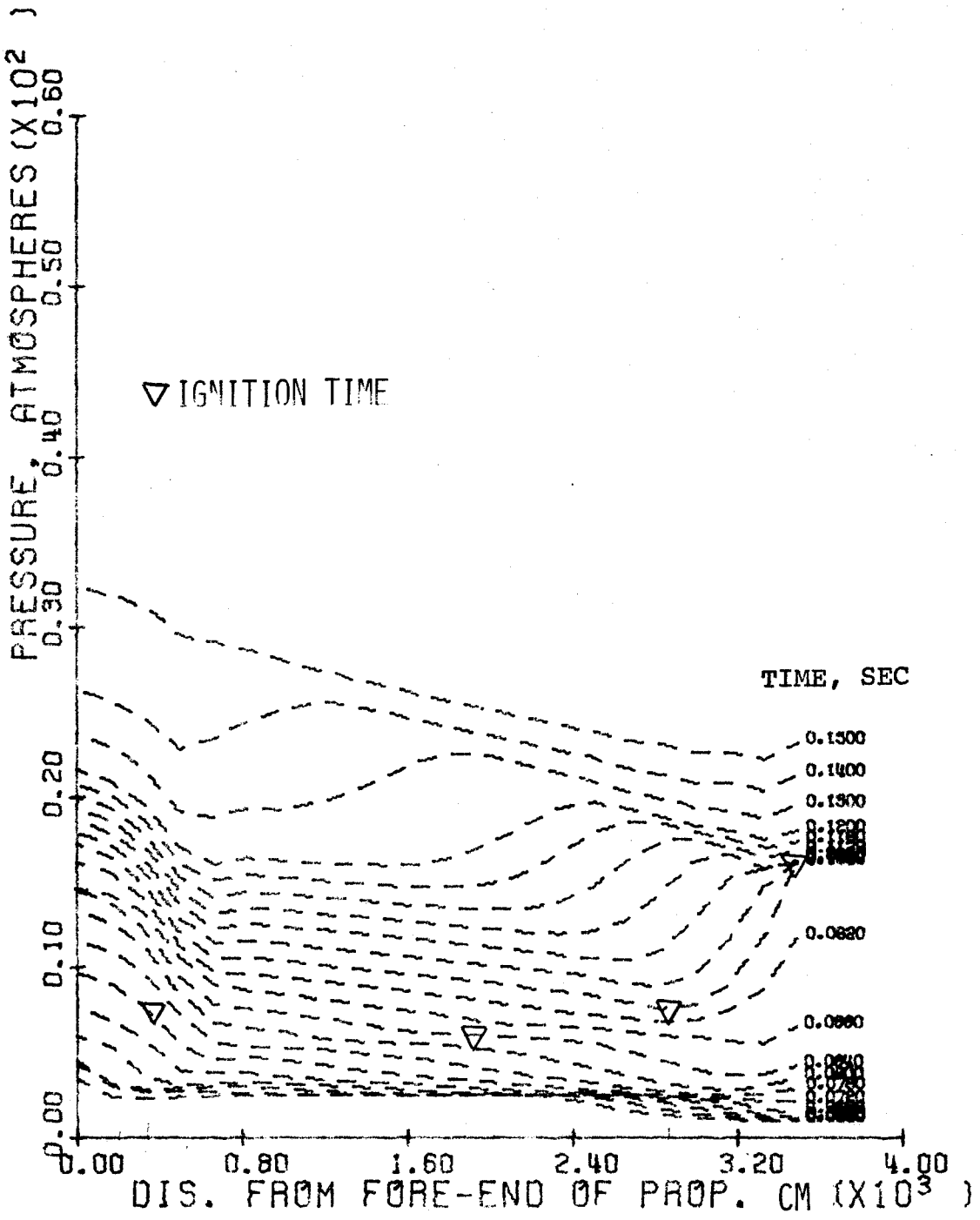

FIG. 5-2 PRESSURE WAVE PROPAGATING DOWN THE PORT AND REFLECTING OFF THE AFT CLOSURE
(SRB1)

As shown in Figs. 5-3, 5-4, and 5-5, the developing flow field during ignition is influenced greatly by the heat loss to the propellant. As the gases are accelerated their static temperature decreases and as they heat the surface their stagnation temperature decreases, which in turn decreases their linear velocity. In Figs. 5-3, 5-4, and 5-5, the first curve (at $t = 0.04$ sec) is before first ignition has occurred; the next three curves are during flame spreading (the point of flame spreading is indicated by a triangle). As the pressure increases following full ignition, the flow field becomes more fully developed, gas velocity decreases as the gas becomes more dense, and the gas temperature becomes more uniform. The last curve (at $t = 0.5$ sec) approximates fully developed flow conditions and is beginning to take on the quasi-steady flow characteristics which are adequately represented by $p(x)$ models.

Flame spreading rates for a range of input conditions are shown on Fig. 5-6. The heavy dashed curve corresponds to SRB1 whose distinguishing characteristic is that the ignition temperature is 850K rather than 750K used in most of the calculations.

After the first upstream portion of the grain is ignited, the mass flow generated by the main propellant grain soon exceeds the mass flow of the igniter. Thus, for the particular case under consideration, as shown in Fig. 5-6, the time of first ignition is dependent on items such as igniter mass flow rate ($\dot{m}_{ig}$), ignition temperature ($T_{ps,ig}$), and convective heating rate, but the flame spreading rate is a motor characteristic which is largely independent of erosive burning, $T_{ps,ig}$, and convective heating rate. Since the insensitivities of flame spreading rate to erosive burning and $T_{ps,ig}$ (as shown on Fig. 5-6) are unexpected and not fully explained, they should not be considered as generalizations.

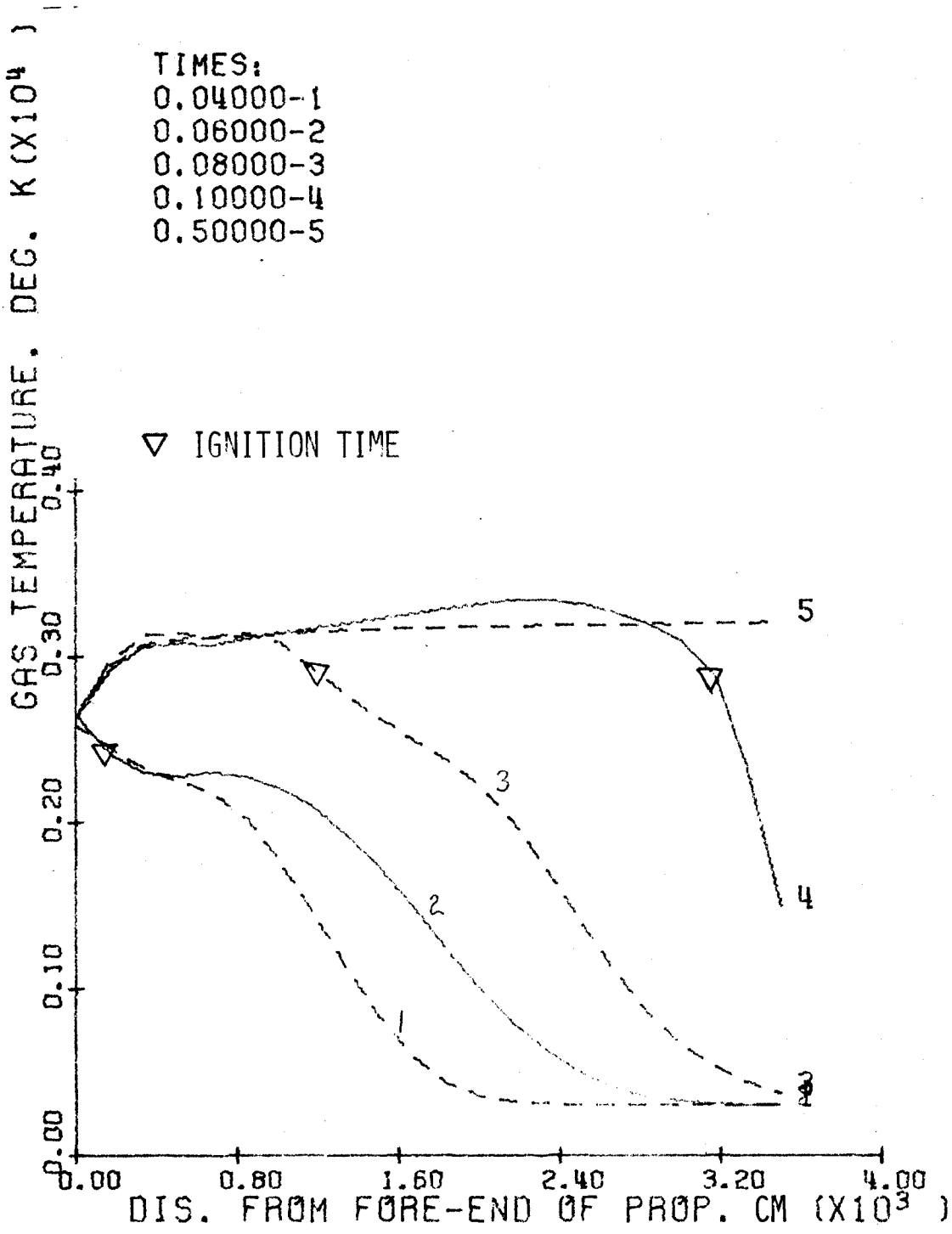

FIG. 5-3 STATIC TEMPERATURE ALONG PORT DURING IGNITION TRANSIENT (SRB1)

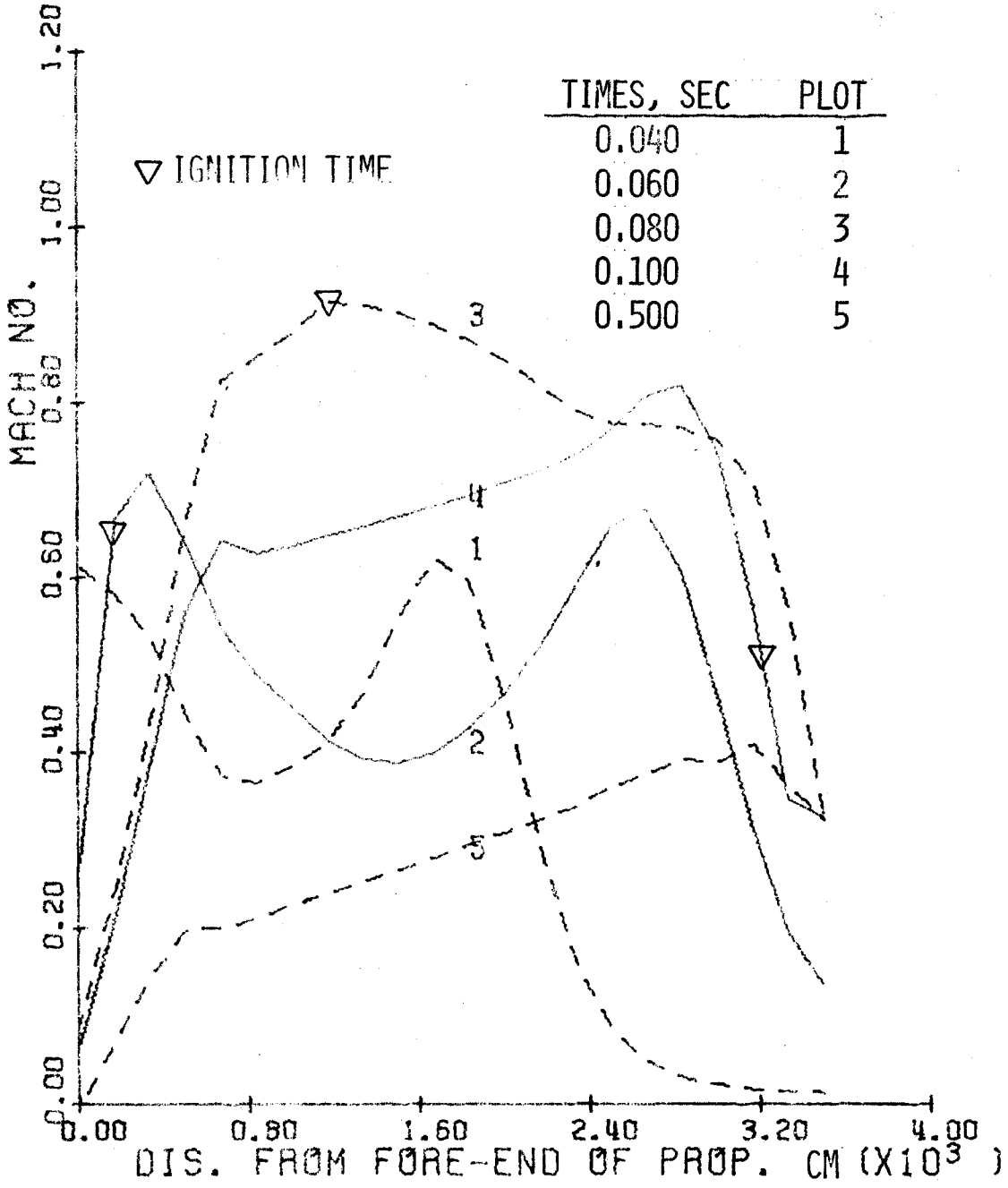

FIG. 5-4 MACH NUMRERS ALONG PORT DURING IGNITION TRANSIENT (SRB1)

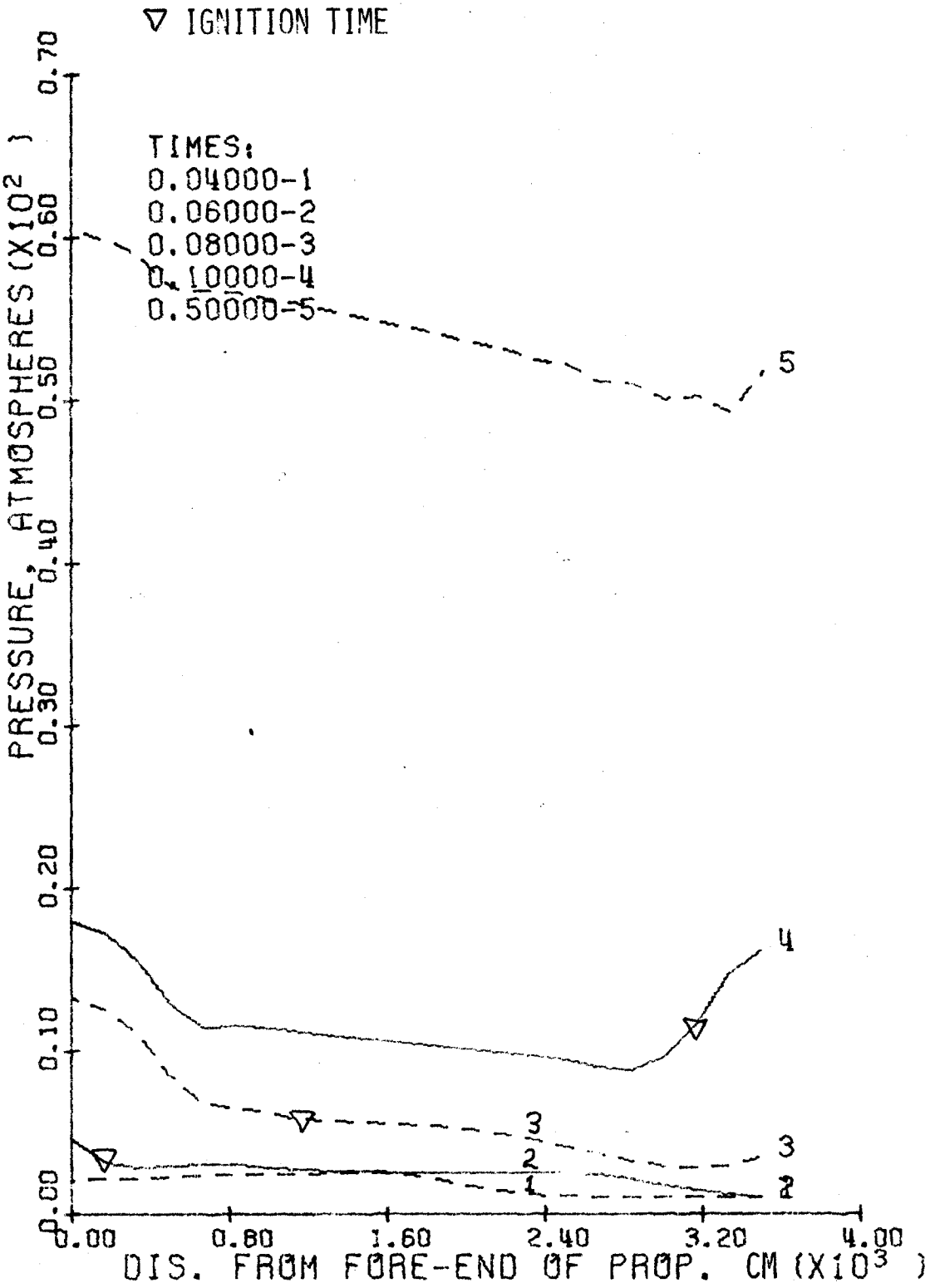

FIG. 5-5 STATIC PRESSURES ALONG PORT DURING IGNITION TRANSIENT (SRB1)

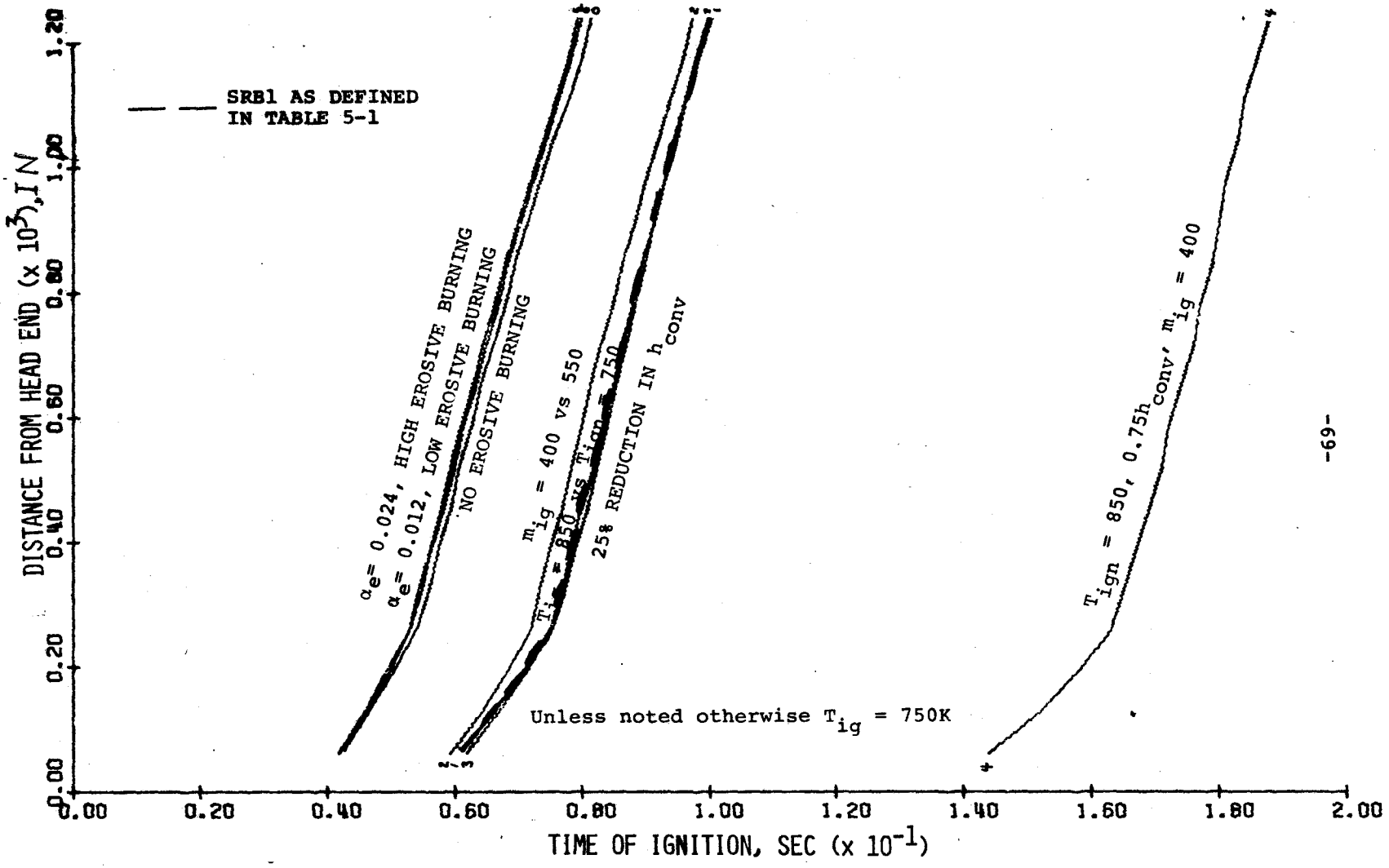

FIG. 5-6 IGNITION TIMES ALONG PROPELLANT FOR A RANGE OF MOTOR AND IGNITER PARAMETERS.

By studying the flow field development characteristics of Figs. 5-1 through 5-5, the reader can get a good understanding of how flame spreading is implicitly an output of the p(x,t) model, i.e.,

- The hot gases from the igniter heat the propellant as they flow down the port.
- The rate at which the propellant is heated rapidly decreases in the direction of flow because igniter gases rapidly give up their heat and require a significant time to reach the nozzle end of the motor.
- After the head end of the grain ignites, the flow rate of hot combustion gases along the port begins to accelerate and, thereby, accelerates the heating of the preheated (but unignited) propellant.
- As the flow rate increases, the acceleration of the combustion gases becomes one of the limiting factors and flame spreading rate becomes largely a characteristic of the motor and not the igniter.
- As the hot combustion gases are driven down the port, the propellant is progressively heated to its ignition point, which is to say that flame spreading is described by successive ignitions.

The intrinsic capability of the p(x,t) model to calculate flame spreading rates is one of its main features.

Figure 5-7 is included to show a case in which the ignition delay is prominent. However, note that after first ignition occurs the p vs t characteristics are similar to those shown in Fig. 5-1, merely delayed by 0.1 seconds.

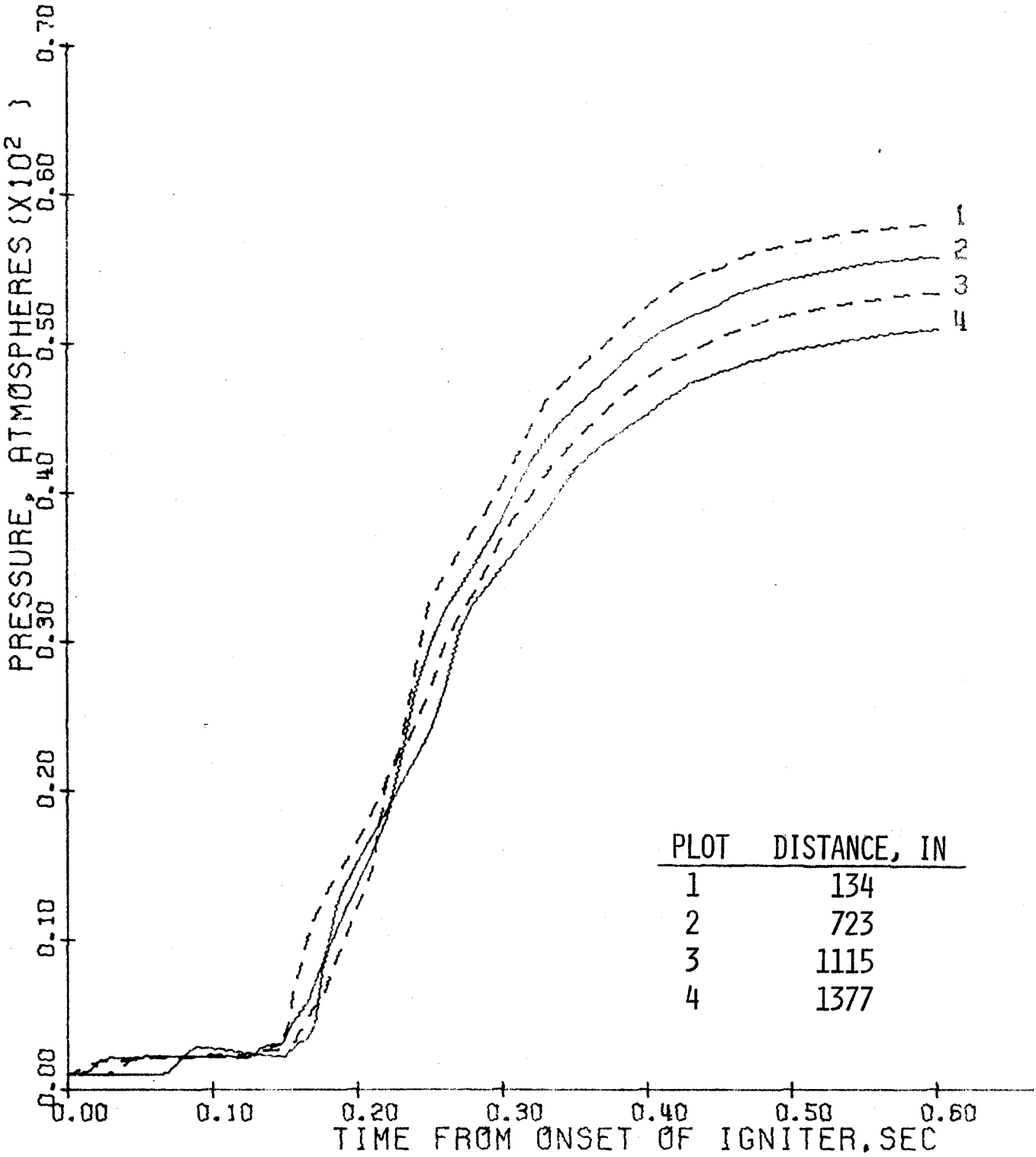

FIG. 5-7 EFFECT OF 27% DECREASE IN IGNITER FLOW RATE AND 25% DECREASE IN CALCULATED CONVECTIVE HEAT TRANSFER COEFFICIENT, COMPARED TO CONDITIONS OF FIG. 5-1.
(SRB4)

6.0 SOLID ROCKET BOOSTER CONSIDERED AS A SEGMENTED MOTOR

The motor configuration considered in this section is intended to approximate that of the Solid Rocket Motor for the Space Shuttle Booster,[25] which (as shown in Fig. 6-1a) consists of four segments. Since the burning surface area in the circumferential slots is inhibited, the burning surface associated with each circumferential slot is relatively small. The output associated with each slot is described in Table 6-1.

As shown in Table 6-2 and Table 6-3 (parts 1 and 2), the input is identical to that for the monolithic motors except that the geometry of the slots is specified as called for in Section 3. Similarly, the output format as shown in Table 6-3 (parts 3 through 5) is the same as for a monolithic motor except that the state and contribution of the slots is included as described in Table 6-1.

Figure 6-2 shows the pressure versus time at four positions along the grain. A direct comparison of the results for the segmented configuration (SRB/SEG1) with the results for the monolithic configuration reveals that the overall pressure response is very similar. However, as shown in Fig. 6-3 the flame spreading characteristics are influenced by the segments. These effects are attributed to the leading edge of each segment disturbing the boundary layer and thereby increasing the convective heat transfer coefficient.

The small influence of the slots on the overall ignition transient is not surprising since the surface areas and volumes associated with the slots are relatively small fractions of the totals, for the particular design considered.

Figures 6-4, 6-5, and 6-6 show the pressure, gas velocity, and gas temperature of the three slots. Figure 6-5 illustrates that the flows entering and exiting the slots are closely coupled to the pressure waves that occur in the main chamber. The flow oscillations in the slots are

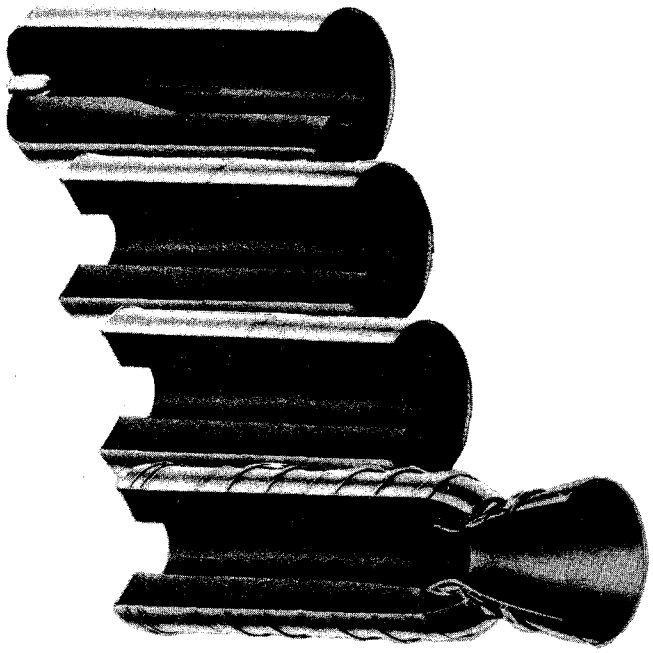

(a) Space Shuttle Solid Rocket Motor

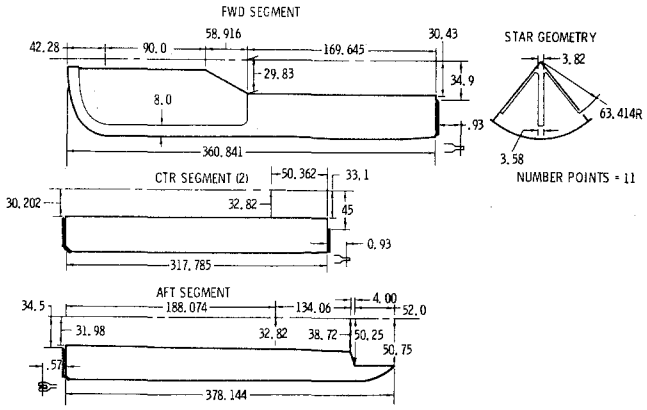

(b) SRM Propellant Grain Design

FIG. 6-1 TYPE OF SEGMENTED GEOMETRY CONSIDERED IN RUN SRB/SEG1 (FIGURES TAKEN FROM AIAA PAPER NO. 75-1170, REF. 25).

Table 6-1

OUTPUT ASSOCIATED WITH SLOTS

Each time the output is printed, the following information is given for each slot:

N	n	increment containing slot -	
PSLOT(N)	$p_{slot,n}$	pressure in slot	atm
TSLOT(N)	$T_{slot,n}$	temperature of slot	K
VSLOT(N)	$V_{slot,n}$	volume of slot	cm^3
SWIDTH(N)	$w_{slot,n}$	width of opening	cm
VELOCITY(N)	$v_{slot,n}$	velocity of gases at slot/main stream interface. When > 0, flow is exiting.	cm/sec
MSLOT/MCH	$(\rho u)_{slot}/(\rho u)_{ch}$	ratio of mass flux from slot to mass flux in main stream	--

Example of output associated with each slot:

PSLOT(ATM)	TSLOT(K)	VSLOT(CM3)	SWIDTH(CM)	VELOCITY(CM/SEC)
1.05	300.23	0.49817E 06	5.8420	-1924.03

Miscellaneous Output:

A) Precedes first time dependent output:

DELTAT=0.1667E-03	CSOUND=0.1061E 06	CPG=0.5872E 00	R=0.3005E 04
Initial time step seconds	Speed of sound at flame temperature conditions,cm/sec	Specific heat of combustion gases, cal/g-K	

B) Part of first time dependent output:

PROPELLANT AREA,CMSQ=2827989.00 CHAMBER VOLUME,CM**3=75151920.0

A_b $\int_0^{x_E} A_p dx$

TABLE 6-2
INPUT DATA FOR SEGMENTED MOTOR (SRB/SEG1)

```
SRB/SEG1 24          ERO TPSCRI=850  SAMPLE FOR MANUAL
&NAME
      THAX=.002
      TPRINT=.001
      DELTAT=.00016

      NDELX=21
      UNIT=-2.
      NPNPXT=0
      NPNPXT=2
      AT=2327.
      XP=3.
      XG=1341.3
      XE=1377.
      GAMA=1.1363
      W=28.21
      TFREF=3361.
      TIGN=2650.
      ROUFSUR=0.01
      FKPR=0.0011
      ROPR  = 1.758
      CPR=.3
      TPSCRI=750.
      TPSCRI=850.
      RREF=1.0783
      BREXP = 0.35
      EBC=0.
      CM=.98
      DE=145.64
      ALFAD=12.31
      NIGTAB=6
      NAPDVX = 22
&END
```

INPUT DIMENSIONS ARE IN INCHES

NOTE: LEAVE COLUMN 1 BLANK IN ALL NAMELIST INPUT

Print at 15-70

				INPUTS IN ADDITION TO THOSE REQUIRED FOR MONOLITHIC MOTOR			
				x_{slot}	$\delta A_{b,slot}$	δV_{slot}	W_{slot}
				XSLOT	DELABS	DELVS	WSLOT
0.	25.						
.020	560.						
.250	560.						
.340	300.						
.450	100.						
.50	0.						
3.	2554.	1018.92	1018.92				
68.42	2554.	1018.92	1018.92				
133.85	2554.	1018.92	1018.92				
199.3	2870.	608.	608.				
264.7	3187.	202.83	202.83				
330.1	3187.	202.83	202.83	361.	411.	30000.	2.3
395.6	3187.	202.83	202.83				
461.0	3187.	202.83	202.83				
526.4	3187.	202.83	202.83				
591.9	3187.	202.83	202.83				
657.3	3187.	202.83	202.83	681.	2660.	20000.	2.3
722.7	3187.	202.83	202.83				
788.1	3187.	202.83	202.83				
853.6	3187.	202.83	202.83				
919.	3187.	202.83	202.83				
984.4	3153.7	202.83	202.83	1001.	3212.	20000.	2.3
1049.9	3127.	202.83	202.83				
1115.3	3203.	202.83	202.83				
1180.7	3278.	202.83	202.83				
1246.1	3354.	202.83	202.83				
1311.6	3709.	202.83	202.83				
1377.0	4500.	202.83	202.83				

TABLE 6-2 (CONTINUED)

INPUT DATA FOR SEGMENTED MOTOR (SRB/SEG1)

```
&NAME
      TMAX=.01
      TPRINT=0.002
      DELFAC=1.3
&END
&NAME
      TPRINT=.005
      TMAX=.11
      DELFAC=2.
&END
&NAME
      TMAX=.2
&END
&NAME
      TMAX=.4
      TPRINT=.01
      DELFAC=1.5
&END
&NAME
      TMAX=.6
      TMAX=.5
      DELFAC=2.
&END
```

TABLE 6-3 (PART 1)

OUTPUT FROM SEGMENTED MOTOR RUN (SRB/SEG1)

- INPUT -


```
HIGH PERFORMANCE ROCKET MOTOR IGNITION TRANSIENT PREDICTION PROGRAM - SEGMENTED - FEB 1976
INCLUDES: SPATIAL & TIME DEVELOPMENT OF P,U,&T AND FLAME SPREADING

 SRB/SEG1 21       NO ERO TPSCRI=850       NEW FCT2

GENERAL:  LIMITS, CODE WORDS, & INITIAL CONDITIONS:
TMAX      LAMBDA      TPRINT      PZONE       DELTAT      NDELX
  0.002     1.00        0.001      7777.00  0.0001600     21

TPI       PAM         UNIT         NINERT   NPNPXT
 298.0     1.00         -2.           0         2

MOTOR CONFIGURATION PARAMETERS:
AT         XP          XG          XE
 2327.00   3.00     1341.30     1377.00

COMBUSTION GAS PROPERTIES
GAMA       W           TFREF       TIGN
 1.136    28.21       3361.0      2650.0

FRICTION TRANSFER AND HEAT TRANSFER COEF.:
RUFSUR     DDRG        DDHC
0.0100      1.00        1.00

PROPELLANT PROPERTIES:
FKPR       ROPR        CPR         TOREF       SIGP       TPSCRI
0.00110  1.758         0.30        298.00     0.00200     850.00

BURNING RATE RELATIONSHIP:
RREF       PREF        BREXP       EBC         EBEX
 1.078     66.08       0.3500       0.0      125.000

PARAMETERS USED IN THRUST CALCULATIONS:
DE         CM          ALFAD       EROAT       EROEXP
 145.64   0.980         12.31       0.0         0.80

IGNITER MASS DISCHARGE VS. TIME TABLE:
  TIME      FLOW RATE
  0.0            25.0
  0.0200        560.0
  0.2500        560.0
  0.3400        300.0
  0.4600        100.0
  0.5000          0.0
```

TABLE 6-3 (PART 2)

OUTPUT FROM SEGMENTED MOTOR RUN (SRB/SEG1)

- INPUT GEOMETRY -

PROPELLANT GEOMETRY TABLE:

LENGTH	PORT AREA	PROPELLANT PERIMETER	WETTED PERIMETER	UPSTRM OF SLOT	BURN AREA OF SLOT	VOLUME OF SLOT	WIDTH OF SLOT
3.00	2554.00	1018.92	1018.92	0.0	0.0	0.	0.0
68.43	2554.00	1018.92	1018.92	0.0	0.0	0.	0.0
133.86	2554.00	1018.92	1018.92	0.0	0.0	0.	0.0
199.30	2870.00	608.00	608.00	0.0	0.0	0.	0.0
264.70	3187.00	202.83	202.83	0.0	0.0	0.	0.0
330.10	3187.00	202.83	202.83	361.00	411.0	30400.	2.30
395.60	3187.00	202.83	202.83	0.0	0.0	0.	0.0
461.00	3187.00	202.83	202.83	0.0	0.0	0.	0.0
526.40	3187.00	202.83	202.83	0.0	0.0	0.	0.0
591.90	3187.00	202.83	202.83	0.0	0.0	0.	0.0
657.30	3187.00	202.83	202.83	681.00	2660.0	28600.	2.30
722.70	3187.00	202.83	202.83	0.0	0.0	0.	0.0
788.10	3187.00	202.83	202.83	0.0	0.0	0.	0.0
853.60	3187.00	202.83	202.83	0.0	0.0	0.	0.0
919.00	3187.00	202.83	202.83	0.0	0.0	0.	0.0
984.40	3153.70	202.83	202.83	1001.00	3212.0	28600.	2.30
1049.90	3127.00	202.83	202.83	0.0	0.0	0.	0.0
1115.30	3203.00	202.83	202.83	0.0	0.0	0.	0.0
1180.70	3278.00	202.83	202.83	0.0	0.0	0.	0.0
1246.10	3354.00	202.83	202.83	0.0	0.0	0.	0.0
1311.60	3709.00	202.83	202.83	0.0	0.0	0.	0.0
1377.00	4500.00	202.83	202.83	0.0	0.0	0.	0.0

BURNING RATE TABLE - R VS P

NDATA	NPPR
0	2

PRESSURE	RATE

****GEOMETRY CONVERTED FROM INCHES TO CENTIMETERS

LENGTH	PORT AREA	PROPELLANT PERIMETER	WETTED PERIMETER	UPSTRM OF SLOT	BURN AREA OF SLOT	VOLUME OF SLOT	WIDTH OF SLOT
7.62	16477.38	2588.06	2588.06	0.0	0.0	0.	0.0
173.81	16477.38	2588.06	2588.06	0.0	0.0	0.	0.0
340.00	16477.38	2588.06	2588.06	0.0	0.0	0.	0.0
506.22	18516.08	1544.32	1544.32	0.0	0.0	0.	0.0
672.34	20561.24	515.19	515.19	0.0	0.0	0.	0.0
838.45	20561.24	515.19	515.19	916.94	2651.6	498166.	5.84
1004.82	20561.24	515.19	515.19	0.0	0.0	0.	0.0

TABLE 6-3 (PART 3)
OUTPUT FROM SEGMENTED MOTOR RUN (SRB/SEG1)
- DURING FLAME SPREADING -

TIME =0.9000E-01 (208 DELTAT) DELTAT =0.5000E-03

N	DISTANCE CM	DISTANCE IN	PRESSURE ATM	PRESSURE PSIA	T DEG K	MACH NO.	RATE CM/SEC	BR/BRN	TAUB CM	FRICT. FACTOR	CONV. COEF.	M/A G/SEC CMSQ	TSURF K	PORT CMSQ
0	7.6	3.0	15.83	232.5	2653.3	0.078	0.65	1.000	0.0208	0.0	0.0315	15.16	850.	16531.1
1	173.8	68.4	15.09	221.7	2938.8	0.233	0.64	1.000	0.0160	0.0	0.0645	40.87	850.	16518.8
2	340.0	133.9	13.40	196.9	3074.2	0.415	0.61	1.000	0.0130	0.0	0.0880	63.06	850.	16511.1
3	506.2	199.3	10.64	156.3	3084.1	0.623	0.56	1.000	0.0100	0.0	0.0920	75.07	850.	18530.9
4	672.4	264.7	9.01	132.3	3066.8	0.749	0.53	1.000	0.0076	0.0	0.0808	76.56	850.	20565.1
5	838.6	330.1	8.81	129.4	3105.6	0.759	0.53	1.000	0.0068	0.0	0.0785	75.45	850.	20564.7
6	1004.8	395.6	8.56	125.8	3143.2	0.774	0.52	1.000	0.0058	0.0	0.0766	74.34	850.	20564.2
7	1170.9	461.0	8.40	123.4	3187.3	0.779	0.52	1.000	0.0051	0.0	0.0746	72.94	850.	20563.8
8	1337.1	526.4	8.15	119.8	3226.0	0.795	0.51	1.000	0.0044	0.0	0.0730	71.79	850.	20563.4
9	1503.3	591.9	7.88	115.8	3255.6	0.814	0.51	1.000	0.0036	0.0	0.0716	70.76	850.	20563.1
10	1669.5	657.3	7.61	111.8	3250.1	0.832	0.50	1.000	0.0027	0.0	0.0701	69.81	850.	20562.6
11	1835.7	722.7	7.36	108.2	3212.9	0.855	0.50	1.000	0.0019	0.0	0.0694	69.90	850.	20562.2
12	2001.9	788.1	7.17	105.3	3113.5	0.891	0.49	1.000	0.0012	0.0	0.0699	72.01	850.	20561.8
13	2168.1	853.6	6.87	100.9	2940.7	0.937	0.48	1.000	0.0005	0.0	0.0704	74.62	850.	20561.5
14	2334.3	919.0	6.60	97.0	2748.6	0.966	0.0	0.0	0.0	0.0030	0.0706	76.55	820.	20561.2
15	2500.4	984.4	6.39	93.9	2577.9	0.989	0.0	0.0	0.0	0.0030	0.0710	78.33	762.	20346.3
16	2666.6	1049.9	6.35	93.3	2397.5	0.982	0.0	0.0	0.0	0.0029	0.0714	80.15	701.	20174.2
17	2832.8	1115.3	6.28	92.3	2161.6	0.976	0.0	0.0	0.0	0.0029	0.0721	83.13	629.	20664.4
18	2999.0	1180.7	6.42	94.3	1850.2	0.971	0.0	0.0	0.0	0.0029	0.0755	91.67	555.	21148.4
19	3165.2	1246.1	6.77	99.5	1466.5	0.956	0.0	0.0	0.0	0.0029	0.0816	108.13	475.	21640.1
20	3331.4	1311.6	7.16	105.2	997.7	0.760	0.0	0.0	0.0	0.0029	0.0754	112.75	387.	23926.0
21	3497.6	1377.0	6.79	129.1	569.1	0.326	0.0	0.0	0.0	0.0030	0.0	75.63	321.	29032.2

PESTAG.ATM= 9.33 PESTAG.PSIA= 137.12 MASS BURNED= 0.4029E 05

THRUST NEWTONS	THRUST LBF	CFLM -	AT CM**2	EPSONG -	EPSON -	PA/PE
1651665.0	371310.7	1.1637	15010.000	7.1604	3.7521	1.992

N	PSLOT(ATM)	TSLOT(K)	VSLOT(CM3)	SWIDTH(CM)	VELOCITY(CM/SEC)
6	8.56	1610.88	0.49816E 06	5.8537	-3423.28

N	PSLOT(ATM)	TSLOT(K)	VSLOT(CM3)	SWIDTH(CM)	VELOCITY(CM/SEC)
10	7.61	1358.39	0.46671E 06	5.8473	967.43

N	PSLOT(ATM)	TSLOT(K)	VSLOT(CM3)	SWIDTH(CM)	VELOCITY(CM/SEC)
15	6.39	857.72	0.46667E 06	5.8420	-7282.38

TABLE 6-3 (PART 4)
OUTPUT FROM SEGMENTED MOTOR RUN (SRB/SEG1)
- AT BEGINNING OF RAPID PRESSURE RISE -

TIME =0.1200E 00 (258 DELTAT) DELTAT =0.1000E-02

N	DISTANCE CM	DISTANCE IN	PRESSURE ATM	PRESSURE PSIA	T DEG K	MACH NO.	RATE CM/SEC	BR/BRN	TAUB CM	FRICT. FACTOR	CONV. COEF.	M/A G/SEC	TSURF CMSQ	TSURF K	PORT CMSQ
0	7.6	3.0	21.32	313.2	2655.9	0.058	0.72	1.000	0.0413	0.0		0.0313	15.06	850.	16583.9
1	173.8	68.4	20.51	301.3	2970.3	0.185	0.71	1.000	0.0362	0.0		0.0683	43.81	850.	16570.9
2	340.0	133.9	18.79	276.0	3096.9	0.335	0.69	1.000	0.0326	0.0		0.0971	71.10	850.	16561.7
3	506.2	199.3	16.12	236.7	3105.1	0.465	0.65	1.000	0.0283	0.0		0.1049	88.15	850.	18559.2
4	672.4	264.7	15.47	227.3	3103.2	0.497	0.64	1.000	0.0253	0.0		0.0897	86.85	850.	20574.1
5	838.6	330.1	16.15	237.2	3135.3	0.465	0.65	1.000	0.0246	0.0		0.0861	84.32	850.	20573.8
6	1004.8	395.6	15.86	233.0	3151.6	0.485	0.65	1.000	0.0235	0.0		0.0863	86.24	850.	20573.2
7	1170.9	461.0	15.88	233.2	3178.2	0.487	0.65	1.000	0.0228	0.0		0.0853	86.20	850.	20572.8
8	1337.1	526.4	15.77	231.7	3201.8	0.494	0.65	1.000	0.0219	0.0		0.0847	86.64	850.	20572.4
9	1503.3	591.9	15.74	231.1	3230.7	0.495	0.65	1.000	0.0211	0.0		0.0837	86.23	850.	20572.0
10	1669.5	657.3	15.84	232.6	3252.5	0.490	0.65	1.000	0.0201	0.0		0.0826	85.65	850.	20571.5
11	1835.7	722.7	16.14	237.1	3284.6	0.472	0.65	1.000	0.0192	0.0		0.0804	83.55	850.	20571.0
12	2001.9	788.1	17.01	249.9	3331.6	0.424	0.66	1.000	0.0185	0.0		0.0763	78.60	850.	20570.6
13	2168.1	853.6	18.23	267.8	3386.8	0.361	0.68	1.000	0.0177	0.0		0.0702	71.20	850.	20570.3
14	2334.3	919.0	19.29	283.4	3439.4	0.311	0.69	1.000	0.0171	0.0		0.0645	64.34	850.	20569.9
15	2500.4	984.4	19.63	288.4	3472.1	0.303	0.70	1.000	0.0164	0.0		0.0637	63.58	850.	20354.7
16	2666.6	1049.9	19.09	280.5	3493.0	0.323	0.69	1.000	0.0158	0.0		0.0651	65.67	850.	20182.3
17	2832.8	1115.3	18.53	272.2	3508.2	0.354	0.68	1.000	0.0150	0.0		0.0677	69.63	850.	20672.0
18	2999.0	1180.7	17.90	262.9	3516.6	0.385	0.68	1.000	0.0142	0.0		0.0670	69.32	850.	21155.7
19	3165.2	1246.1	17.62	258.9	3531.5	0.391	0.67	1.000	0.0134	0.0		0.0693	72.85	850.	21647.0
20	3331.4	1311.6	17.10	251.1	3486.0	0.382	0.66	1.000	0.0088	0.0		0.0628	65.87	850.	23932.5
21	3497.6	1377.0	17.72	260.3	3383.4	0.326	0.0	0.0	0.0	0.0		0.0	62.53	874.	29036.7

PESTAG.ATM= 18.82 PESTAG.PSIA= 276.48 MASS BURNED= 0.1279E 06

THRUST NEWTONS	THRUST LBF	CFLM -	AT CM**2	EPSONG -	EPSON -	PA/PE
3760539.0	845406.6	1.3141	15010.000	7.1604	6.6401	2.102

N	PSLOT(ATM)	TSLOT(K)	VSLOT(CM3)	SWIDTH(CM)	VELOCITY(CM/SEC)
6	15.86	2162.83	0.49816E 06	5.8897	-1434.37

N	PSLOT(ATM)	TSLOT(K)	VSLOT(CM3)	SWIDTH(CM)	VELOCITY(CM/SEC)
10	15.64	2309.84	0.48896E 06	5.8827	726.69

N	PSLOT(ATM)	TSLOT(K)	VSLOT(CM3)	SWIDTH(CM)	VELOCITY(CM/SEC)
15	19.63	2055.78	0.48896E 06	5.8754	2025.19

TABLE 6-3 (PART 5)
OUTPUT FROM SEGMENTED MOTOR RUN (SRB/SEG1)
- APPROACHING FULL CHAMBER PRESSURE -

TIME =0.4700E 00 (574 DELTAT) DELTAT =0.1250E-(

N	DISTANCE CM	DISTANCE IN	PRESSURE ATM	PRESSURE PSIA	T DEG K	MACH NO.	RATE CM/SEC	BR/BRN	TAUB CM	FRICT. FACTOR	CONV. COEF.	M/A G/SEC CMSQ	TSURF K	PORT CMSQ
0	7.6	3.0	60.75	892.4	2651.5	0.002	1.04	1.000	0.3789	0.0	0.0051	1.55	850.	17457.2
1	173.8	68.4	60.25	885.0	2928.3	0.071	1.03	1.000	0.3725	0.0	0.0754	50.05	850.	17440.5
2	340.0	133.9	59.49	873.8	3060.8	0.145	1.03	1.000	0.3663	0.0	0.1245	98.10	850.	17424.8
3	506.2	199.3	57.53	845.2	3103.4	0.199	1.02	1.000	0.3567	0.0	0.1421	129.36	850.	19065.8
4	672.4	264.7	57.24	840.8	3118.1	0.201	1.01	1.000	0.3530	0.0	0.1236	129.76	850.	20742.4
5	838.6	330.1	57.15	839.5	3131.1	0.210	1.01	1.000	0.3525	0.0	0.1250	134.74	850.	20742.1
6	1004.8	395.6	56.88	832.6	3140.3	0.225	1.01	1.000	0.3503	0.0	0.1291	143.04	850.	20741.0
7	1170.9	461.0	56.38	828.2	3149.0	0.237	1.01	1.000	0.3491	0.0	0.1322	149.86	850.	20740.3
8	1337.1	526.4	55.94	821.8	3157.0	0.251	1.01	1.000	0.3474	0.0	0.1357	157.13	850.	20739.4
9	1503.3	591.9	55.57	816.3	3163.7	0.264	1.00	1.000	0.3458	0.0	0.1392	164.31	850.	20738.6
10	1669.5	657.3	55.09	809.3	3171.3	0.278	1.00	1.000	0.3438	0.0	0.1426	171.27	850.	20737.6
11	1835.7	722.7	54.56	801.5	3175.9	0.297	1.00	1.000	0.3419	0.0	0.1478	181.12	850.	20736.7
12	2001.9	788.1	54.01	793.4	3180.2	0.308	0.99	1.000	0.3400	0.0	0.1495	185.57	850.	20735.7
13	2168.1	853.6	53.63	787.9	3185.2	0.327	0.99	1.000	0.3384	0.0	0.1547	195.47	850.	20734.9
14	2334.3	919.0	52.85	776.3	3186.7	0.338	0.99	1.000	0.3361	0.0	0.1559	199.03	850.	20733.7
15	2500.4	984.4	52.54	771.8	3193.4	0.363	0.98	1.000	0.3345	0.0	0.1634	212.38	850.	20518.0
16	2666.6	1049.9	51.17	751.6	3190.7	0.383	0.98	1.000	0.3309	0.0	0.1659	217.99	850.	20344.0
17	2832.8	1115.3	51.19	752.0	3197.6	0.396	0.98	1.000	0.3298	0.0	0.1693	225.75	850.	20833.5
18	2999.0	1180.7	50.18	737.1	3197.3	0.394	0.97	1.000	0.3270	0.0	0.1643	219.64	850.	21316.2
19	3165.2	1246.1	50.53	742.3	3205.5	0.411	0.97	1.000	0.3266	0.0	0.1697	230.56	850.	21807.7
20	3331.4	1311.6	49.69	729.9	3207.5	0.364	0.97	1.000	0.3204	0.0	0.1497	200.72	850.	24092.4
21	3497.6	1377.0	52.08	765.0	3226.4	0.324	0.0	0.0	0.0	0.0	0.0	187.02	874.	29196.6

PESTAG.ATM= 55.27 PESTAG.PSIA= 811.92 MASS BURNED= 0.1731E 07

THRUST NEWTONS	THRUST LBF	CFLM -	AT CM**2	EPSUNG -	EPSON -	PA/PE
13021060.0	2927268.0	1.5494	15010.000	7.1604	7.1604	0.789

N	PSLOT(ATM)	TSLOT(K)	VSLOT(CM3)	SWIDTH(CM)	VELOCITY(CM/SEC)
0	56.66	3153.66	0.49797E 06	6.5436	219.92

N	PSLOT(ATM)	TSLOT(K)	VSLOT(CM3)	SWIDTH(CM)	VELOCITY(CM/SEC)
10	55.09	3378.36	0.47347E 06	6.5306	1569.60

N	PSLOT(ATM)	TSLOT(K)	VSLOT(CM3)	SWIDTH(CM)	VELOCITY(CM/SEC)
15	52.54	3374.29	0.47454E 06	6.5120	1961.87

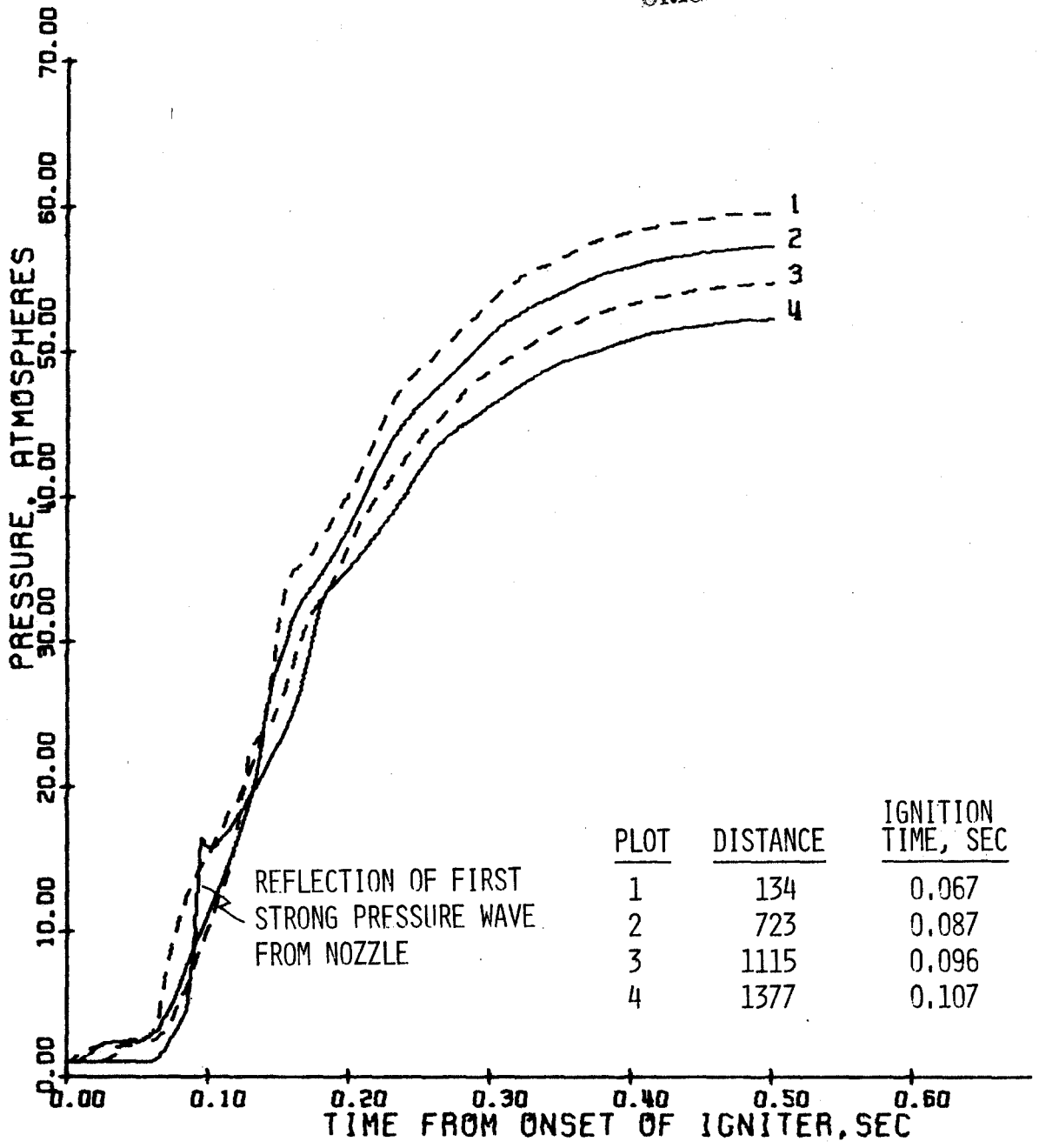

PLOT	DISTANCE	IGNITION TIME, SEC
1	134	0.067
2	723	0.087
3	1115	0.096
4	1377	0.107

FIG. 6-2 PRESSURE DEVELOPMENT ALONG PORT OF SEGMENTED MOTOR
(SRB/SEG1 FOUR SEGMENT MOTOR)

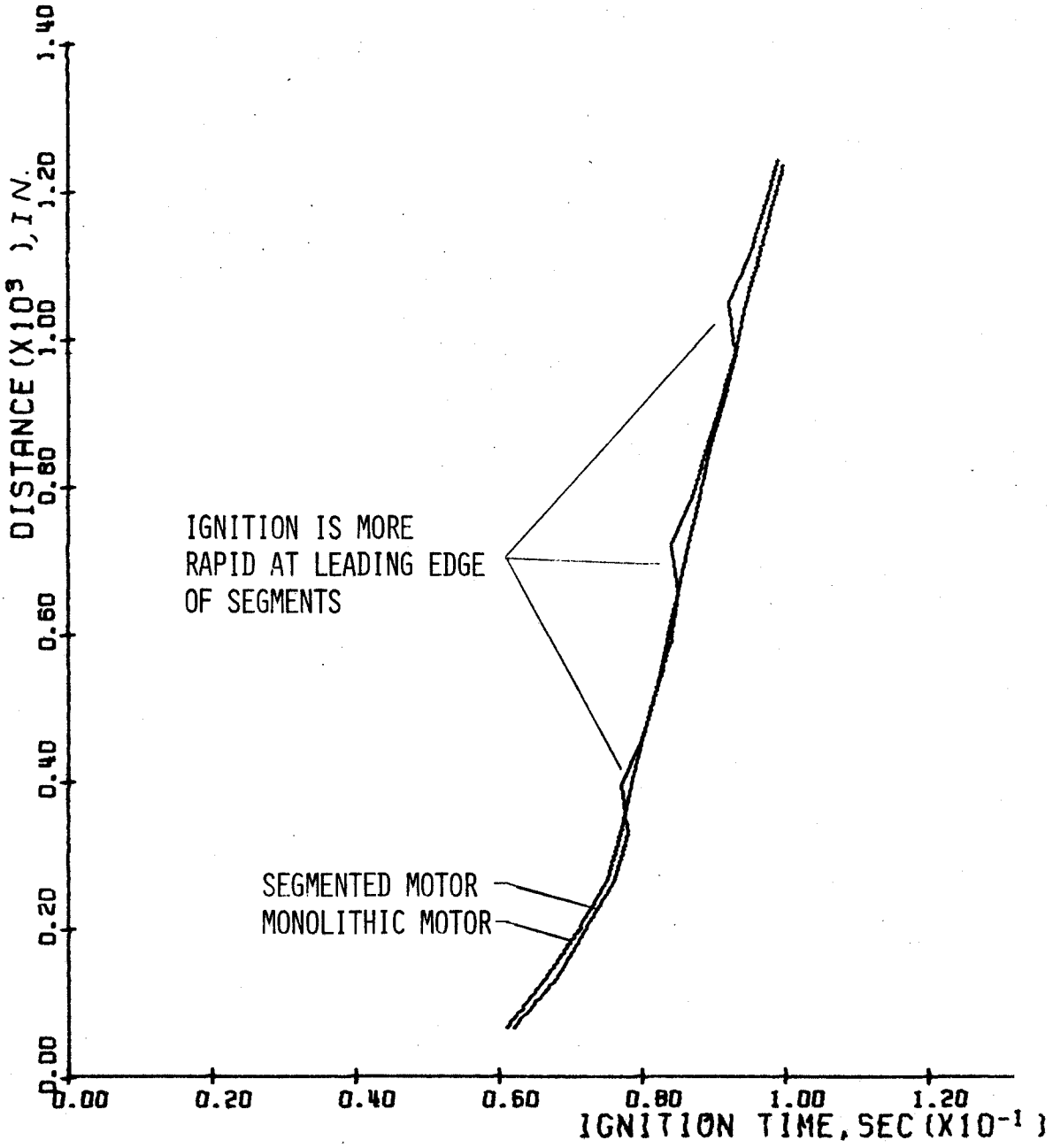

FIG.6-3 FLAME SPREADING TIMES OF SEGMENTED MOTOR COMPARED WITH FLAME SPREADING TIMES OF MONOLITHIC MOTOR (SRB/SEG1 COMPARED TO SRB1)

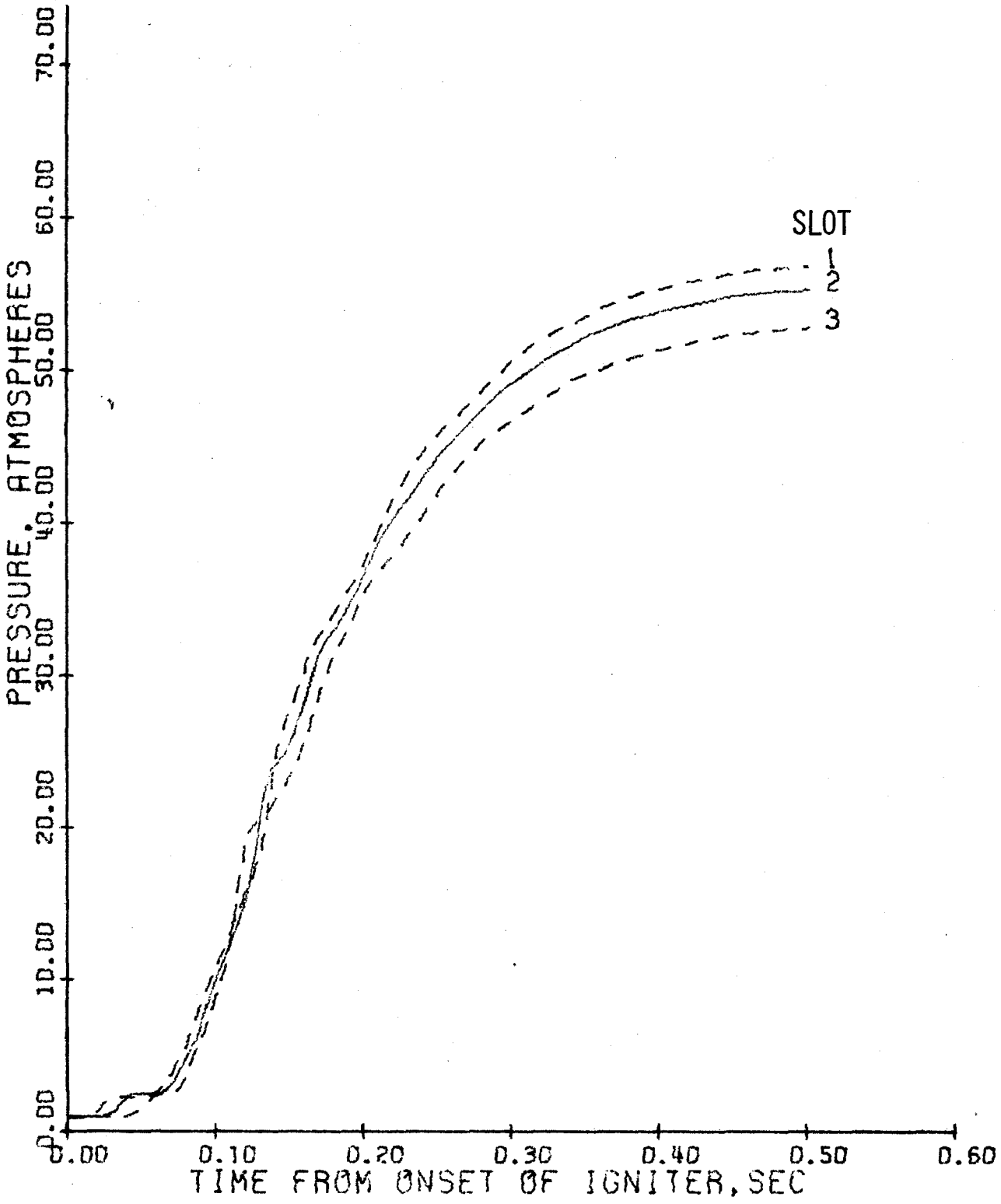

FIG. 6-4 PRESSURE TRANSIENTS IN SLOTS.

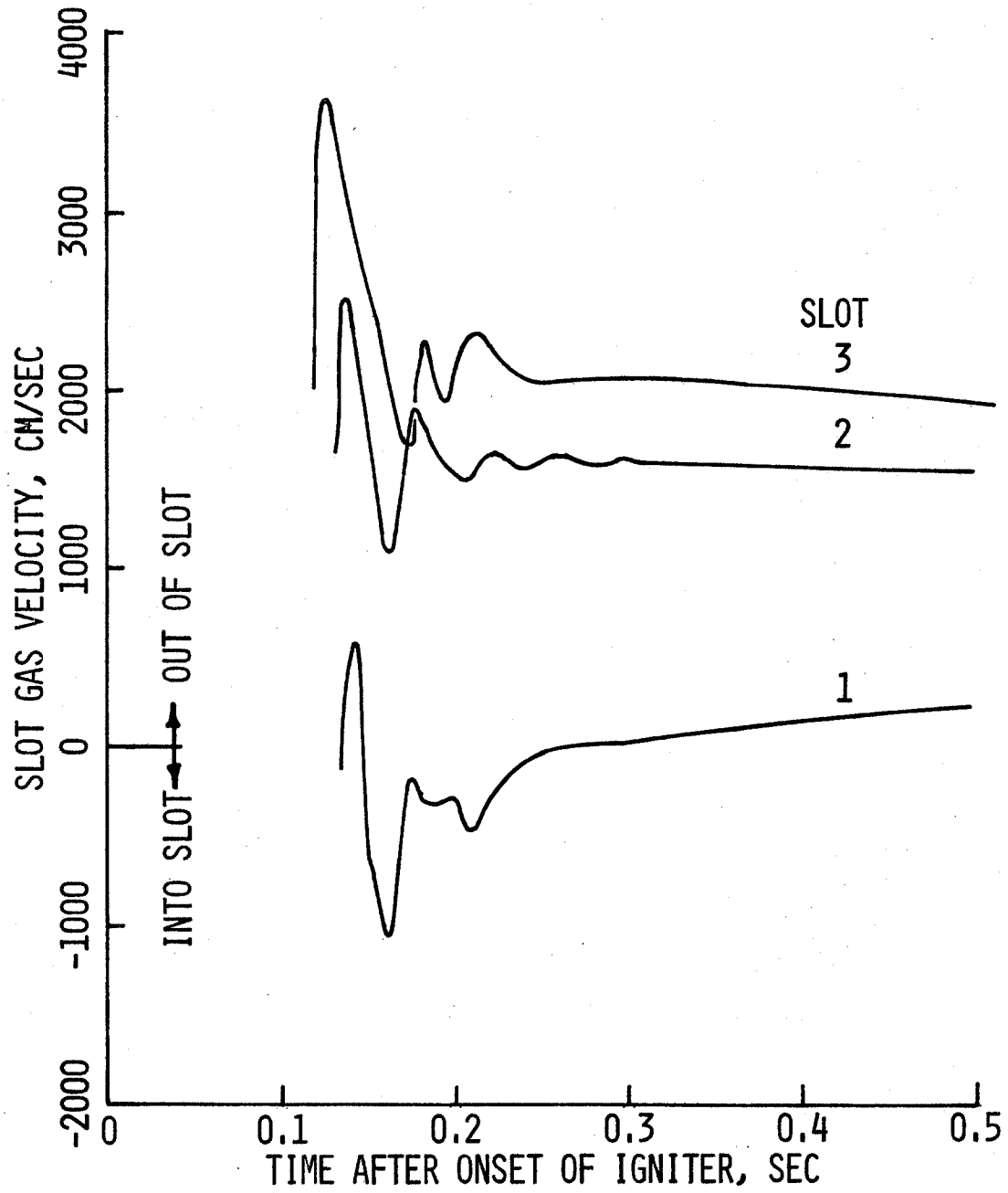

Fig. 6-5 Following ignition of burning surface in slots, the gas velocity entering and exiting the slot is very sensitive to pressure oscillation in the main chamber.

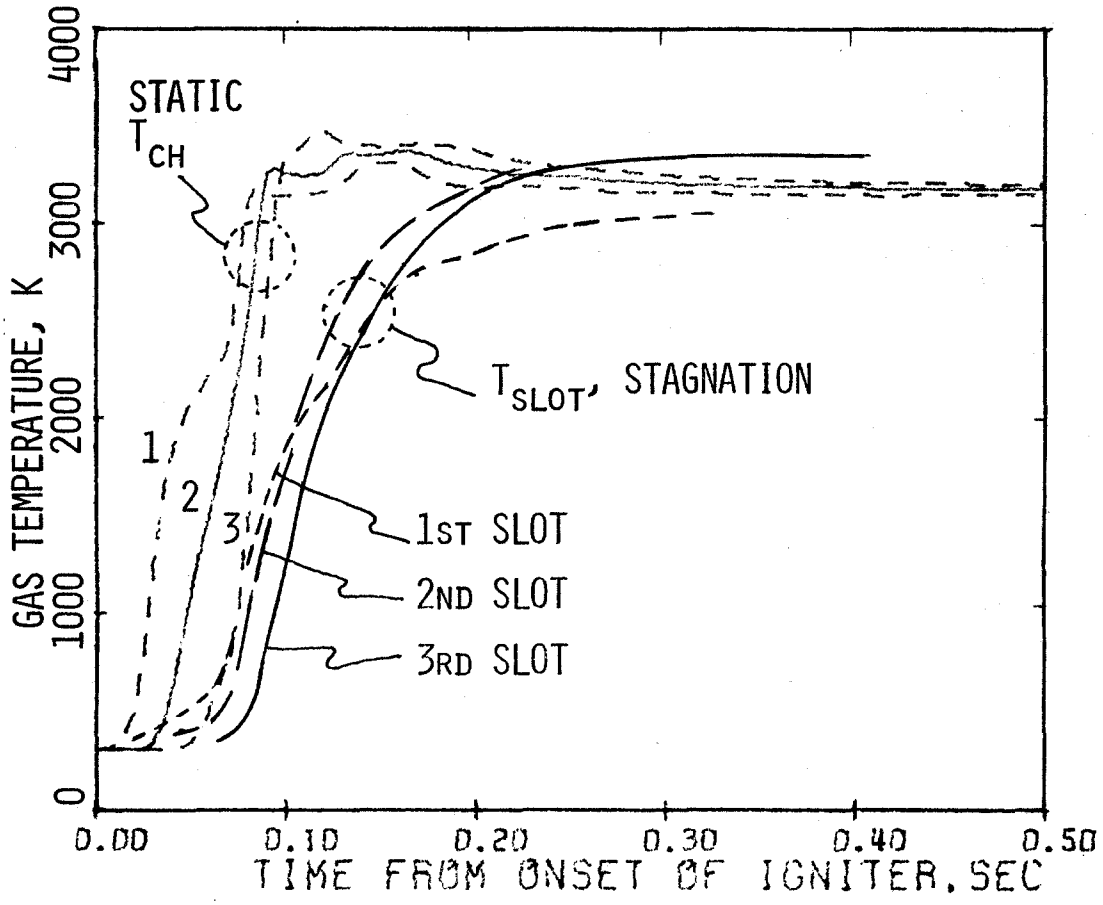

Fig. 6-6 Mean gas temperatures in slots lag the gas temperatures in the main stream.

complex, since each slot has its own characteristic filling and venting time. During the flame spreading interval, the net flow is entering the slots. After ignition of the burning surface area in the slots and during the early stages of chamber pressurization, the small amount of mass generated by the relatively small burning surface in each slot serves to partially pressurize the volume in the slot. The two downstream slots with their larger surface areas produce a net outflow of gas during the early phase of chamber pressurization, whereas the upstream slot begins to produce an outflow toward the end of chamber pressurization. As shown by the temperature differences (between the chamber and slot gases) in Fig. 6-6, the time required to flush the warm gases from the slots is appreciable.

A comparison of the pressure oscillations predicted for the monolithic motor (Fig. 5-1) with those of the segmented motor reveals that the volumes between the segments and mass flow entering and exiting the slots serve to damp the longitudinal waves. This illustrates a very important intrinsic feature of the solution -- the ability to analyze certain aspects of longitudinal combustion instability in segmented motors. Indeed, a logical follow-up of the present study is to extend the computer program and use it as part of a study to determine the extent to which the slots in the present SRB design reduce the possibility of axial mode combustion instability.

As shown in Fig. 6-1, the nozzle of the head-end igniter is very close to star-point tips in the first segment. It has been pointed out[26] that treating the head-end region as a uniformly heated port (as in the present analysis) results in unrealistically long induction periods (see Fig. 2-1 definition). A better simulation would be obtained by considering at least three zones of heating and ignition in the first segment: (1) the more intense heating and rapid ignition of the star-point tips, (2) the increasing heating

rate in the axial slots as the gas generated by the burning star-point tips augments the axial flow of hot gases, and (3) the conventional heating of the aft portion of the first segment. Thus, the net effect will be to reduce the predicted induction time which is a major contributor to the uncertainty associated with motor-to-motor variation in time-to-full-chamber-pressure. Recall that the results of Section 5 showed that flame spreading rate is relatively insensitive to the variations that may occur within the motor, whereas time to first ignition is affected greatly by small variations.

The analysis of the interaction of the slot flow and the main chamber flow is based on the assumption that the slots have been properly designed and that the aerodynamic interactions between the two flows will not produce appreciable pressure drops across the slots. Reference 27 describes analytical and experimental methods for determining the severity of aerodynamic interactions and prescribes a design approach to eliminate the undesirable affects. The user of the program is cautioned to insure that the particular slots being analyzed conform to the assumptions and conditions stated in Section 2.

7.0 CONCLUSION

The analytical model described in this report provides for the first time a means of analyzing the complexities of ignition transients and pressure peaks of large, high-performance, segmented SRB's. This is accomplished by accounting for (1) the temporal and spatial development of the flow field set up by the igniter discharge, (2) ignition and flame spreading coupled to chamber flow, (3) the large velocity, pressure, and temperature gradients that occur during the early phases of ignition, and (4) the interactions that combine to produce peak pressures (i.e., compression of chamber gases during pressurization, erosive burning, and mass-added effect of igniter discharge).

As the pursuit of higher performance rocket motors continues and the present configurations are upgraded (i.e., by increasing loading density, using high-performance propellant, and extending ambient temperature range), the methods described in the report will enable analysts to predict maximum pressures with much greater confidence than was heretofore possible.

The calculated results in this report are intended to introduce the user to the computer program and are not intended to be a comprehensive investigation of a particular SRB design. Nevertheless, the results of Section 5 and 6 produced several interesting insights. Once the head-end section of the SRB ignites, the subsequent flame spreading rate is a motor property that is largely unaffected by changes in the igniter, the erosive burning contribution, and the propellant ignition temperature; whereas, the time of first ignition is strongly dependent on igniter characteristics and propellant ignition temperature. The contributions of the burning surface areas and volumes in the slots of the present SRB design do not greatly influence the times of the important ignition events. The interactions

of the main chamber flow with the slots tend to damp axial pressure waves which are set up toward the end of flame spreading.

The ignition prediction and analysis procedures described in the report can be applied to a wide variety of rocket motor applications and are not limited to large, segmented boosters. Special purpose applications can be achieved by extensions to the present program, e.g., aft-end ignition; flame spreading delays produced by restrictors (e.g., used to reduce ignition spikes); ignition of degraded or wet propellant surfaces; case expansion (and A_p/A_t increases) during pressurization of low safety factor motor cases; and nozzle closures. In its present form the program contains many of the elements necessary for the analysis of axial mode combustion instability in segmented motors.

REFERENCES

1. Peretz, A., Caveny, L. H., Kuo, K. K., and Summerfield, M., "The Starting Transient of Solid-Propellant Rocket Motors With High Internal Gas Velocities," AMS Report No. 1100 and NASA CR-136274, April 1973, Princeton University, Princeton, N.J. (Order from NTIS as N 74-13506); also summarized in AIAA Journal, Vol. 11, No. 12, December 1973, pp. 1719-1727.

2. DeSoto, S. and Friedman, H. A., "Flame Spreading and Ignition Transients in Solid Grain Propellants," AIAA Journal, Vol. 3, March 1965, pp. 405-412.

3. Sforzini, R. H., "Extension of a Simplified Computer Program for Analysis of Solid-Propellant Rocket Motors," NASA CR-129024, Auburn Univ., Auburn, Ala., April 1973.

4. Caveny, L. H. and Summerfield, M., "Micro-Rocket Impulsive Thrusters," Aerospace and Mechanical Science Report No. 1014, Nov. 1971, Princeton University, Princeton, N.J.

5. Bradley, H. H. Jr., "Theory of a Homogeneous Model of Rocket Motor Ignition Transients," AIAA Preprint No. 64-127, Jan. 1964.

6. Most, W. J. and Summerfield, M., "Starting Thrust Transients of Solid Rocket Engines," AMS Report No. 873, July 1969, Princeton University, Princeton, N.J.

7. Threewit, T. R., Rossini, R. A., and Uecker, R. L., "The Integrated Design Computer Program and the ACP-1103 Interior Ballistics Computer Program," Report No. STM-180, Dec. 1964, Aerojet-General Corp., Sacramento, Ca.

8. Vellacott, R. J. and Caveny, L. H., "A Computer Program for Solid Propellant Rocket Motor Design and Ballistic Analysis," ARS Preprint No. 2315-62, Waco, Texas, Jan. 1962.

9. Carlson, L. W. and Seader, J. D., "Heat Transfer Characteristics of Hot-Gas Ignition," AIAA Journal, Vol. 5, No. 7, July 1967, pp. 1272-1279.

10. Wrubel, J. A. and Carlson, L. W., "Study of Heat Transfer Characteristics of Hot-Gas Igniters," Technical Rept. AFRPL-TR-67-267, July 1967, Rocketdyne, Canoga Park, Ca.

11. Kilgroe, J. D., "Studies on Ignition and Flame Propagation on Solid Propellants," UTC 2229-FR, Nov. 1967, United Technology Center, Sunnyvale, Ca.

12. Humble, L. V., Lowdermilk, W. H. and Desmon, L. G., "Measurements of Average Heat-Transfer and Friction Coefficients for Subsonic Flow of Air in Smooth Tubes at High Surface and Fluid Temperatures," Rept. 1020, 1951, NASA.

13. Cohen, N. S., Derr, R. L., and Price, C. F., "Study of Ignition and Extinguishment in Multiple Stop-Restart Duty Cycles," 8th JANNAF Combustion Meeting, Vol. II (CPIA Publication 220), Nov. 1971.

14. Shapiro, A. H. and Smith, R. D., "Friction Coefficients in the Inlet Length of Smooth Round Tubes," NACA TN No. 1785, Nov. 1948.

15. Lenoir, J. M. and Robillard, G., "A Mathematical Method to Predict the Effects of Erosive Burning in Solid Propellant Rockets," Sixth Symposium (International) on Combustion, Reinhold, New York, 1957, pp. 663-667.

16. Lawrence, W. J., Matthews, D. R., and Deverall, L. I., "The Experimental and Theoretical Comparison of the Erosive Burning Characteristics of Composite Propellants," ICRPG/AIAA 3rd Solid Propulsion Conference (June 4-6, 1968), AIAA Paper No. 68-531.

17. Goodman, T. R., "Application of Integral Methods to Transient Nonlinear Heat Transfer," Advances in Heat Transfer, Vol. 1, Academic Press, 1964, pp. 51-122.

18. Courant, R., and Hilbert, D., Methods of Mathematical Physics, Vol. 2, Interscience Publishers, Inc., New York, July 1966, pp. 407-550.

19. Kuo, K. K., Vichnevetsky, R. and Summerfield, M., "Theory of Flame Front Propagation in Porous Propellant Charges under Confinement," AMS Report 1000, Aug. 1971, AMS Dept., Princeton University, Princeton, N.J. (Order from NTIS as AD 762063.)

20. Richtmyer, R. D. and Morton, K. W., Difference Methods for Initial-Value Problems, Interscience Publishers, New York, 1967.

21. Salvadori, M. G. and Baron, M. L., Numerical Methods in Engineering, Prentice Hall, Inc., Englewood Cliffs, N.J., 1961.

22. Vichnevetsky, R., Computer Methods for Partial Differential Equations (Course Notes - Spring 1975), Rutgers, The State University of New Jersey, New Brunswick, N.J.

23. Shapiro, A. H., The Dynamics and Thermodynamics of Compressible Fluid Flow, Vol. II, The Ronald Press Co., New York, 1954.

24. Isaacson, E. and Keller, H. B., Analysis of Numerical Methods, Wiley, New York, 1966, pp. 58-61.

25. Thirkill, J. "Solid Rocket Motor for the Space Shuttle Booster, AIAA Paper No. 75-1170, Sept. 1975.

26. Thurston, J. R., Personal Communication, Thiokol Corp., Wasatch Division, 5 March 1976.

27. Glick, R. L., Thurman, J. L. and Caveny, L. H., "The Internal Ballistics of Slotted Tube Solid Propellant Rocket Motors," Journal of Spacecraft and Rockets, July 1967, pp. 525-530.

APPENDIX A

Performance Parameters

The motor performance equations are presented to specify the manner in which the motor parameters are applied. A compatible set of combustion gas properties is established by starting with calculated combustion gas properties (obtained from thermochemistry computer programs) and then adjusting the calculated properties to obtain agreement with measured mass flow rates and thrusts. Careful attention should be given to accounting for items such as heat loss, combustion efficiencies, and ambient temperature. The measured value of c* that is normally used to calculate the mass discharge is established from motor p vs t data and weight of propellant burned, w_{pr}, by the following equation

$$c^*_{meas} = \frac{gA_t \int p_{E,stag}}{w_{pr}} \qquad \text{(A-1)}$$

The quantity c^*_{meas} is used to relate instantaneous mass flow rate, m_n, to throat area, A_t, and chamber pressure, $p_{E,stag}$

$$m_n = A_t p_{E,stag} g/c^*_{meas} \qquad \text{(A-2)}$$

From isentropic one-dimensional compressible flow theory, mass discharge rate can be expressed in terms of the gas properties as follows.

$$m = p_{E,stag} A_t g \frac{\gamma^{1/2}\left(\frac{2}{\gamma+1}\right)^{\frac{\gamma+1}{2(\gamma-1)}}}{\sqrt{gR_g T_{E,stag}/\bar{W}}} \qquad \text{(A-3)}$$

Ideally, c^* is defined in terms of the chamber gas properties as

$$c^* = \frac{\sqrt{gR_g T_f/\overline{W}}}{\gamma^{1/2}\left(\frac{2}{\gamma+1}\right)^{\frac{\gamma+1}{2(\gamma-1)}}} \qquad \text{(A-4)}$$

i.e., the chamber temperature is the same as the flame temperature under no loss, equilibrium conditions.

To have a compatible set of relationships, the consistency between c^*_{meas} and $T_{ch,act}$ established by Eq. (A-5) is maintained throughout the analysis.*

$$T_{ch,act} = \frac{\overline{W}}{gR_g}\left[c^*_{meas}\gamma^{1/2}\left(\frac{2}{\gamma+1}\right)^{\frac{\gamma+1}{2(\gamma-1)}}\right]^2 \qquad \text{(A-5)}$$

Thus, the input value of $T_{f,ref}$ used in the program should be $T_{ch,act}$.

The ratio of specific heats, γ, is an average effective value for the motor and nozzle. When possible, this value was determined from experimental data. Because of shifting equilibrium during flow through the nozzle, this value is little more than empirical correlation constant. When satisfactory experimental data is not available, an effective value based on thermochemical calculations can be deduced

---

*Using $T_{ch,act}$ has the effect of lumping other losses (i.e., nozzle discharge and two phase flow) with combustion efficiency losses. A more thorough approach to establishing $T_{ch,act}$ could be based on the Standard Performance Prediction program recently developed by the U.S.A.F. Rocket Propulsion Laboratory or the Thiokol Performance Prediction program recently developed by the Wasatch Division of the Thiokol Corporation.

from the relationship between theoretical gas properties at chamber and exit condictions,

$$\frac{T_{ch}}{T_{ex}} = \left(\frac{p_{ch}}{p_{ex}}\right)^{\frac{\gamma - 1}{\gamma}} \tag{A-6}$$

or between the theoretical gas properties at chamber and nozzle throat conditions,

$$\frac{T_{ch}}{T_{t}} = \left(\frac{p_{ch}}{T_{t}}\right)^{\frac{\gamma - 1}{\gamma}} \tag{A-7}$$

Thrust is expressed in terms of a thrust coefficient as

$$F = C_{F\lambda m} p_{E,stag} A_t \tag{A-8}$$

The particular thrust coefficient used in the program is

$$C_{F\lambda m} = C_m \left[C_{FV} \lambda_N + (1 - \lambda_N) \frac{p_{ex}}{p_{E,stag}} \varepsilon_{ex} \right] - \frac{p_{am}}{p_{E,stag}} \varepsilon_{ex} \tag{A-9}$$

where

$$C_{FV} + \left\{ \left[\frac{2\gamma^2}{\gamma - 1} \left(\frac{2}{\gamma + 1} \right)^{\frac{\gamma + 1}{\gamma - 1}} \right] \left[1 - \left(\frac{p_{ex}}{p_{E,stag}} \right)^{\frac{\gamma - 1}{\gamma}} \right] \right\}^{1/2}$$

$$+ \varepsilon_{ex} \frac{p_{ex}}{p_{E,stag}} \tag{A-10}$$

and

$$\lambda_N = (1 + \cos \alpha_n)/2 \tag{A-11}$$

The value of motor coefficient, C_m, used in the equation is for nozzle-end stagnation pressure and should not be confused with values that were determined from the relationship between head-end pressure and measured thrust. Also, note that C_m does not multiply the last term in Eq. (A-9).

APPENDIX B

MODIFIED* C.G.S UNITS FOR PROPELLANT COMBUSTION CALCULATIONS

and

APPROXIMATIONS TO GAS PROPERTIES

Gas Law: $p/\rho = (R_g/W)T$

p -[atm] , T -[K]

ρ -[g/cm^3] , W -[g/g-mole] (B-1)

$$R_g = 82.05\left[\frac{cm^3 atm}{g\text{-}mol\text{-}K}\right]$$

Speed of sound:

$$c = (g\gamma p/\rho)^{1/2} = (g\gamma TR_g/W)^{1/2} [cm/sec] \quad (B-2)$$

$$g = 1.013 \times 10^6\left[\frac{g}{atm\text{-}cm\text{-}sec^2}\right]$$

Viscosity: Empirical fit for typical combustion products

$$\mu = 1.185 \times 10^{-6} W^{0.5} T^{0.6} [g/cm\text{-}sec] \quad (B-3)$$

Thermal conductivity of low density combustion gases:
Polyatomic Eucken equation:

$$\lambda = \left(c_p + \frac{5}{4}\frac{R_u}{W}\right)\mu \ [cal/cm\text{-}sec\text{-}K] \quad (B-4)$$

c_p -[cal/g-K]

$$R_u = 1.987\left[\frac{cal}{g\text{-}mol\text{-}K}\right]$$

Mass flow rates:

$$r\rho_c A_b = \frac{p_{E,stag} A_t g}{c^*} \quad [g/sec] \quad (B-5)$$

r -[cm/sec] , ρ -[g/cm^3] ,

A_b -[cm^2] , p -[atm]

---

*Pressure in atmosphere rather than dynes/cm^2.

$$c^* = \frac{(gTR_g/W)^{1/2}}{\Gamma} \quad \text{units same as speed of sound} \qquad \text{(B-6)}$$

Reynolds number:

$$Re = \frac{\rho u D}{\mu} \qquad \text{(B-7)}$$

$$\rho = \frac{p}{T(R_g/W)} \qquad \text{(B-8)}$$

Specific heat:

$$c_{p,g} = \frac{\gamma}{\gamma-1}\frac{R_u}{W} \qquad \text{(B-9)}$$

Internal energy:

$$e + \frac{u^2}{2J_c}[\text{cal/g}] \qquad \text{(B-10)}$$

Prandtl number (Eucken formula):

$$Pr = \frac{\nu}{\alpha} = \frac{c_p \mu}{\lambda} = \frac{c_p}{c_p + 1.25R_u/W} \qquad \text{(B-11)}$$

☆U.S. GOVERNMENT PRINTING OFFICE 1977—740-049/134 REGION NO. 4